CHARACTERIZATION OF *IN VITRO* TUMOR NECROSIS FACTOR-α-INDUCED HEPATIC CELL DEATH

BY

MISS THANAWAN SOIMANEE

A THESIS SUBMITTED IN PARTIAL FULFILMENT OF
THE REQUIREMENTS FOR THE DEGREE OF
THE MASTER OF SCIENCE (BIOMEDICAL SCIENCES)
GRADUATE PROGRAM IN BIOMEDICAL SCIENCES
FACULTY OF ALLIED HEALTH SCIENCES
THAMMASAT UNIVERSITY
ACADEMIC YEAR 2026

CHARACTERIZATION OF *IN VITRO* TUMOR NECROSIS FACTOR-α-INDUCED HEPATIC CELL DEATH

BY

MISS THANAWAN SOIMANEE

A THESIS SUBMITTED IN PARTIAL FULFILMENT OF THE REQUIREMENTS FOR THE DEGREE OF THE MASTER OF SCIENCE (BIOMEDICAL SCIENCES) GRADUATE PROGRAM IN BIOMEDICAL SCIENCES FACULTY OF ALLIED HEALTH SCIENCES THAMMASAT UNIVERSITY ACADEMIC YEAR 2026

THAMMASAT UNIVERSITY
FACULTY OF ALLIED HEALTH SCIENCES

THESIS

BY

MISS THANAWAN SOIMANEE

ENTITLED

CHARACTERIZATION OF *IN VITRO* TUMOR NECROSIS FACTOR-α-INDUCED HEPATIC CELL DEATH

was approved as partial fulfillment of the requirements for
the degree of Master of Science (Biomedical sciences)

on May 18, 2026

Chairman	Sittiruk Roytrakul
	(Sittiruk Roytrakul, Ph.D)
Member and Advisor	Chareeporn Akekawatchai
	(Associate Professor Chareeporn Akekawatchai, Ph.D.)
Member and Co-adviser	Onruedee
	(Assistant Professor Onruedee Khantisitthiporn, Ph.D.)
Member and Co-adviser	Phatchariya Phan.il
	(Assistant Professor Phatchariya Phannasil, Ph.D.)
Member	Narisa K. Bordeerat
	(Associate Professor Narisa Kengtrong Bordeerat, Ph.D.)
Dean	Seksun Samosornsuk
	(Associate Professor Seksun Samosornsuk, Ph.D)

Dissertation	Characterization of *In vitro* Tumor Necrosis Factor-α-induced Hepatic Cell Death.
Author	Thanawan Soimanee
Degree	Master of Science
Major Field/Faculty/University	Clinical Biochemistry, Pharmacology and Toxicology Faculty of Allied Health Sciences Thammasat University
Dissertation Advisor	Assoc. Prof. Chareeporn Akekawatchai, Ph.D.
Dissertation Co-Advisor	Asst. Prof. Phatchariya Phannasil, Ph.D.
Dissertation Co-Advisor	Asst. Prof. Onruedee Khantisitthiporn, Ph.D.
Academic Year	2026

ABSTRACT

Hepatocyte death triggers liver inflammation and fibrosis, ultimately driving the progression to hepatocellular carcinoma. Various mediators in the inflammatory liver microenvironment have been identified as inducers of hepatocyte death, including the proinflammatory cytokine tumor necrosis factor-α (TNF-α). While TNF-α-induced hepatocyte death is established as a potential therapeutic target for chronic liver diseases, its molecular mechanisms remain unclear. This study aimed to characterize an *in vitro* model of TNF-α-mediated hepatocyte death using the HepG2 cell line. The cells were treated with various concentrations of TNF-α in combination with cycloheximide (CHX), a protein synthesis inhibitor, at different time points. Cell viability was assessed using the 3-(4,5-dimethylthiazol-2-yl)-2,5-diphenyltetrazolium bromide assay (MTT assay). Additionally, cell cycle arrest and apoptotic cell death were evaluated using DNA-binding dye staining and AnnexinV-7AAD labeling, respectively, followed by flow cytometric analysis. Further molecular characterization was performed using Western blot analysis, coupled with comprehensive proteomic and bioinformatic evaluations. Treatment with TNF-α alone reduced cell viability, but did not have any effect on cell growth, cell cycle and apoptotic cell death. Western blot

analysis indicated no cleavage of the apoptotic markers, caspase-3 and PARP-1, and no expected shift in cell cycle regulation. Notably, TNF-α treated cells may exhibit SA-β-gal activity, a hallmark of cellular senescence, without cell cycle or growth arrest. Cells treated with CHX alone exhibited decreased viability, growth and S-phase cell cycle arrest, and a limited degree of apoptosis. Consistently, molecular analysis revealed no cleavage of caspase-3 and PARP-1 and downregulated p21 expression. Importantly, cells treated with a combination of TNF-α and CHX showed an additive reduction of viability, growth and S-phase cell cycle arrest, but notably enhanced induction of apoptosis (up to 75.8% from 50 μM CHX and 100 ng/mL TNF-α co-treatment). The co-treatment also caused a clear cleavage of caspase-3 and PARP-1, with p21 downregulation. The results indicate that TNF-α alone does not induce cell cycle arrest or apoptosis, while the translational inhibitor, CHX removes the survival pathways, effectively allowing TNF-α to drive the cells toward caspase-3/PARP-1-dependent apoptosis. Additionally, proteomic analysis using MetaboAnalyst 6.0 revealed six candidate proteins from a total of 19,482 proteins expressed differentially in all treatments: phospholipase A2 homolog, ZNF5930S, zinc finger protein 557, oligodendrocyte transcription factor 2, haloacid dehalogenase-like hydrolase domain-containing 5 and adenine phosphoribosyltransferase. The protein-protein interaction network generated by STITCH 5.0 predicted interactions among the latter three proteins, CHX and TNF-α, suggesting their potential roles in TNF-α/CHX-induced cell cycle and apoptosis. Collectively, this molecular characterization of TNF-α/CHX-induced hepatocyte apoptosis provided a valuable *in vitro* model for investigating hepatocyte stress and death in inflammatory environments.

Keywords: Hepatocyte death, TNF-α, Cycloheximide, Apoptosis, Cell cycle, S-phase arrest, Proteomics

ACKNOWLEDGEMENT

This work would not have been possible without the love and support of so many people and one very special cat.

My sincere gratitude to all committee members: Associate Professor Dr. Chareeporn Akekawatchai, Assistant Professor Dr. Onruedee Khantisitthiporn, Associate Professor Dr. Narisa Kengtrong Bordeerat, Assistant Professor Dr. Phatchariya Phannasil, and Dr. Sittiruk Roytrakul, for participating in my thesis dissertation examination.

I would also like to express my sincere gratitude to the Thammasat University Research Unit in Diagnostic Molecular Biology of Chronic Diseases related to Cancer (DMB-CDC), Thailand, for the generous support and resources that made this research possible. This work would not have come to life without your belief in its importance.

To my family and friends, you are the foundation upon which everything in my life is built. Through every moment of self-doubt, every late night, and every time I felt like giving up, your love was the quiet voice that told me to keep going. Words will never be enough to express how deeply grateful I am for your endless sacrifices, your warmth, and the unconditional love you have given me every single day. This achievement belongs to you just as much as it belongs to me.

To my collaborators, I could not have walked this road without you by my side. You were my sounding board, my cheerleaders, and my dearest friends all at once. Thank you for every kind word, every shared struggle, every laugh that made the difficult moments bearable. You each left a piece of yourselves in this work, and I will carry the memory of our time together long after this journey is done. I am so lucky to have had you with me.

And to my sweet Kanomkeng, my little companion who asked for nothing and gave everything. You curled up beside me through the hardest chapters, and somehow, without a single word, you made everything feel okay. Thank you for your warmth, your purrs, and your gentle presence. You are so deeply loved.

Thanawan Soimanee

TABLE OF CONTENTS

LIST OF TABLES

LIST OF FIGURES

LIST OF FIGURES (Cont.)

LIST OF ABBREVIATIONS

Symbols/Abbreviations	Terms
%	Percent
α	Alpha
β	Beta
κ	Kappa
mL	Milliliter
ng	Nanogram
μM	Micromolar
ActD	Actinomycin D
APRT	Adenine phosphoribosyltransferase
ASH	Alcoholic steatohepatitis
ATP	Adenosine triphosphate
Bax	Bcl-2-associated X proteins
Bid	BH3 interacting-domain death agonist
CHX	Cycloheximide
CLD	Chronic liver disease
D-GalN	D-galactosamine
DAMPs	Damage-associated molecular patterns
ECM	Extracellular matrix
FADD	FAS-associated death domain
FBS	Fetal bovine serum
GAPDH	Glyceraldehyde 3-phosphate dehydrogenase
H_2O_2	Hydrogen peroxide
HCC	Hepatocellular carcinoma

LIST OF ABBREVIATIONS (cont.)

Symbols/Abbreviations	Terms
HDHD5	Haloacid dehalogenase-like hydrolase domain-containing 5
HMGB1	High-motility Group Box-1
HSCs	Hepatic stellate cells
IκBα	IKK phosphorylates the inhibitor-α NFκB
IL-1β	Interleukin 1 beta
IL-6	Interleukin 6
MLKL	Mixed lineage kinase domain-like
MMP	Matrix metalloproteinase
NAFLD	Non-alcohol fatty liver disease
NASH	Non-alcoholic steatohepatitis
NFκB	Nuclear factor κB
OC90	Otoconin-90
OLIG2	Oligodendrocyte transcription factor 2
OS	Oxidative stress
p21	Cyclin-dependent kinase inhibitor 1
PARP-1	Poly (ADP-ribose) polymerase 1
PDGF	Platelet-derived growth factors
PE	Phycoerythrin
RIPK	Receptor-interacting protein-kinase
ROS	Reactive oxygen species
SA-β-Gal	Senescence-associated β-galactosidase

LIST OF ABBREVIATIONS (cont.)

Symbols/Abbreviations	Terms
SASP	Senescence-associated secretory phenotype
SDS-PAGE	Sodium Dodecyl Sulfate-Polyacrylamide Gel Electrophoresis
TACE	TNF-converting enzyme
TAK1	TGFβ-activated kinase 1
TGF-β	Transforming growth factor beta
TIMP1	Tissue inhibitor of metalloproteinase 1
TNF-α	Tumor necrosis factor alpha
TNFR1	Tumor necrosis factor receptor 1
TRADD	TNFRSF1A-Associated Via Death Domain
TRAF	TNF receptor-associated factor
ZNF557	Zinc finger protein 557
ZNF593OS	Putative transmembrane protein

CHAPTER 1
INTRODUCTION

1.1 Background to research

Chronic liver disease (CLD) is a major cause of death worldwide. Major etiologies of CLD consist of viral hepatitis, alcoholic steatohepatitis (ASH), non-alcoholic steatohepatitis (NASH), autoimmune disease and genetic diseases. A clinical sign of CLD caused by all etiologies is the development of liver fibrosis in the liver,[1] which leads to liver cirrhosis and eventually hepatocellular carcinoma (HCC). Liver fibrosis is a deposition of extracellular matrix (ECM) proteins, mostly collagen type I and type III, resulting in fibrosis scar conformation. This progressive process causes the disruption of regular liver physiology and function,[2] and the degree of liver fibrosis is correlated with evidence of HCC.[1] The processes of liver fibrosis and inflammation are very complex and involve many cell types in the liver. Exposure to toxic substances, metabolic disease, and viral diseases contributes to hepatocyte damage and death, leading to the release of apoptotic bodies, damage-associated molecular patterns (DAMPs), pro-fibrogenic cytokines and growth factors in the damaged liver, which participate in determining the normal tissue healing process or pathogenic outcomes. The multidirectional interactions among hepatocytes, hepatic stellate cells (HSCs), Kupffer cells and innate immune cells in the liver promote HSC transdifferentiation into proliferative and extracellular matrix (ECM) producing myofibroblasts, leading to liver inflammation and fibrosis. Understanding the molecular and cellular mechanisms underlying the establishment of liver fibrosis and inflammation is critical for the development of diagnosis, treatment, and care of CLD patients.

Hepatocyte death in the liver is primarily a key event of liver inflammation and fibrosis. Typically, hepatocyte damage leads to major types of cell death, necrosis and apoptosis. The two mechanisms cause the secretion of proinflammatory cytokines, fibrogenic growth factors, and other mediators, thereby promoting hepatic inflammation and fibrosis.[1] Hepatocyte damage has also been shown to result in a stable cellular stage with resistance to apoptosis and a lack of response to mitogenic stimuli, termed hepatocellular senescence. This cellular process disrupts homeostasis and the

microenvironment by releasing senescence-associated secretory phenotype (SASP) factors in the liver. Recently, cellular senescence has been increasingly described and initially known as an anti-tumor mechanism. However, in chronic liver damage, hepatocyte senescence is also implicated in hepatic inflammation, fibrosis, and possibly hepatocarcinogenesis.[3, 4] While hepatocyte death has been well characterized and is regarded as a therapeutic target in CLD, hepatocyte senescence is less well described.

Among the profibrogenic mediators released in the damaged liver, tumor necrosis factor-α (TNF-α) is a prominent cytokine known as a key player in chronic inflammation and fibrosis. Many studies demonstrated that TNF-α has dual effects on hepatocytes. The activation of tumor necrosis factor receptor 1 (TNFR1) by TNF-α appears to induce either survival or death of hepatocytes. Previous studies indicated TNF-α alone did not induce apoptotic cell death, possibly due to its ability to activate NFκ-B signaling pathways leading to survival and inflammation.[5, 6] However, TNF-α in combination with the inhibitors of transcription and translation processes can induce apoptosis in many *in vitro* and *in vivo* studies.[7-9] Although TNF-α has also been demonstrated to cause cellular senescence in many cell types, the direct evidence of hepatocyte senescence induced by TNF-α is still limited.[10-13] Accumulating evidence indicates that TNF-α-associated hepatocyte damage triggers various intracellular alterations, causing different forms of cell death and senescence. These processes drive pathological consequences, especially the release of inflammatory and fibrogenic mediators to promote liver inflammation and fibrosis.[1, 14] However, the precise molecular mechanisms underlying TNF-α-mediated hepatocyte death and senescence require further investigation.

1.2 Significance and rationale of research

Liver fibrosis and inflammation are clinical signs of CLD, caused by various factors including hepatotropic viruses, alcohol abuse, and improper nutrition. Apparently, the development of liver fibrosis results from hepatocyte death and chronic inflammation in the liver, which generate proinflammatory and profibrotic cytokines, especially TNF-α. While TNF-α is well-established as a key mediator in liver inflammation and fibrosis, the direct interaction of TNF-α with hepatocytes is not fully understood. Particularly, a comprehensive understanding of the molecular alterations during TNF-α-mediated hepatocyte death and senescence and how these changes contribute to the inflammatory and fibrogenic environment in the liver is required. Based on the previous *in vitro* and *in vivo* studies suggesting that TNF-α-mediated apoptotic cell death requires translational arrest induced by cycloheximide (CHX),[7] this study aimed to characterize an *in vitro* model of hepatocyte senescence and death using hepatocellular cell line, HepG2, treated with a combination of TNF-α and CHX. This model was characterized by evaluating cell death and senescence, as well as by identifying the key molecular pathways and comprehensive proteomic profiles associated with TNF-α/CHX-mediated hepatocyte damage. The characterization of the *in vitro* hepatocyte death and senescence mediated by TNF-α provides understanding in cellular and molecular mechanisms underlying chronic liver inflammation and fibrosis, leading to the development of more effective diagnosis, treatment and care of CLD.

CHAPTER 2
REVIEW OF LITERATURE

2.1 Chronic liver disease

Chronic liver disease (CLD) is a major cause of health issues, with almost 2 million deaths and almost 4% of all deaths worldwide. Interestingly, 1 out of 3 liver associated death represent in females. In high-income countries, alcohol consumption is the main cause of liver cirrhosis, whereas approximately 32.4% of non-alcoholic fatty liver disease, one-fourth of the mature population, progresses to end-stage liver disease in Europe and America. Furthermore, virus infection, especially virus hepatitis B (HBV) and virus hepatitis C (HCV), is largely related to liver cancer in Asia up to 75% of all liver cancer progression.[15] In Thailand, the frequency of liver cirrhosis is 75.3 per 100,000 population. This presents a higher rate in males than in females.[16] The disease is associated with various clinical conditions, including steatohepatitis (ASH), non-alcoholic steatohepatitis (NASH), fatty liver disease, autoimmune disease, genetic diseases, and hepatotropic viral infection. The pathogenesis and progression of CLD have been well-described (**Figure 2.1**). CLD is known to be initiated by hepatocellular damage and inflammation, leading to liver fibrosis. Typically, the degree of fibrosis correlates with liver function and represents a major risk factor for progression to liver cirrhosis and eventually hepatocellular carcinoma (HCC).[1] The common etiologies of liver fibrosis, including hepatitis B and C virus infection, alcoholic steatohepatitis (ASH), and non-alcoholic steatohepatitis (NASH), cause chronic liver damage, consequently resulting in an accumulation of extracellular matrix (ECM), especially type I and III collagens deposition, and formation of fibrosis scar. Liver fibrosis is well-known as a sign of CLD. It could be a consequence of the disruption of epithelial or endothelial barrier and hepatocyte cell death, chronic inflammation with cytokine release, activation of hepatic stellate cells (HSCs), and progression of ECM production in the liver.[1, 2] Understanding molecular and cellular mechanisms underlying the establishment of liver fibrosis is critical for the development of diagnosis, treatment, and care for CLD patients.

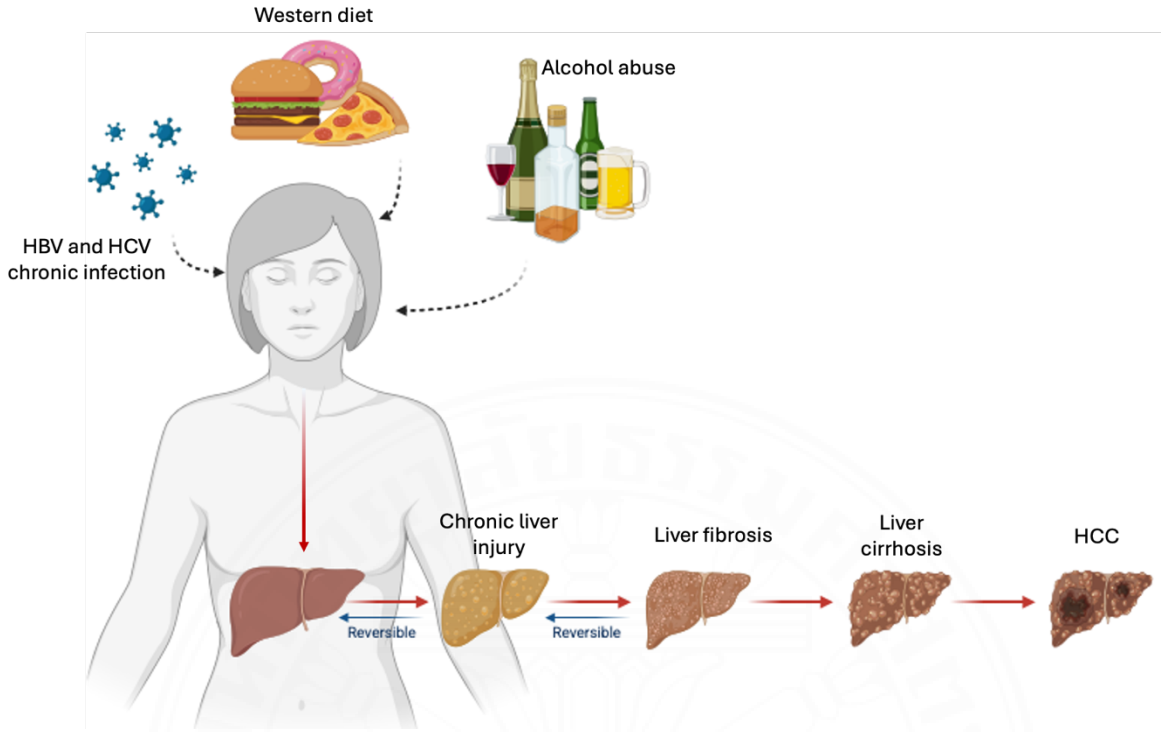

Figure 2.1 The progression of chronic liver disease: Modified from.[2] Created with BioRender.com

2.2 Mechanistic concepts of liver fibrosis

Liver fibrosis is a complex process involving many cell types in the liver (**Figure 2.2**). Initially, chronic hepatic damage caused by different factors such as toxic substances, metabolic and viral disease results in hepatocyte apoptotic death that leads to the release of damage-associated molecular patterns (DAMPs) and apoptotic bodies. These released mediators activate hepatic stellate cells (HSCs) directly, resulting in HSC transdifferentiation to myofibroblast activation. The released DAMPs also induce the recruitment and activation of immune cells, especially cytokine-secreting lymphocytes and monocytes. The local macrophages, known as Kupffer cells, also produce proinflammatory and profibrogenic cytokines, promoting HSC transdifferentiation and myofibroblast activation. On a molecular basis, there is a complex network of cytokine-producing signaling participating in the activation of HSCs, including the signaling of transforming growth factor (TGF-β) and platelet-derived growth factor (PDGF). Multidirectional interactions among activated HSCs, Kupffer cells, and other immune cells promote the transdifferentiation into proliferative ECM-producing myofibroblasts. The overactivation of ECM-producing cells results in excessive ECM accumulation, leading to liver fibrosis which destroys the physiological architecture and function of the liver. Thus, one approach to prevent death from chronic liver disease is to hamper the progression of fibrogenesis in the liver.[1]

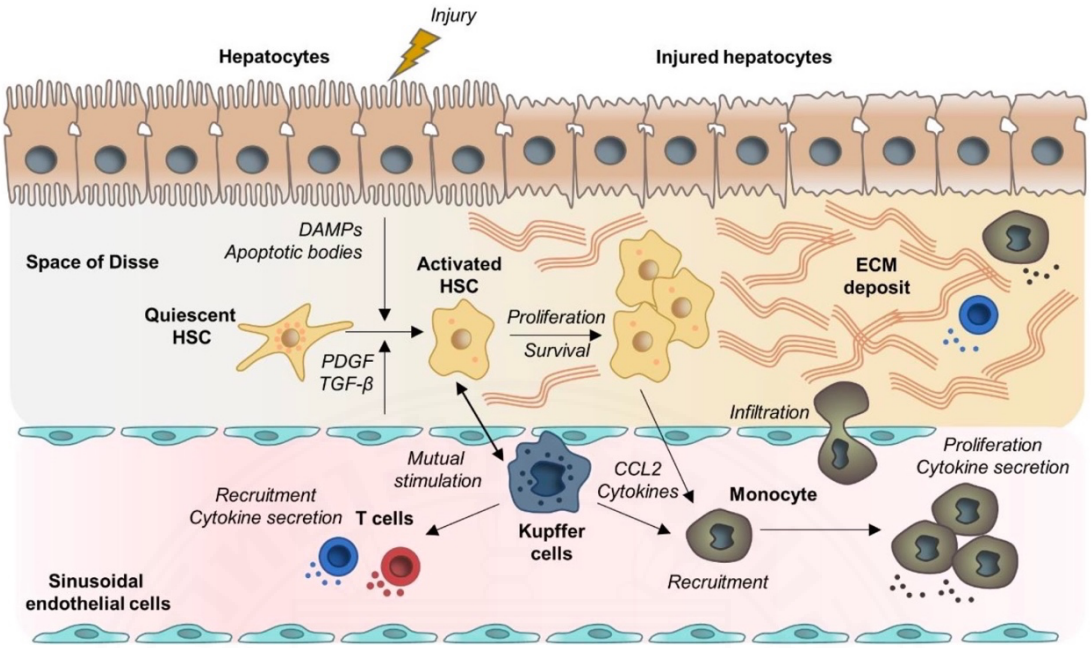

Figure 2.2 Mechanistic concepts for liver fibrosis. During chronic liver injuries, complex multidirectional interactions among hepatocytes, HSCs and Kupffer cells, as well as innate immune cells, promote the process of HSC transdifferentiation into proliferative and extracellular matrix (ECM) producing myofibroblasts, leading to liver fibrosis. Abbreviation: Platelet Derived Growth Factor; TGF-β: Transforming Growth Factor Beta; CCL2: chemokine (C-C motif) ligand 2.[1]

2.2.1 Hepatocyte death: necrosis, apoptosis, and senescence

Hepatocyte death is known as an initial event in liver disease caused by all etiologies. Dead hepatic cells secrete DAMPs and apoptotic bodies to activate other cell types in the liver, especially HSCs and Kupffer cells, which, in turn, coordinately promote ECM production by proliferative myofibroblasts.[1] Typically, damaged hepatocytes undergo two distinct types of cell death, necrosis and apoptosis. DAMPs can be released passively from necrotic hepatocytes due to a disrupted cell membrane.[17, 18] DAMPs are characterized as a family of molecules comprising nucleic acids, intracellular proteins, adenosine triphosphate (ATP), and mitochondria or nucleic compounds such as high-motility Group Box-1 (HMGB1).[17] Accumulating studies indicated an important role of DAMPs, particularly HMGB1, which is highly released from necrotic hepatocytes as a danger signal, in the recruitment of immune cells, and immune activation and inflammation in the necrotic areas in the liver.[18-21] In contrast, hepatocyte apoptosis is believed to secrete low levels of DAMPs because cellular components remain intact within apoptotic bodies.[17, 18] However, apoptotic hepatocytes release the apoptotic bodies, which can be engulfed by HSCs and Kupffer cells, resulting in immune activation and profibrogenic response.[22, 23] The hepatocyte apoptosis also elicits a profibrogenic response through the activation of the Fas death receptor system.[24, 25] Presently, hepatocyte apoptosis and necrosis and their molecular mechanisms have been well-characterized, and the inhibition of hepatocyte death is one of the approaches aiming to develop effective treatment of chronic liver disease.[1]

In recent years, cellular senescence has been increasingly recognized as a contributor to CLD and HCC, even though the precise mechanisms are still largely unclear. Understanding the roles of cellular senescence in the pathogenesis of CLD and HCC is required for the theoretical basis for the clinical treatment of liver diseases.[3] Basically, a cell responds to endogenous and exogenous stress by entering a state of cell-cycle arrest, termed senescence.[14] This cellular process prevents passing DNA damage onto daughter cells and is well-known as an anti-tumor mechanism. The senescent cells lose ability to divide, but they continue to maintain metabolic activity for a certain duration. In acute damage, cellular senescence contributes to tumor suppression, wound healing and tissue homeostasis by arresting the cell cycle and releasing specific factors, known as senescence-associated secretory phenotypes

(SASP). SASPs consequently promote the clearance of the senescent cells by immune cells and stimulate tissue-healing mechanisms. However, in persistent chronic damage, immunosurveillance is deregulated, allowing the accumulation of senescent cells that are implicated in tissue dysfunction and chronic inflammation, and various diseases.[14] Extensive research has indicated that cellular senescence becomes critical in specific physiological and pathological conditions that depend on stress signals, including embryonic development, tissue repair, tumorigenesis and tumor suppression, aging and chronic inflammation-related disorders, including fibrosis[26, 27] and HCC.[3]

The characteristics of senescent cells have been extensively studied. The senescence phenotype is primarily described as a stable cellular stage with no response to mitogenic stimuli and resistance to apoptosis, known as "senescence without death" contributing to age-related diseases.[28] Research progress on cellular senescence indicates the complexity and heterogeneity of the senescent program. Cellular senescence is termed by different phenotypes dependent on stressors or insults, cell types and physiological context. Thus, how to best characterize and describe the senescence phenotypes remains to be determined.[3] At present, no single molecular or cellular phenotype can define cellular senescence, and multiple hallmarks of the senescent program have been proposed, including cell cycle arrest, chromatin reorganization, cell-surface markers, secretory phenotypes, lysosomal compartmentalization, morphological changes and metabolic alterations.[14] Accumulating studies demonstrate the characterization by alteration of cell shape and nuclear envelope integrity, lysosomal function, and shifts in gene expression proflies, and increased activity of key cell cycle arrest regulators such as p53/p21 and $p16^{INK4a}$, the triggering of DNA damage response mechanism, reorganization of chromatin architecture, elevated levels of senescence-associated β-galactosidase (SA-β-Gal) and development of senescence-associated secretory phenotype (SASP).[29] The cellular senescence induced by various stressors requires further clarification in different pathological conditions, including chronic inflammation-related liver diseases and HCC.[3, 14]

Hepatocyte senescence has been established as an anti-tumor mechanism during hepatocarcinogenesis and a therapeutic target of HCC.[3] Hepatocellular senescence inhibits the division and proliferation of damaged

hepatocytes and alters tissue homeostasis and the microenvironment by releasing SASP. Characteristics of hepatocellular senescence are described by several phenotypes, including telomere shortening and dysfunction, SA-β-galactosidase activity, SASP release, cell proliferative arrest, cell enlargement, and levels of p21 and $p16^{INK4a}$ markers.[3] Although the molecular mechanisms and biological function of hepatocellular senescence in CLD remain largely unclear, different approaches of senescence-induced therapy to support its protective roles in tumorigenesis have been extensively studied.[3]

2.2.2 Cell cycle regulation during cell death and senescence

Typically, hepatocytes respond to harmful stimuli such as DNA damage, cellular stress, chemical exposure and viral infection, by choosing one of three main fates: repairing DNA, undergoing apoptosis, or entering a state of permanent growth arrest called cellular senescence.[30] Growing evidence supports that persistent cellular stress often leads cells to undergo aging-related changes, known as cellular senescence[31, 32] and disruption of the decision pathways can significantly contribute to cancer development and aging. Cellular senescence and apoptosis are tightly linked to the dysregulation of cell cycle, and cell cycle arrest is frequently observed as a fundamental response to cellular stress. The arrest represents an initial checkpoint or a prerequisite that enables the initiation of the complex senescence program.[33] Upon cellular damage, such as DNA lesions or stress signals, a key regulatory protein, most notably p53, commonly known as the guardian of the genome's protector, becomes activated. Activated p53 induces the transcription of p21, a cyclin-dependent kinase inhibitor (CDKI), which suppresses CDK activity and temporarily ceases cell cycle progression.[34, 35] This transient arrest allows the cell to evaluate the extent of damage and initiate repair mechanisms. When cellular damage is too severe to be repaired but not immediately lethal, cells may transition from a reversible cell cycle arrest to an irreversible state of cellular senescence.[36, 37] Importantly, cell cycle arrest itself is not equivalent to senescence.[38] Arrested cells temporarily withdraw from the cell cycle to repair damage and may subsequently re-enter proliferation. In contrast, senescent cells permanently lose the ability to re-enter the cell cycle, performing an irreversible senescence.[33, 39] The transition from transient cell cycle arrest to permanent senescence is termed "geroconversion".[40] A key characteristic that distinguishes senescence-

associated arrest from temporary quiescence is the significant reorganization of chromatin. During senescence, cells actively silence the genes involved in cell proliferation by forming dense chromatin structures called senescence-associated heterochromatin foci (SAHF).[41] Even though senescent cells are growth-arrested, they often remain metabolically active or become hypermetabolic, leading to the secretion of bioactive molecules collectively referred to as the senescence-associated secretory phenotype (SASP). These molecules can adversely affect neighboring cells, impair tissue repair, and contribute to organ-level ageing.[42, 43]

Cellular senescence at the molecular level is mainly driven by two key signaling pathways. The first involves p53, a transcription factor, and its target p21, which acts as a CDK inhibitor.[44] When DNA damage is detected, the ATM/ATR kinase complex activates p53, leading to increased p21 expression. The p21 subsequently binds to CDK-cyclin complexes, blocking the G1-to-S-phase transition and preventing DNA replication.[34, 45] This p53/p21 pathway typically induces a temporary cell cycle arrest, giving cells time to repair DNA. After repairing, p21 levels decrease, allowing cell proliferation to resume.[46] However, when severe stress, such as oncogenic stress or telomere shortening, induces irreparable damage, the CDKN2A gene is activated, leading to the expression of p16, a tumor suppressor and CDK inhibitor.By binding directly to CDK4 and CDK6, p16 prevents their interaction with cyclin D. Normally, the cyclin D-CDK4/6 complex phosphorylates the retinoblastoma (Rb) protein, but p16 prevents this phosphorylation, keeping Rb in its active hypophosphorylated state. Active Rb subsequently associates with E2F, thereby repressing genes needed for S-phase entry. Moreover, the Rb/E2F complex attracts chromatin-modifying enzymes like histone methyltransferases, leading to chromatin condensation and SAHF formation. As a result, the cell cycle is permanently halted at G1, establishing a profound state of cellular senescence.[41, 45]

The interplay between cell cycle arrest and apoptosis is also essential in determining cell fate, whether it survives or undergoes programmed death. When a cell finds that transient arrest cannot repair its DNA damage, it may trigger apoptosis as a more severe safeguard. Research shows that p53 levels are crucial in influencing this choice.[47] During early cell cycle arrest, moderate p53 activation promotes p21 expression and G1 arrest. In contrast, severe or sustained damage results in elevated p53 levels, which drive the transcription of proapoptotic genes, such as *BAX*, *PUMA*, and *NOXA*. Under these circumstances, anti-apoptotic proteins, including members of the Bcl-2 family, are concurrently expressed in an attempt to maintain cellular homeostasis. However, excessive activation of apoptotic regulators eventually disrupts this balance, triggering cell death.[48, 49] Once apoptotic signaling is initiated, caspase-3 becomes activated and cleaves p21, effectively removing the protein responsible for maintaining cell cycle arrest. The loss of p21 signifies that cell cycle control is no longer required, as the cell is now irreversibly committed to apoptosis. Thus, degradation of p21 serves as a molecular switch that facilitates the transition from cell cycle arrest to programmed cell death.[50-52]

In summary, cell cycle arrest is an early protective mechanism activated in response to DNA damage or cellular stress through the p53-p21 signaling pathway, leading to reversible inhibition of CDK activity. This phase primarily provides time for DNA repair. If damage persists at a moderate level, cells may undergo irreversible growth arrest via the p16-Rb pathway, resulting in cellular senescence. Conversely, when damage exceeds a critical threshold and repair mechanisms fail, cells abandon survival pathways and activate the apoptotic machinery, involving Bcl-2 family proteins and caspases, to eliminate damaged cells. This decisive checkpoint serves as a critical safeguard to prevent the propagation of genetically unstable cells.[45, 47, 48]

2.2.3 Liver inflammation and cytokine release in the damaged liver

Inflammatory responses in acute liver injury are part of the protective hepatic wound healing process. Immune responses usually eradicate pathogens or other etiologic agents and resolve acute hepatitis, resulting in liver tissue regeneration. However, in cases of ineffective immune responses or persistent etiologic agents in the liver, hepatic damage remains, driving repetitive hepatocyte death and inflammation. Over time, these processes support compensatory liver regeneration, leading to liver fibrosis, cirrhosis, and eventually HCC.[2]

A key regulator of hepatic inflammation appears to be macrophages. The released DAMPs and apoptotic bodies from damaged hepatocytes apparently cause the activation of Kuffer cells, and recruitment of infiltrated monocyte-derived macrophages.[53-57] In the early stage of liver injury, the resident Kuffer cells secrete proinflammatory cytokines, interleukin-1β (IL-1β), tumor necrosis factor-α (TNF-α), chemokine (C-C motif) ligand 2 (CCL2), and CCL5, consequently promoting the activation of HSCs and the attraction of other immune cells, including monocyte-derived macrophages to the liver area.[58] Mutual activation of proinflammatory macrophages and HSCs consequently amplifies and perpetuates a profibrogenic environment in the liver. In contrast, in the progressive liver injury and inflammation, macrophages become anti-inflammatory and release anti-inflammatory mediators such as IL-10 and tumor growth factor-β (TGF-β).[59] At the late stage of liver injury, the abundance of TGF-β in the liver allows switching of the resident macrophages to immunosuppressive cell types, causing the immune invasion and tumorigenesis.[1, 60] Apparently, macrophages and the cytokines they release play critical roles in the acquisition of liver inflammation and fibrosis.

Another key process promoting hepatic damage, inflammation and fibrosis is oxidative stress (OS). An imbalance between cellular prooxidant and antioxidant factors causes the production of reactive oxygen species (ROS), comprising profibrogenic mediator superoxides, hydrogen peroxide (H_2O_2) and hydroxyl radicals.[61] During normal cellular mechanisms, hepatocytes, HSCs and macrophages generate low levels of ROS, which serve as messengers in various intracellular signaling.[62] However, production of ROS at high levels results in disruption of cellular lipids, proteins and DNA, leading to hepatocyte necrosis and apoptosis. ROS also

stimulates HSCs and Kuffer cells and other inflammatory cells to produce proinflammatory and profibrogenic factors.[54, 63] Thus, OS is one of the therapeutic targets for liver inflammation and fibrosis.[64]

2.3 Tumor necrosis factor-α: a central player in chronic liver inflammation and fibrosis

Among profibrogenic mediators released in the injured liver, tumor necrosis factor alpha (TNF-α) is a prominent inflammatory cytokine, potentially playing roles in liver fibrosis in both non-infectious and infectious liver diseases.[65, 66] This proinflammatory cytokine is secreted from many cell types, including activated monocytes/macrophages and triggers multiple intracellular signaling pathways to cell proliferation and apoptosis in target cells. Although roles of TNF-α in hepatic fibrosis has not been fully described, it is evident that TNF production during hepatic damage causes prolonged inflammation, resulting in the stimulation of liver-resident HSCs to transdifferentiate into the fibrogenic myofibroblasts. These cellular activities are known to support liver fibrogenesis.[5, 67]

2.3.1 TNF-α ligand-receptor system

TNF-α is synthesized as a 26-kDa precursor protein (mTNF), which is cleaved proteolytically by TNF-converting enzyme (TACE) to generate a soluble 17-kDa form (sTNF). Both mTNF and sTNF are functionally active and able to transmit signaling through binding to tumor necrosis factor receptors (TNFRs), TNFR1 and TNFR2 on the cell surface, whereas mTNF preferentially activates TNFR2.[67] Studies in gene-knockout mice to evaluate the specific involvement of TNFRs in liver fibrosis indicated that TNFR1, but not TNFR2, is important in HSC activation. HSCs isolated from TNFR1, but not TNFR2, knockout mice showed a reduction in the ECM production.[68] Importantly, TNFR1 knockout mice presented a reduction of hepatic damage and fibrosis induced by CCL_4.[68-70] Inhibition of TNFR1 also reduces hepatocellular injury and fibrosis, and steatosis in non-alcoholic fatty liver disease (NAFLD).[71] These previous studies support the importance of TNFR1, not TNFR2, in the establishment of liver fibrosis. TNFR2 is expressed in hematopoietic and endothelial cells, playing roles in homeostasis, and until now, it is less well characterized in liver damage and fibrosis.[6, 67]

2.3.2 TNF-α signaling

TNF-α is known as a multifunctional cytokine, inducing either cell survival or death. The activation of TNF-α in hepatocytes causes multiple signaling pathways, consequently leading to different cellular outcomes. The TNF-α activation is known to be responsible for cell survival and proliferation, inflammation, immune response, and cell death.[6, 67] The established signaling pathways of TNF and TNFR1 are demonstrated in Figure 2.3. The binding of TNF-α to the extracellular domains of TNFR1 causes the formation of complex I, comprising the membrane-bound signaling core TNFR1-TNFR1-associated death domain (TRADD), receptor-interacting protein-kinase (RIPK) 1, and TNF receptor-associated factor (TRAF) 2. Polyubiquitin chains are added to the complex, thereby activating downstream signal molecules. Then, the complex leads to the activation of TGFβ-activated kinase 1 (TAK1), which is linked to c-Jun N-terminal kinase (JKN)/p38 signaling and the inhibitor of κB (IκB) kinase (IKK). The IKK complex, which is composed of IKKα, IKKβ, and the regulatory nuclear factor κB (NFκB) essential modulator (NEMO, also named IKKγ), is activated. Consequently, IKK phosphorylates the inhibitor-α NFκB (IκBα), which becomes degraded by K48-linked polyubiquitination, eventually allowing transcription factor NFκB to enter the nucleus and activate the transcription process of numerous proteins in inflammation, proliferation and cell survival.[6, 72] The NFκB signaling pathways have been shown to be important in the cytoprotective effects of TNF and required for TNF/TNFR1-mediated liver regeneration.[73-75]

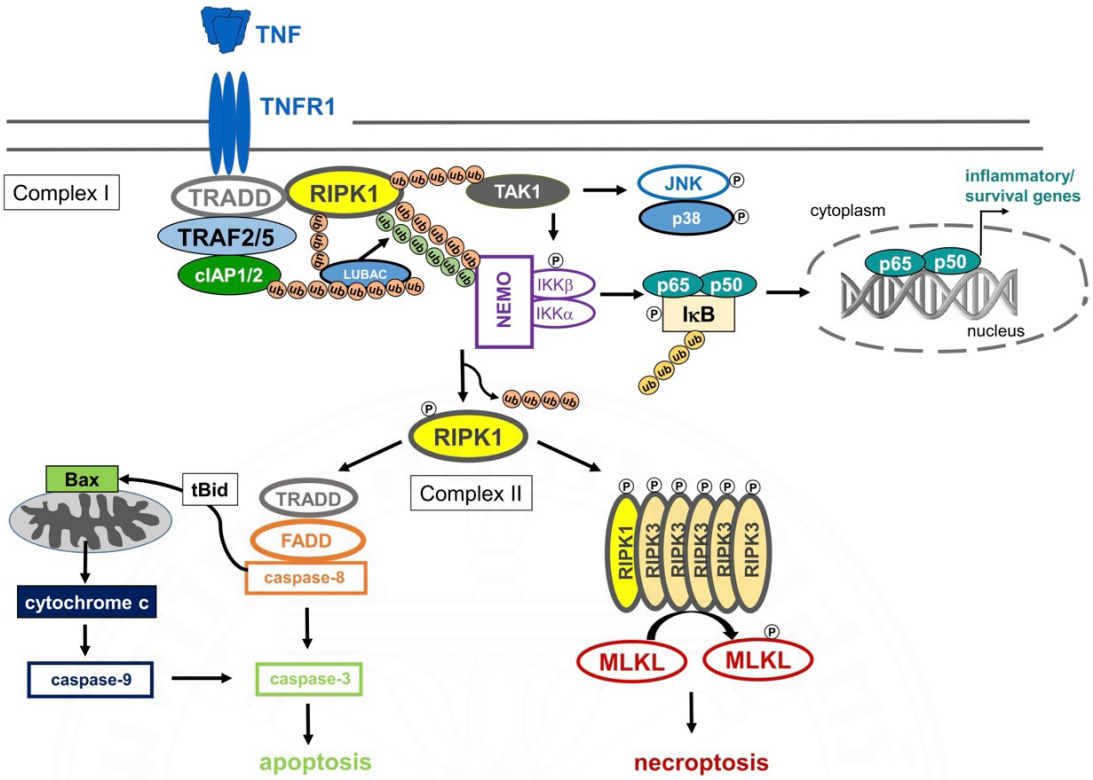

Figure 2.3 TNFR1 signaling pathways. The binding of TNF to TNFR1 results in the formation of complex I, which transmits signals to the downstream NFκB system, leading to cell survival and inflammation. Upon recruitment of FADD to TRADD, the death-inducing signaling complex (complex II) is formed and signals through caspase-8-dependent pathways and the mitochondrial pathway of Bax, cytochrome c and caspase-9. These activation pathways result in apoptotic cell death. Alternatively, the presence of phosphorylated RIPK1 and RIPK3 causes the phosphorylation MLKL, leading to a proinflammatory form of cell death, necroptosis.[6]

In contrast, the death-inducing signaling complex (complex II) is formed by recruiting FAS-associated death domain (FADD) to TRADD, which allows recruitment of procaspase-8 to the complex. This results in the activation of proapoptotic pathways downstream of TNFR1.[6, 72] The activated caspase-8 then proteolytically cleaves procaspase-3 to obtain active caspase-3, the major executioner of apoptosis.[6] TNF-mediated caspase-3 activation also mediates a mitochondrial apoptotic pathway involving cleavage of BH3 interacting-domain death agonist (Bid) to truncated Bid (tBid), activation of Bcl-2-associated X proteins (Bax), cytochrome C release, and finally activation of caspase-9 and caspase-3.[6] Additionally, TNF may activate TNFR1 signaling pathways to the caspase-independent cell death, termed necroptosis. The phosphorylated RIPK1 and RIPK3 complex, which is assembled to form a complex of amyloid microfilaments, called necrosome, causes phosphorylation of mixed lineage kinase domain-like (MLKL), leading to a proinflammatory necroptosis.[6, 72]

2.3.3 Roles of TNF-α in liver inflammation and fibrosis

TNF-α is a key player in inflammatory responses and TNF-α-targeted drugs are among the promising therapy for inflammatory-dependent diseases.[65] Accumulating studies support the roles of TNF-α in hepatic cell death, liver inflammation and fibrosis (**Figure 2.4**).[67] Hepatocyte apoptosis is known to be an initial event of fibrogenesis. Hepatocyte is stimulated by proapoptotic proteins, TNF-α, FasL and TRAIL, inducing cell apoptosis and release of apoptotic bodies. The apoptotic bodies are then engulfed by HSCs and Kupffer cells, causing the upregulation of profibrogenic factors such as TGF-β and death ligands such as TNF-α.[23] Prolonged activation of HSCs and Kuffer cells further enhances hepatocyte apoptosis and inflammation by a feedforward loop mechanism.[23, 76]

TNF-α is suggested to have pleiotropic effects on HSCs based on several studies. The *in vitro* study demonstrated that TNF-α treatment suppresses collagen-α1 gene expression, apoptosis and proliferation of HSCs.[77, 78] However, TNF-α is demonstrated to enhance liver fibrosis by upregulating matrix metalloproteinase (MMP) and a tissue inhibitor of metalloproteinase-1 (TIMP1) expression in HSCs.[79] Several previous studies also support proliferative and profibrogenic effects of TNF-α

on HSCs.[80, 81] Thus, overall TNF-α is known to promote liver fibrosis by promoting the fibrogenic HSC activity. Interestingly, TNF-α is associated with an interaction between hepatocytes and activated HSCs, which is apparently involved in liver fibrogenesis. TNF-α treatment induces production of a profibrogenic protein, periostin, in human hepatoblastoma cell line, HepG2.[82] This consequently activates the production of fibrotic matrix proteins, fibronectin collagen type I, elastin, and tenascin, which are components required for fibrogenesis.[67, 83]

During hepatic damage, a major source of TNF-α is hepatic macrophages. The activated macrophages secrete various profibrogenic cytokines such as TNF-α, and TGF-β and chemokines, leading to activation of HSCs.[1, 67] TNF-α derived from hepatic macrophage is associated with the NFκB-dependent HSC survival, which is required for liver fibrosis.[80] Notably, liver macrophages are unlikely to participate in HSC transdifferentiation.[67] Hepatic B lymphocytes also contribute to fibrogenic responses by secreting inflammatory cytokines and chemokines in the damaged liver. Insufficiency of hepatic B cells protects CCL4-treated mice from liver HSC activation and fibrosis because hepatic B cells are able to induce production of inflammatory cytokines and chemoattractants including TNF-α.[67] Apparently, accumulating studies strongly indicated a prominent role of TNFα in the activity of many cell types during hepatic damage, inflammation, and fibrosis.

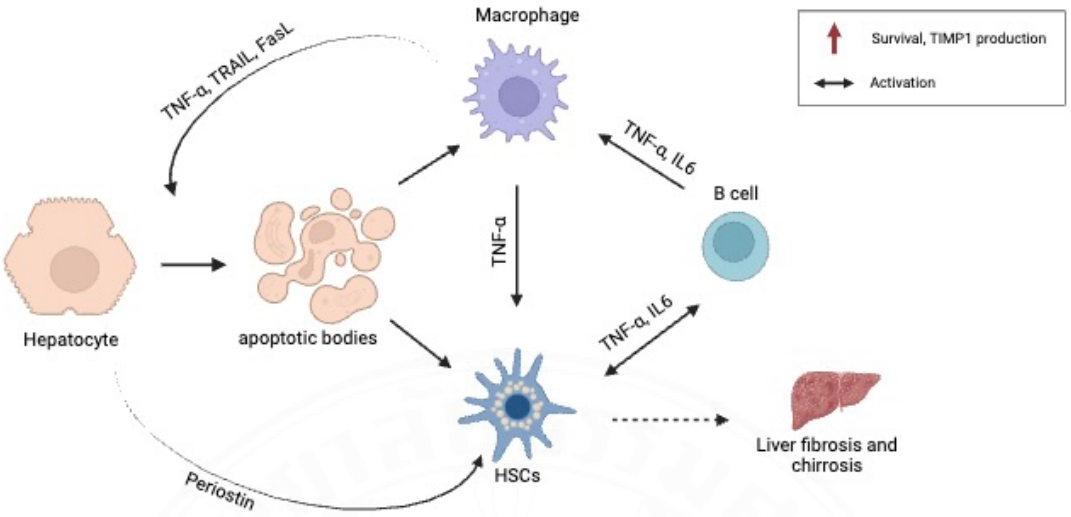

Figure 2.4 TNF-α-mediated liver fibrosis and cirrhosis. In the damaged liver, apoptotic hepatocytes release apoptotic bodies, which are engulfed by macrophages and HSCs. The macrophages, subsequently upregulate the expression of death ligands (e.g., TNF-α, TRAIL and FasL), amplifying hepatocyte cell death. When HSCs engulf apoptotic bodies, this triggers an enhanced profibrogenic response. Periostin secreted from TNF-α-induced apoptotic hepatocytes mediates collagen production in HSCs and HSCs also promote B cell survival. In fibrotic liver, B cells produce proinflammatory cytokine and chemoattractants (e.g., TNF-α, IL-6, MCP-1, and MIP-1α) to accelerate liver fibrosis and cirrhosis. Modified from.[67] Created with BioRender.com.

2.4 Roles of TNF-α in hepatocyte death and senescence

Hepatocyte death is a key event to drive liver inflammation and fibrosis. As described earlier, TNF-α, a prominent cytokine released from hepatic macrophages and other immune cells, may have dual effects on hepatocytes.[5, 84] The activation of TNFR1 by TNF-α in hepatocytes induces cell proliferation, and apoptosis or necroptosis that is closely linked to inflammation.[65] The molecular mechanisms determining cell fate decisions are very complicated and not fully understood. It is well-established that TNF-α activates the intracellular signaling complex I and complex II pathways to either cell survival, inflammation and cell death, respectively (**Figure 2.3**). These signaling pathways are possibly regulated by TNF-α concentrations in the damaged liver area that differ depending on the etiologic agents. *In vitro* and *in vivo* experiments indicated that TNF-α induced hepatocyte death at high concentrations, whereas, at low concentrations, activated cell survival (**Figure 2.5**). The pleotropic effects were due to the activity of YAP, a member of Hippo signaling pathway, which is known to regulate proliferation, differentiation, and death.[5, 85] The pleotropic effects of TNF-α are suggested to be involved in a balance between survival and death of hepatocytes and have been emphasized in many inflammatory diseases.

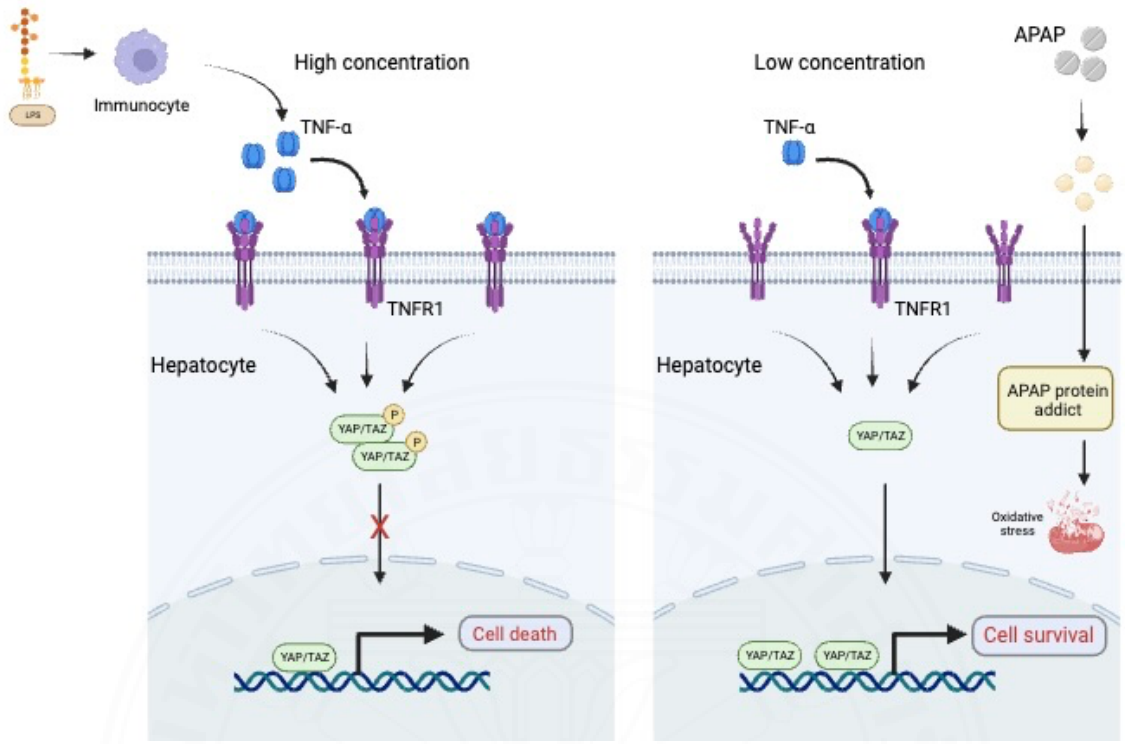

Figure 2.5 Hepatocyte proliferation and apoptosis are modulated by TNF-α via the Yap signaling pathway. High concentrations of TNF-α induce hepatocyte death via TNFR1-mediated phosphorylation and subsequent inactivation of YAP1. Conversely, low concentrations of TNF-α promote YAP1 activation, contributing to cell survival and proliferation. Modified from.[5] Created with BioRender.com.

One of the well-characterized hepatocyte deaths induced by TNF-α is apoptotic cell death. TNF-α activates hepatocyte apoptosis through the caspase-dependent pathways, while it also induces a survival pathway through the NF-kB activation system (**Figure 2.3**).[6] Interestingly, TNF-α alone is unable to trigger hepatocyte apoptosis.[86, 87] The ability of TNF-α to induce apoptosis appears to depend on secondary signaling pathways, and existing literature remains controversial. An *in vitro* study indicated that TNF-α treatment with the deletion of IKK2, a crucial kinase required for NF-κB activation, did not sensitize hepatocytes to apoptosis,[88] whereas the study on hepatitis C virus infection supports that TNF-α-mediated hepatocyte apoptosis requires the NF-κB inhibition.[89] Moreover, other studies suggest that the inhibition of transcriptional and translational processes can sensitize hepatocytes to TNF-α-induced apoptosis.[7, 90] Different inhibitors for transcription and translation, such as cycloheximide (CHX), actinomycin D (ActD) and D-galactosamine (D-GalN), have been used in the *in vitro* and *in vivo* models of TNF-α-mediated hepatocyte apoptosis.[7-9] Presently, TNF-α-induced hepatocyte apoptosis is well-established as a key event triggering liver inflammation and fibrosis, and a solid *in vitro* model is required for in-depth studies on its specific intracellular mechanisms.

Hepatocellular senescence has increasingly been recognized as an important modulator of hepatocarcinogenesis in recent years.[4] Accumulating studies support the existence of hepatocyte senescence during acute and late phases of liver injuries, with the differential outcomes of hepatocyte senescence.[4] In the early stage of liver injury, senescent hepatocytes secrete proinflammatory cytokines and chemokines such as CCL2, IL-1, IL-6 and IL-10 and growth factors such as TGF-β to eliminate causative agents and enhance tissue repair. In contrast, the progression to chronic damage causes the senescent hepatocytes to gradually produce SASPs, which may alter the microenvironment favoring fibrogenesis and inflammation and hepatocarcinogenesis.[4] Indeed, purpose of SASP secretion from senescent hepatocytes is for the activation of immune cells to eliminate precancerous hepatic senescence, also known as senescence surveillance, along with prevention of malignant cell establishment.[3, 91] Particularly, TNF-α is considered a key factor of cellular senescent induction in many cell types[12, 92, 93] and has also been studied in hepatocytes. A study

in human hepatoma HepG2 cell line indicated that TNF-α treatment did not induce apoptosis but exhibited the ability to induce reactive oxygen species (ROS), and mitochondrial DNA (mtDNA) lesions and depletion.[10] Presently, hepatocyte senescence induced by TNF-α and its precise mechanisms also require further characterization.

Accordingly, accumulating studies indicate TNF-α-mediated hepatocyte death and senescence. However, their precise mechanisms are not fully understood, particularly intracellular mechanisms underlying hepatocyte apoptosis and senescence, which potentially drive the establishment of pathogenic inflammation and fibrosis in the liver. Hence, an *in vitro* model of TNF-α-induced cell death and senescence is needed for studying cellular and molecular mechanisms of hepatocyte death and senescence during chronic inflammation.

CHAPTER 3
AIMS, HYPOTHESIS, AND OBJECTIVE

3.1 Experimental framework

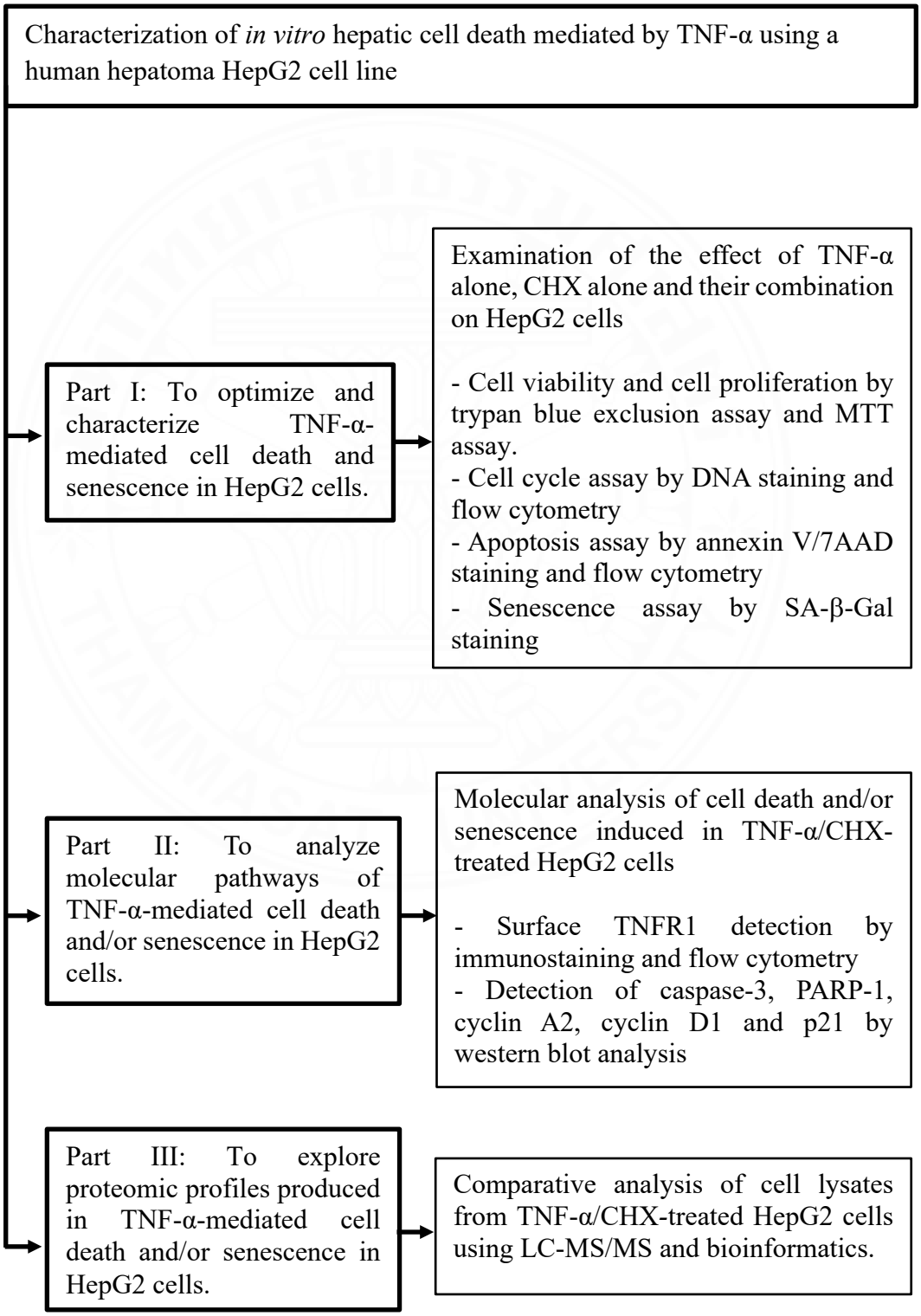

3.2 Central hypothesis

Proinflammatory cytokine TNF-α may induce hepatocyte death and/or senescence in a HepG2 hepatoma cell line, serving as *in vitro* model for hepatocyte stress and death in an inflammatory liver environment.

3.3 Main aim

This study aims to characterize *in vitro* TNF-α-mediated hepatocyte death and/or senescence using the human hepatoma cell line HepG2.

3.4 Specific aims

3.4.1 Specific aim 1: To optimize and characterize TNF-α-mediated cell death and senescence in HepG2 cells.

3.4.2 specific aim 2: To analyze molecular pathways of TNF-α-mediated cell death and/or senescence in HepG2 cells.

3.4.3 specific aim 3: To explore proteomic profiles produced in TNF-α-mediated cell death and/or senescence in HepG2 cells.

CHAPTER 4
RESEARCH METHODOLOGY

4.1 Materials

4.1.1 General chemicals, reagents and antibodies

Various general chemicals and reagents from major suppliers are listed in **Table 1**. **Table 4.2** details the preparation of general solutions and buffers. **Tables 4.3** and **4.4** present lists of antibodies, their suppliers, and applications in flow cytometry and Western blotting. The basic reagents and media used for cell culture are provided in **Table 4.5**.

Table 4.1 Chemicals and reagents

Name	Main suppliers and manufacturers
Acrylamide 4K-solution 40% mix 37.5:1	Euroclone lid. UK, Pero, Italy
Ammonium persulfate (APS)	Bio-Rad, Japan
BCA protein assay kit	EMD Millipore Corp, MA, USA
Bromophenol blue	Sigma-Aldrich, MO, USA
Cycloheximide (CHX)	Sigma-Aldrich, MO, USA
Dimethyl sulfoxide (DMSO)	Biobasic inc, Singapore
Enhanced chemiluminescence (ECL) substrate	Bio-Rad, USA
Ethanol	RCI Lab, BKK, TH
Ethylene glycol tetraacetic acid (EGTA)	Sigma-Aldrich, MO, USA
Ethylenediaminetetraacetic acid (EDTA)	Biobasic inc, Singapore
Glycerol	Ajax chemicals, NSW, AUS
Glycine	Bio-Rad, USA

(Continued over page)

Table 4.1 Chemicals and reagents (Cont.)

Name	Main suppliers and manufacturers
1M HEPES ($C_8H_{18}N_2O_4S$)	Gibco-BRL, Grand Island, NY, USA
Hydrochloric acid (HCl)	QREC, NZ
Imperial™ protein stain	Termo, Rockford, IL, USA
Magnesium dichloride ($MgCl_2$)	Ajax Chemicals, NSW, AUS
Methanol	Millipore, Burlington, MA, USA
MUSE™ Annexin V and Dead Cell Kit	Cytek Bioscience, San Diego, CA
MUSE Cell Cycle Assay Kit	Cytek Bioscience, San Diego, CA
N, N, N′, N′-Tetramethylethylenediamine (TEMED)	Biobasic inc, Singapore
Non-fat dry milk	Biobasic inc, Singapore
Phenylmethylsulfonyl fluoride (PMSF)	Sigma-Aldrich, MO, USA
Phosphatase inhibitor cocktail 2	Sigma-Aldrich, MO, USA
Phosphatase inhibitor cocktail 3	Sigma-Aldrich, MO, USA
Potassium chloride (KCl)	Millipore, Burlington, MA, USA
Protease inhibitor (PI) cocktail tablets	Roche, Mannheim, Germany
Protein standard (for western blot)	Millipore, Burlington, MA, USA
Restore™ Western blot stripping buffer	Termo Scientific, Rockford, IL, USA
Radioimmunoprecipitation assay (RIPA) buffer	Sigma-Aldrich, MO, USA

(Continued over page)

Table 4.1 Chemicals and reagents (Cont.)

Name	Main suppliers and manufacturers
Senescence detection kit	Abcam, Cambridge, UK
Sodium chloride (NaCl)	Elago Enterprises, NSW, AUS
Sodium dodecyl sulfate (SDS)	Sigma-Aldrich, MO, USA
Sodium fluoride (NaF)	Ajax chemicals, NSW, AUS
Sodium orthovanadate (Na_3VO_4)	Sigma-Aldrich, MO, USA
Thiazolyl blue tetrazolium bromide (MTT)	Invitrogen, Biobasic inc, Singapore
Trichloroacetic acid	Millipore, Burlington, MA, USA
Triton X-100	Biobasic inc, Singapore
Tumor necrosis factor-alpha (TNF-α)	R&D system Biotechne, USA
Tween-20	Biobasic inc, Singapore
β-mercaptoethanol	Gibco-BRL, Grand Island, NY, USA

Table 4.2 General solutions and buffers

Name	Content
0.4% Trypan blue	0.4% (w/v) Trypan blue in 1X PBS
0.5 M Tris base pH 6.8	0.5 M Tris-base in DI water and adjusted pH with HCl
1.5 M Tris base pH 8.8	1.5 M Tris-base in DI water and adjusted pH with HCl
1% Paraformaldehyde (PFA)	1% (w/v) PFA in 1X PBS
10% Ammonium persulfate (APS)	10% (w/v) APS (freshly prepared) in deionized water
10% Sodium dodecyl sulfate (SDS)	10% (w/v) SDS in deionized water
10X Running buffer	30 g/L Tris-base, 144 g/L glycine, 10 g/L SDS

(Continued over page)

Table 4.2 General solutions and buffers (Cont.)

Name	Content
10X TBS buffer pH 7.4	88 g/L NaCl, 2 g/L KCl, 24 g/L Tris-base (adjusted pH with HCl)
10X Transfer buffer (stock)	60.5 g/L Tris-base, 144 g/L glycine
1X Transfer buffer (working)	10X transfer buffer (stock) in deionized water (1:10)
1X Staining solution (for SA-β-Galactosidase staining assay)	Citric-phosphate β-gal staining solution with potassium ferrocyanide/ferricyanide staining supplement
4% Paraformaldehyde (PFA)	4% (w/v) PFA in 1X PBS
6X Loading buffer	Tris pH 6.8, 30% (v/v) glycerol, 10% (v/v) SDS, 0.012% (w/v) bromophenol blue
70% Glycerol	70% (v/v) glycerol in PBS pH 7.4
BCA solution	Bicinchoninic acid, sodium carbonate, sodium tartrate, and sodium bicarbonate in 0.1M NaOH, pH 11.25
BSA protein standard	Bovine serum albumin (BSA) standard 2 mg/mL
Cupric sulfate	4% cupric sulfate
Fixative solution (for cell cycle)	70% (v/v) ethanol in Deionized water (freshly prepared)
Lysis buffer (Triton X-100 based lysis buffer)	50 mM HEPES pH 7.5, 150 mM Nacl, 1.5 mM $MgCl_2$, 1 mM EGTA, 0.5 mM EDTA, 10% (v/v) glycerol and 1% (v/v) triton X-100
MTT solution (stock)	5 mg 3-(4,5-dimethylthiazol-2-yl)-2,5-diphenyltetrazolium bromide (MTT), 1 mL PBS
MTT solution (working)	MTT in PBS (1:10)

(Continued over page)

Table 4.2 General solutions and buffers (Cont.)

Name	Content
1X Phosphate buffered saline (PBS)	137 mM sodium chloride (NaCl), 2.7 mM potassium chloride (KCl), 8.1 mM sodium phosphate dibasic, 1.47 mM potassium phosphate monobasic
Ponceau S staining 0.5%	0.5 g (w/v) Ponceau S, 0.5 g (w/v) trichloroacetic acid
Radioimmunoprecipitation assay (RIPA) buffer	50 mM Tris-HCl, pH 8.0, with 150 mM sodium chloride, 1.0% Igepal CA-630 (NP-40), 0.5% sodium deoxycholate, and 0.1% sodium dodecyl sulfate.
Separating gel 5 ml/gel 1.0 mm (12.5%)	31% (v/v) of 40% (w/v) Acrylamide, 1.5 M Tris-base pH 8.8, 1% (v/v) of 10% SDS, 0.6% (v/v) 10% APS, 0.1% (v/v) TEMED
Separating gel 5 ml/gel 1.0 mm (15%)	46% (v/v) of 40% (w/v) Acrylamide, 1.5 M Tris-base pH 8.8,1% (v/v) of 10% SDS, 0.6% (v/v) 10% APS, 0.1% (v/v) TEMED
Stacking gel 5 mL (4%)	10% (v/v) of 40% (w/v) Acrylamide, 0.5 M Tris-base pH 6.8,1% (v/v) of 10% SDS, 0.7% (v/v) 10% APS, 0.2% (v/v) TEMED
Human staining buffer (immunostaining for FACS)	1X PBS containing 1% (v/v) human serum group AB, 0.04% NaN_3
Tris-buffered saline (TBS)	8.8 g/L NaCl, 0.2 g/L KCl, 2.4 g/L Tris-base (adjusted pH by HCl)
TBST	TBS containing 0.1% (v/v) Tween-20
X-Gal stock solution (20 mg/mL)	20 mg X-Gal with 1 mL DMSO

Table 4.3 Primary antibodies used in flow cytometry and Western blot

Name	Conc./dilution	Application	Sources
Human TNF RI/TNFRSF1A PE conjugated antibody (monoclonal mouse IgG, clone 16803): FAB225P	10 µL/reaction	FACS	R&D Systems, Minneapolis, MN
PE-conjugated mouse IgG1 (monoclonal mouse IgG1k, clone 11711): IC002P	10 µL/reaction	FACS	R&D Systems, Minneapolis, MN
Anti-procaspase-3 (H-277) rabbit polyclonal IgG: sc-7148	1: 500	WB	Santa Cruz, CA, USA
PARP-1 monoclonal antibody mouse IgG1, clone 1D7D4: 66520-1-Ig	1: 40000	WB	Proteintech, USA
p21 Waf1/Cip1 (12D1) rabbit mAB IgG: 2947	1: 2000	WB	Cell signaling, Massachusetts, USA
Cyclin A2 polyclonal antibody rabbit IgG: 18202-1-AP	1: 3000	WB	Proteintech, USA
Cyclin D1 monoclonal antibody mouse IgG2b, clone 2G3G5: 60186-1-Ig	1: 1000	WB	Proteintech, USA
GAPDH monoclonal antibody mouse IgG2b, clone 1E6D9: 60004-1-Ig	1: 50000	WB	Proteintech, USA

(Continued over page)

Table 4.4 Secondary antibodies used in Western blot

Name	Conc./dilution	Application	Sources
Goat anti-rabbit IgG-HRP: sc-2004	1: 10000	WB	Santa Cruz, CA, USA
Anti-mouse IgG, HRP-linked antibody: 7076	1: 10000	WB	Cell signaling, Massachusetts, USA

Table 4.5 Reagents and medium used in cell culture

Name	Suppliers
0.25% Trypsin-EDTA	Gibco-BRL, Grand Island, NY, USA
Dimethyl sulfoxide (DMSO)	Ameresco, Solon, Ohio, USA
Dulbecco's Modified Eagle Medium (DMEM) 1X with 1 g/L D-glucose, L-Glutamine and 110 mg/L Sodium pyruvate	Gibco-BRL, Grand Island, NY, USA
Fetal bovine serum (FBS) (Heat-inactivated at 56°C for 30 min	Gibco-BRL, Paisley, PA, UK
1M HEPES	Gibco-BRL, Grand Island, NY, USA
Penicillin-Streptomycin (10^5 unit/mL penicillin and 10^5 µg/mL streptomycin)	Gibco-BRL, Grand Island, NY, USA
1X Phosphate buffered saline (PBS)	Gibco-BRL, Grand Island, NY, USA

4.2 Cell culture and maintenance

The human hepatocellular carcinoma cell line, HepG2, was obtained from the American Type Culture Collection (ATCC HB-8065, Manassas, VA, USA). Cells were cultured and maintained in complete growth medium, consisting of DMEM-low glucose and supplemented with 10% (v/v) inactivated fetal bovine serum (FBS), 1M HEPES and 1% penicillin/streptomycin. Cells were subcultured every 3 days according to the following protocol. The cultures were washed once with 1X PBS, and cells were detached by adding trypsin-EDTA solution. After the enzyme reaction was stopped by neutralizing with complete medium, cells were resuspended, seeded into a new flask at a splitting ratio of 1:3, and cultured at 37°C in a 5% CO_2 atmosphere.

4.3 Cellular assays

4.3.1 Assessment of cell viability by trypan blue exclusion assay and 3-(4,5-dimethylthiazol-2-yl)-2,5-diphenyltetrazolium bromide assay

Cells were washed with 1X PBS and detached using trypsin-EDTA solution, which facilitates dissociation of cells from the culture dish surface. Trypsin was then inactivated with complete medium. Cells were resuspended and transferred to a sterile 50-mL centrifuge tube. To evaluate cell viability using the trypan blue exclusion assay, 50 µL trypan blue reagent (**Table 4.2**) was mixed thoroughly with 50 µL of cell suspension. Then, 10 µL of the mixture was carefully loaded into a counting chamber to count viable cells under a microscope and calculated as cells/mL.

To assess cell viability using the MTT assay, cells were suspended in complete medium at a density of 1×10^6 cells/mL and seeded into 96-well plates to yield 2×10^5 cells per well and incubated overnight at 37°C with 5% CO_2. The MTT stock solution was prepared at a concentration of 5 mg/mL (**Table 4.2**) by reconstituting in 1X PBS. A fresh MTT working solution (**Table 4.2**) was prepared at a 1:10 dilution, and 50 µL was added to each well. The plates were incubated for 3 hours to allow the formation of insoluble formazan crystals. Subsequently, the crystals were dissolved by adding 150 µL of DMSO to each well and mixing thoroughly. An absorbance was then measured at 570 nm using an ELISA plate reader (BioTek Instruments, USA). Cell

viability was calculated as a percentage relative to the untreated control cells, which were defined as 100% viability.

4.3.2 Growth arrest assay

Cells were seeded into 24-well plates at a density of 2×10^5 cells/mL in complete medium and incubated overnight at 37°C with 5% CO_2. The initial 24-hour culture, designated as passage 0, was harvested by trypsinization and resuspended in the complete medium. Viable cell concentrations (cells/mL) were determined by trypan blue exclusion assay. The cell suspension was then adjusted to the initial seeding density, transferred to fresh plates, and incubated for additional 24 hours, defined as passage 1. This subculturing was repeated for up to three passages to evaluate proliferative capacity.

4.3.3 Cell cycle analysis by DNA staining and flow cytometry

Cell cycle progression was evaluated using the MUSE Cell Cycle Assay Kit (Cytek Bioscience, USA) according to the manufacturer's instructions. Briefly, Cells were harvested by trypsinization, washed with cold PBS and spun down at 1,500 rpm for 5 minutes. After discarding the supernatant, cells were resuspended gently in 1X PBS, leaving approximately 50 μL of 1X PBS per 1×10^6 cells. Cells were then fixed in freshly prepared, ice-cold 70% ethanol for at least 3 hours (can be stored at –20°C for 2-3 months). A 200 μL ethanol-fixed cell suspension, concentration ranging from 5×10^5 to 1×10^6 cells/mL, was centrifuged at 300 g for 5 minutes, and the supernatant was removed, and the cell pellet was resuspended in 0.25 μL 1X PBS. A 200 μL of Muse Cell Cycle reagent was then added to the cell suspension. The sample was incubated in the dark at room temperature for 30 minutes and analyzed on Muse cell analyzers (Merk Millipore Co., Darmstadt, Germany).

4.3.4 Apoptosis analysis by Annexin V/7AAD staining and flow cytometry

Apoptotic cell death was assessed using MuseTM Annexin V and Dead Cell kit (Cytek Bioscience, San Diego, CA) following the manufacturer's protocols. Briefly, cells were suspended and adjusted to a concentration of 1×10^6 cells/ml in binding buffer. A 90 µL Muse Annexin V & cell death reagent was added to a tube containing 90 µL of the cell suspension. The cell suspension was then incubated at room temperature for 20 minutes before detection and analysis on the Muse cell analyzer (Merk Millipore Co., Darmstadt, Germany). Survival cells were annexin $V^-/7AAD^-$ cells, whereas apoptotic cells included early ($annexin^+/7\text{-}AAD^-$) and late ($annexin^+/7\text{-}AAD^+$) populations.

4.3.5 Detection of cellular senescence by SA-β-Galactosidase staining

Cellular senescence was detected using the Senescence Detection kit (Abcam, Cambridge, UK) according to the manufacturer's protocol. The 20X X-Gal stock solution was prepared (**Table 4.2**) and stored in a polypropylene container at –20°C, protected from light. A staining mix was freshly prepared by combining 235 µL of the staining solution and 2.5 µL of the staining supplement. Then, 12.5 µL of the 20 mg/mL X-gal stock solution in DMSO was added to the staining mix. Cells were seeded at a density of 2.5×10^5 cells and incubated overnight. After washing with 1X PBS, the cells were exposed to the designated treatments and incubated at 37°C in a 5% CO_2 atmosphere for the indicated times. Treated cells were washed once with 1X PBS and then fixed with the fixative solution (**Table 4.2**). They were incubated in the fixative for 15 minutes at room temperature to ensure thorough fixation. Following fixation, the cells were washed twice with 500 µL of 1X PBS to eliminate excess fixative. To visualize the cellular response, 250 µL of a prepared staining solution mix was carefully added to each well. The plate was then covered to prevent evaporation and placed in a zip-lock bag to minimize CO_2 exposure. The plate was incubated overnight at 37°C to allow for optimal staining. After the incubation period, the cells were examined under an inverted light microscope (Nikon ECLIPSE Ts2, Tokyo, Japan) to detect blue coloration indicative of senescence.

4.3.6 Tumor necrosis factor receptor 1 detection by immunofluorescent staining and flow cytometry

Cells suspension in human staining buffer at a concentration of 1-3×10^6 cells/mL was spun down, and cells were fixed in 4% PFA (**Table 4.2**) for 10-15 minutes at room temperature, then washed with 1X PBS and resuspended in human staining buffer. For staining, 50 µL of the cell suspension (1-5×10^6 cells/mL) was transferred into round-bottom polystyrene FACS tubes. The cells were labeled with 10 µL of PE-conjugated anti-human TNFRI/TNFRSF1A antibody per reaction (**Table 4.3**) and incubated on ice for 30 minutes in the dark. After incubation, the labeled cells were washed with staining buffer and 1X PBS, then resuspended in 1% PFA (**Table 4.2**). Samples were mixed immediately prior to analysis. Flow cytometric acquisition was performed using a BD FACS Lyric system (BD Biosciences, CA, USA). Background fluorescence was defined and subtracted using isotype-matched control antibodies, PE-conjugated mouse IgG1 (**Table 4.3**). Receptor expression was evaluated as the percentage of positive cells. Data analysis and population gating were conducted using FlowJo™ software Version 10.8.1 (BD Biosciences, USA).

4.4 Protein detection by Western blot analysis

4.4.1 Lysate preparation and protein quantitation

Approximately 1 × 10^6 cells were lysed in 400 µL freshly prepared lysis buffer supplemented with 1X protease inhibitor cocktail (PI), 2 mM sodium orthovanadate (Na_3VO_4), 10 mM sodium fluoride (NaF), 2 mM phenylmethylsulphonyl fluoride (PMSF), and phosphatase inhibitor cocktails 2 and 3 (**Table 4.1** and **Table 4.2**) and incubated on ice for 20 to 30 minutes. Following incubation, if the cells are adhesive, a gentle scraping technique may be used to detach them from the surface and the solution was centrifuged at 14,000 rpm for 15 minutes to remove insoluble material. The supernatants were then carefully transferred to fresh microtubes. Total protein in cell lysates was measured by BCA protein assay kit (Novagen®, EMD Millipore Corp, MA, USA) as recommended by the manufacturer. Briefly, BSA standard, ranging from 20 to 2000 µg/mL, was used to generate a standard curve. Ten microliters of either BSA standard or protein sample were added to 100 µL of BCA working reagent in a 96-well

plate. The plate was covered and shaken for 30 seconds. Then, the reaction was incubated at 37°C for 30 minutes or at room temperature for 2-16 hours. After cooling to room temperature, the samples were measured at 570 nm using a microplate reader (BioTek Instrument, USA). Protein concentration was determined, and samples were adjusted with lysis buffer to normalize total protein content, yielding 40-50 µg per sample.

4.4.2 Protein separation by sodium dodecyl sulfate–polyacrylamide gel electrophoresis (SDS-PAGE)

Discontinuous polyacrylamide gels consisting of 4% stacking gel and 15% resolving gel compartments (**Table 4.1** and **Table 4.2**) were prepared using a standard casting apparatus (Biorad, USA). The gel was placed into the electrophoresis chamber (Biorad, USA). Approximately 40-50 µg of samples and 0.2-0.4 µg/µL Western blot protein markers (Genedirex, Inc) were loaded into each 3 µL per 1.0 mm gel pore well. After loading, the chamber was connected to the power supply, and a constant voltage of 170V or 200V was applied for 60 minutes or until the ion front reached the bottom of the gels. Immobilon-P PVDF membrane (Millipore, Sigma, USA), with a pore size of 0.2 µm and dimensions of 9 × 6 cm, was activated in methanol for 15 to 30 minutes, followed by thorough rinsing with distilled water (DW) and stored in a transfer buffer (**Table 4.2**). Following SDS-PAGE, proteins were transferred onto PVDF membranes using a wet-transfer system in 1X transfer buffer (**Table 4.2**). The transfer proceeded at a constant voltage of 90V for 90 minutes in a refrigerated environment.

4.4.3 Western blotting

Membranes were immunoprobed with specific antibodies to detect the protein of interest. The membranes were first blocked in a 5% non-fat dry milk solution (Pacific Science, USA) for at least 1 hour at room temperature or incubated overnight at 4°C with gentle shaking. Then, the membranes were briefly washed three times with TBST (Tris-buffered saline with 0.1% Tween-20) for 15 minutes (**Table 4.2**). To verify protein transfer, gels were stained overnight with Coomassie blue (Thermo Scientific, USA) and subsequently destained with water. The membrane was incubated with a primary antibody (**Table 4.3**) targeting apoptosis marker caspase-3 (1:500, Santa Cruz Biotechnology), cell cycle marker for p21 (1:1,000, Cell Signaling Technology), cyclin A2 (1:3,000, Protein Tech), cyclin D1 (1:2,000, Protein Tech), and GAPDH (1:50,000, Protein Tech). All antibodies were diluted in 5% non-fat dry milk blocking solution and incubated at 4°C with gentle shaking overnight. Following primary antibody incubation, the membrane was washed three times briefly with TBST for 15 minutes each to remove unbound protein. After an incubation period, the membrane was probed with a secondary antibody (**Table 4.4**), including goat anti-rabbit (1:10,000, Santa Cruz Biotechnology) and anti-mouse IgG, HRP-linked antibody (1:10,000, Cell Signaling Technology) in 5% non-fat dry milk blocking solution with gentle shaking for 1 hour at room temperature. The membrane was then washed 3 times with TBST for 15 minutes each to remove excess secondary antibodies. Substrate reagents A and B (1:1 dilution) were freshly prepared and added to the membrane for detection. The membrane was incubated in the dark for 5 minutes to allow the reaction to develop. Finally, the membrane was exposed to X-ray film (Smart Science, TH) to detect chemiluminescent signals. Semi-quantitative analysis of the target proteins was performed using densitometry, and the results were normalized to GAPDH and presented as.

4.5 Proteomic methodology: Sample preparation, liquid chromatography-tandem mass spectrometry and label-free quantification

Proteomic analysis was performed on cell lysates obtained from the CHX and/or TNF-α treatment at various time points (**Figure 4.1**). Cell lysates were prepared for label-free liquid chromatography-tandem mass spectrometry (LC-MS/MS) analysis. Briefly, cell pellets collected following the designed treatments and time points were suspended in 250 µL of RIPA buffer supplemented with 1X protease inhibitor cocktail (PI), 2 mM sodium orthovanadate (Na_3VO_4), 10 mM sodium fluoride (NaF), 2 mM phenylmethylsulphonyl fluoride (PMSF), and phosphatase inhibitor cocktails 2 and 3. Cell lysates were further processed at the National Center for Genetic Engineering and Biotechnology (BIOTEC), Thailand. Lysate samples were measured for protein concentration using the Lowry method, with BSA as the standard [94]. Protein samples were then subjected to in-solution digestion. Initially, the frozen protein mixture was diluted with 10 mM ammonium bicarbonate (AMBIC) and disulfide bonds in the protein were reduced by dithiothreitol (DTT) at a final concentration of 5 mM in 10 mM AMBIC, followed by incubation at 60°C for 1 hour. The alkylation was performed with 15 mM iodoacetamide (IAA) in 10 mM AMBIC. All lysates were incubated at room temperature in the dark for 45 minutes. Subsequently, the samples were digested with porcine trypsin at an enzyme-to-protein ratio of 1:20. The digestion was carried out at 37°C for 16 hours. Following digestion, the peptide mixtures were extracted, purified, and stored at –80°C, before nano-liquid chromatography tandem mass spectrometry (nano-LC-MS/MS) analysis.

Each sample was mixed with 0.1% formic acid before loading into the Ultimate 3000 Nano/Capillary LC System (Thermo Scientific, UK). This system connects to a ZenoTOF 7600 mass spectrometer (SCIEX). The peptides were then separated using a nano analytical column (75 µm i.d. × 15 cm, Acclaim PepMap RSLC C18, 2 µm, 100 Å, nanoViper; Thermo Scientific, UK). For chromatographic separation, C18 reverse-phase chromatography was employed and maintained at 60°C for optimal stationary phase (SP) performance. The mobile phase (MP) consisted of solvent A, 0.1% formic acid in water, and solvent B, 0.1% formic acid in 80% acetonitrile. A gradient elution from 5% to 55% solvent B was applied over 30

minutes at a constant flow rate of 0.30 µL/min. Ionization was achieved using CaptiveSpray electrospray ionization (ESI) with an electric field of 3300V. The ionized peptides were introduced into the mass spectrometer's ion analyzer, and the results were displayed as mass chromatograms, indicating peptide features specific to each sample condition. The acquired data were represented as mass-to-charge ratio (m/z) and relative intensity within the m/z range of 350-1800. Each sample group was analyzed in triplicate to ensure reproducibility.

Protein identification and label-free quantification were carried out using MaxQuant software Version 2.1.4.0 (Max-Planck Institute for Biochemistry), which employs the Andromeda search engine to align MS/MS spectra against the Uniprot *Homo sapiens* database (http://www.uniprot.org/). A label-free quantification (LFQ) strategy was adopted throughout the analysis pipeline. Database searches were performed using the digestion enzyme, with a maximum of two missed cleavage permitted. An initial precursor mass tolerance of 0.6 Da was set for the preliminary database search. Cysteine carbamidomethylation was designated as a static modification, while methionine oxidation and N-terminal acetylation of protein were considered dynamic modifications. Additionally, only peptides comprising a minimum of seven amino acid residues were retained as part of the search filtering criteria. Protein identification was accepted only when supported by a minimum of two peptides, at least one of which was unique to the protein sequence. Data quality and reliability were ensured by applying a 1% false discovery rate (FDR) threshold at both the peptide-spectrum match and protein levels, using a target-decoy strategy based on reversed protein sequences. Both known contaminant sequences and the *H. sapiens* proteome FASTA file were incorporated into the MaxQuant search database during spectral processing.

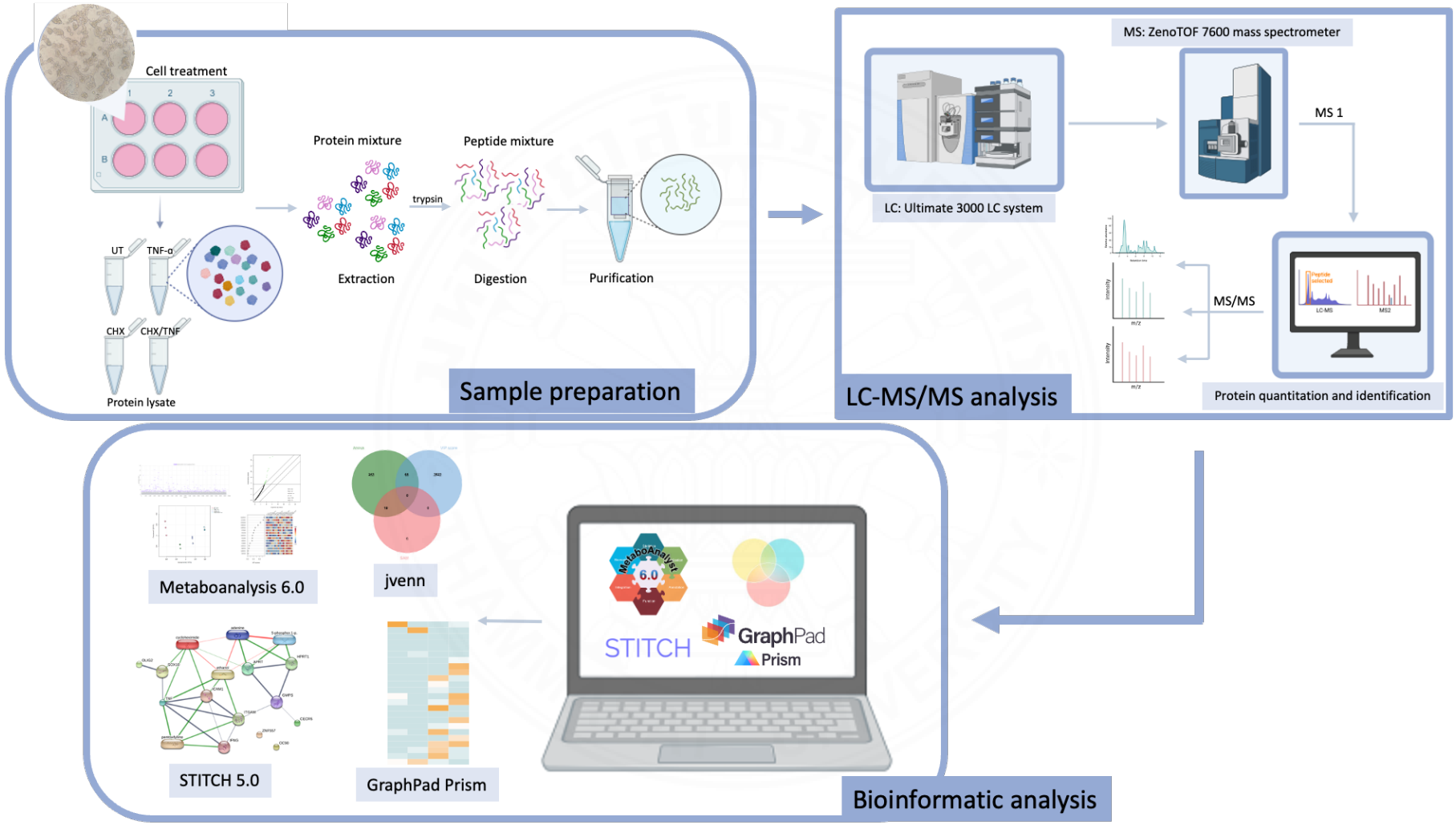

Figure 4.1 Proteomic workflow

4.6 Data processing and bioinformatics analysis

The MaxQuant ProteinGroups.txt file was loaded into Perseus software version 1.6.6.0 (https://maxquant.org/).[95] Then, any potential contaminants that could not be matched to proteins in Universal Proteomics Standard Set 1 (UPS1) were excluded from the analysis. Mass intensity values underwent $\log_2$ transformation prior to conducting pairwise comparisons via unpaired t-tests. Perseus software was used to substitute missing values with a constant value (0) through imputation. Bioinformatics tools were used to analyze protein expression profiles obtained by LC-MS/MS.

The web-based platform MetaboAnalyst 6.0 was used to analyze the data through built-in statistical tools (http://metaboanalyst.ca/)[96] Proteins with significant differential expression across groups were identified using one-way Analysis of Variance (ANOVA), with *p-values* and a false discovery rate (FDR) < 0.05 as the significant threshold. To evaluate sample grouping and determine variable contributions, partial least squares-discriminant analysis (PLS-DA) was performed using the One-Factor Analysis module (at 95% confidence region), with Variable Influence on the Projection (VIP) scores. Additionally, to identify key differentially expressed proteins, Significant Analysis of Microarray (SAM) was applied using the modified t-statistic d-score, formulated as $d(i) = \frac{\bar{x}_{i,2} - \bar{x}_{i,1}}{s_i + s_0}$; d(i), difference in group means for metabolite i; s_i, pooled standard deviation for metabolite i; s_0, a small constant "fudge factor" added to stabilize variance. These three approaches were conducted to select key candidate proteins for further analysis with jVenn web application (https://jvenn.toulouse.inrae.fr/). The Venn diagram displays three protein groups: the first includes proteins uniquely expressed in each group; the second comprises proteins common between groups; and the third shows all proteins expressed across all groups. A heatmap was generated in GraphPad Prism 9.5.1 (GraphPad Software, LLC.)[97] to visualize the patterns of differentially expressed proteins across various experimental conditions and time points. This method offers an intuitive overview of expression trends, enabling rapid identification of protein clusters with similar profiles.

The STITCH Version 5.0 web platform (Search Tool for Interacting Chemicals) was used to generate protein-protein interaction networks and assess their biological significance (http://stitch.embl.de/). Lists of candidate proteins were analyzed using the *Homo sapiens* STITCH database. Protein-protein interaction networks were generated with the interaction confidence score at a medium level (0.400). Edges connecting nodes (proteins or chemicals) were weighted according to the type and strength of confidence; edge line thickness indicates the strength of data support, including experimental confidence, co-expression, co-occurrence, text mining, database annotations, neighborhood, gene fusion and predictions. The maximum number of interactors to display is over 20. Additionally, biological characterization of candidate proteins was conducted using STITCH and Uniprot (http://www.uniprot.org/).

4.7 Statistical analysis

Statistical analysis was performed in GraphPad Prism 9.5.1 (GraphPad Software, LLC.). A Student's unpaired t-test was used to compare the means of two independent groups. The statistical significance was set at $p < 0.05$, with results expressed as mean ± Standard Error of the Mean (SEM).

CHAPTER 5
RESULTS

5.1 Characterization of a human hepatoma HepG2 cell line in response to the inflammatory cytokine TNF-α

5.1.1 HepG2 cell culture and treatment

In this study, the human hepatoma cell line HepG2 was used as a model for human hepatocytes. HepG2 cells were cultured and maintained in DMEM-low glucose and supplemented with 10% (v/v) inactivated fetal bovine serum (FBS), 1M HEPES, and 1% penicillin/streptomycin. HepG2 cells were subpassaged according to the following protocol. The cells were washed with 1x PBS (pH 7.4), then trypsinized with 0.25% (w/v) trypsin-EDTA solution, and the enzymatic reaction was stopped by adding complete medium. The cells were resuspended, transferred to a new flask, and further cultured at 37 °C and 5% CO_2.

An *in vitro* model of hepatic cell death and senescence was established using HepG2 cells induced by TNF-α and cycloheximide (CHX). Cells were treated with TNF-α, CHX, or co-treated with CHX/TNF-α at various concentrations and time points to optimize the treatment conditions. The treated cultures were then assessed for cellular characteristics, including cell viability, cell growth, cell cycle and apoptosis, as described in this section.

5.1.2 Effect of TNF-α treatment on cell viability of HepG2 cells

To examine the effect of TNF-α treatment on HepG2 cell viability, cells were cultured in the culture medium without FBS (untreated culture) and with the medium containing various concentrations of TNF-α, 20, 100 and 500 ng/mL at specific time points, 1, 3, 6, 24, 48, 72 and 120 hours. Cell viability of treated cells relative to untreated cells was determined using 3-(4,5-dimethylthaizol-2-yl)-2,5-diphenylterazolium bromide (MTT) assay (**Figure 5.1**). Within 24 hours of TNF-α exposure, 20, 100 ng/mL TNF-α did not affect HepG2 cell viability at 1, 3, and 6 hours, whereas the higher concentration of 500 ng/mL significantly reduced cell viability at 3, 6 and 24 hours (all $p < 0.0001$). However, by 24 hours of exposure, the percentage of cell viability reduction in 20, 100 and 500 ng/mL TNF-α cultures was 6.8%, 10.7% and 21.2%, respectively. At 48 hours, TNF-α at 20 and 100 ng/mL did not exhibit any significant effect on HepG2 cells, whereas the 500 ng/mL concentration continued to reduce cell viability by approximately 16.7% ($p < 0.0001$). With longer exposure, cell viability in 20 and 100 ng/mL TNF-α-treated cultures decreased significantly by 19.6% and 20.5% ($p < 0.001$ and $p < 0.01$, respectively) at 72 hours and by 23.8% and 44.2% (all $p < 0.0001$) at 120 hours. These results demonstrate that increasing TNF-α concentrations and exposure time led to a significant reduction in HepG2 cell viability, indicating dose- and time-dependent effects. However, high percentages of reduction with the low doses, 20 and 100 ng/mL TNF-α were observed following prolonged exposure for 72 to 120 hours.

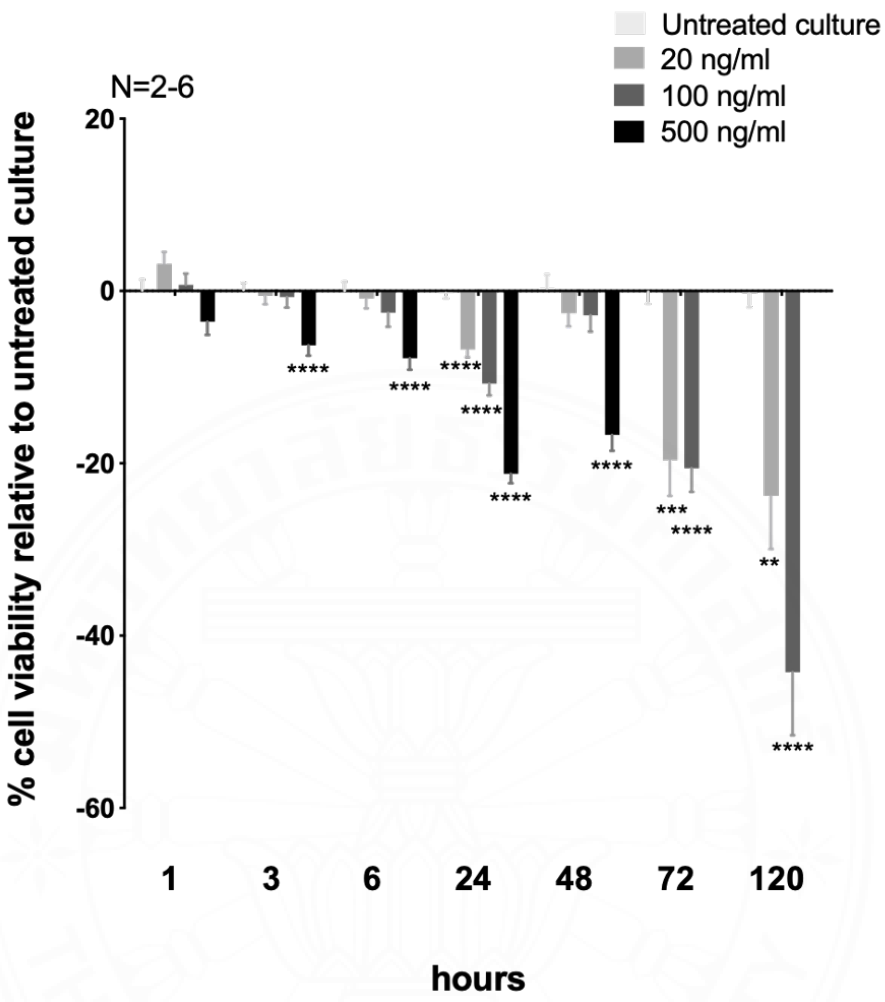

Figure 5.1 Effect of TNF-α treatment on cell viability of HepG2 cells assessed by MTT assay. The percentages of cell viability relative to untreated control were evaluated in the TNF-α-treated cultures at concentrations of 20, 100 and 500 ng/mL for 1, 3, 6, 24, 48, 72 and 120 hours. **, $p < 0.01$, ***, $p < 0.001$ and ****, $p < 0.0001$.

5.1.3 Effect of CHX treatment on cell viability of HepG2 cells

To examine the effect of CHX treatment on HepG2 cell viability, cells were either left untreated (control culture) or cultured in medium supplemented with CHX at concentrations of 12.5, 25, 50 and 100 μM for 3, 6, 12 and 24 hours. Cell viability of the treated cells was assessed by MTT assay. **Figure 5.2** demonstrates that CHX treatment at all concentrations and time points significantly decreased HepG2 cell viability compared with the untreated control culture ($p < 0.0001$). The highest reductions were observed at 24 hours in the cultures with 12.5, 25, 50 and 100 μM CHX treatment by 21.8%, 27.3 %, 29.8%, 34.5%, respectively. Overall, the results indicate that CHX reduced HepG2 cell viability in a dose- and time-dependent manner.

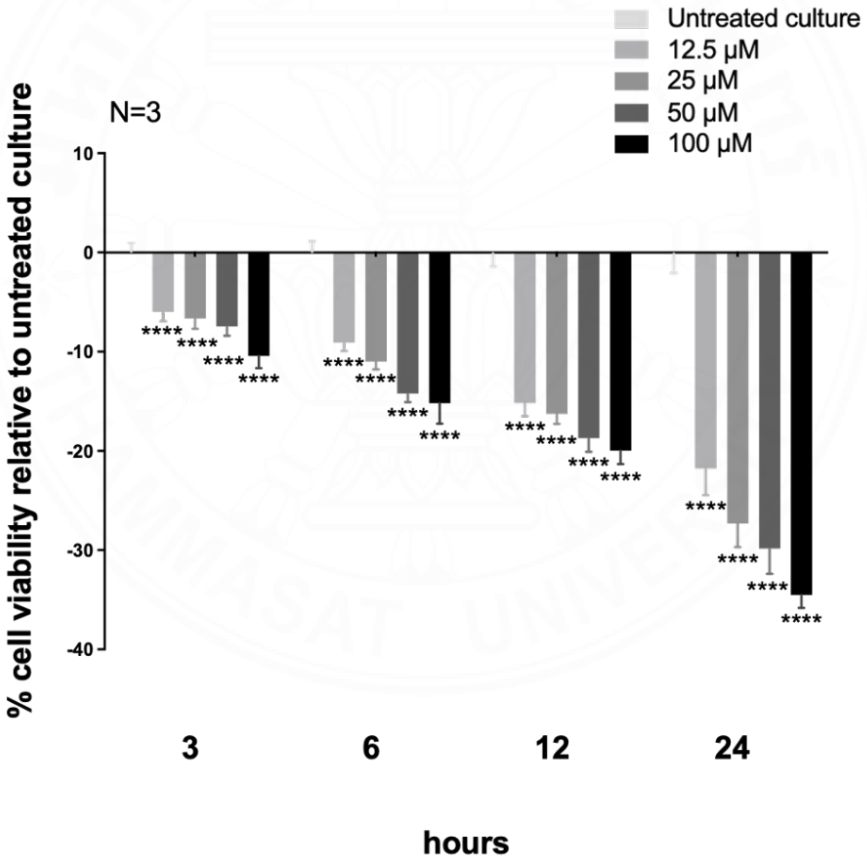

Figure. 5.2 Effect of CHX treatment on cell viability of HepG2 cells assessed by MTT assay. The percentages of cell viability relative to untreated culture were evaluated in the CHX-treated cultures at concentrations of 12.5, 25, 50 and 100 μM for 3, 6, 12 and 24 hours. ****, $p < 0.0001$.

5.1.4 Effect of TNF-α alone and CHX/TNF-α co-treatment on cell viability of HepG2 cells

Several previous studies have shown that CHX enhances TNF-α-mediated hepatic cell death.[9] Based on the results showing the optimal reduction in cell viability with 20 or 100 ng/mL TNF-α or 25 or 50 μM CHX at 24 hours, the CHX/TNF-α co-treatment was applied to HepG2 cells, and their viability was assessed by MTT assay at 24 hours of culture. Cells were left untreated (control culture) or treated with CHX (25 or 50 μM), TNF-α (20 or 100 ng/mL), or their respective combinations (25 μM CHX with 20 ng/mL TNF-α, and 50 μM CHX with 100 ng/mL TNF-α) for 24 hours. **Figure 5.3A** and **5.3B** show the reduction in OD values and their respective percentages relative to untreated controls, comparing the cultures co-treated with combined CHX and TNF-α to individual treatments with CHX and TNF-α. Compared with the untreated control, cell viability of cultures treated with 20 or 100 ng/mL TNF-α was significantly reduced by 5.8% ($p < 0.01$) and 5.8% ($p < 0.001$), respectively. Compared with a single treatment of 25 μM CHX, the culture co-treated with 100 ng/mL TNF-α exhibited a 35.3% reduction of cell viability ($p < 0.01$). Similarly, compared with a single treatment of 50 μM CHX, those treated with combinations of 50 μM CHX and either 20 or 100 ng/mL TNF-α showed 36.3% and 38.4% reductions in cell viability ($p < 0.01$ and $p < 0.001$, respectively). Overall, these results indicated a modest but significant effect of TNF-α alone and the additive effects of co-treatment with CHX at the concentrations tested over 24 hours.

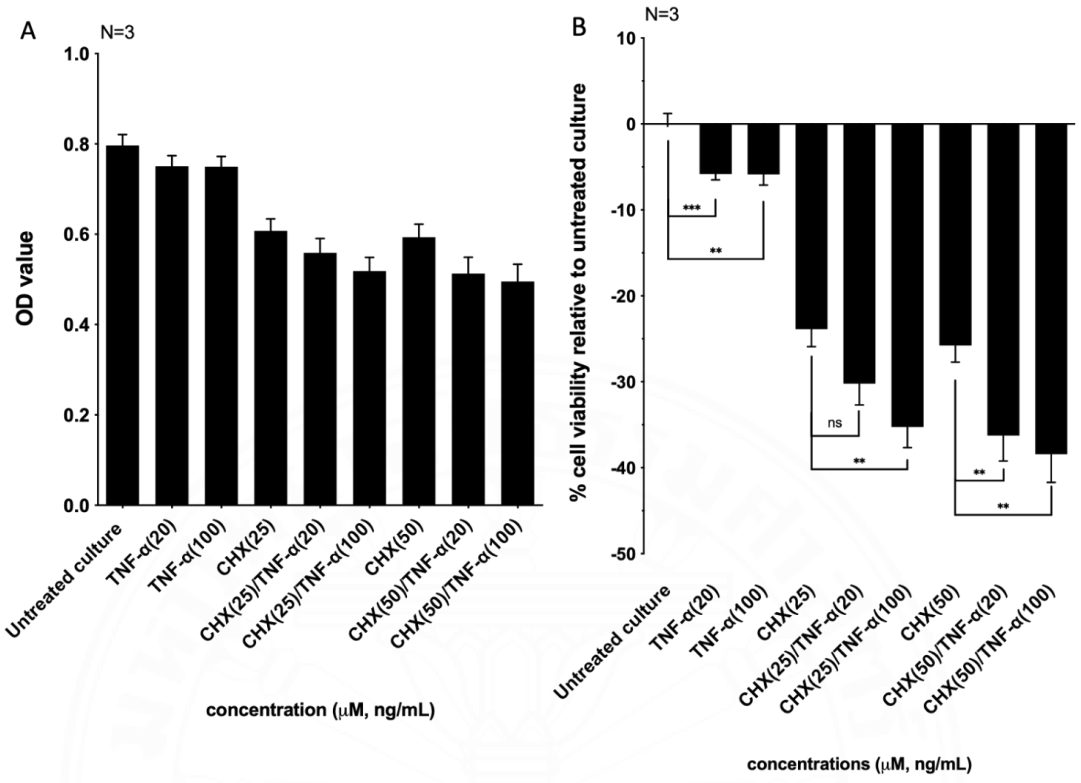

Figure 5.3 Effect of CHX/TNF-α co-treatment on cell viability of HepG2 cells at 24 hours of culture, assessed by MTT assay. (**A**) OD values from MTT assay for the untreated controls and cultures treated with 20 ng/mL TNF-α, 100 ng/mL TNF-α, 25 μM CHX, 25 μM CHX/20 ng/mL TNF-α, 25 μM CHX/100 ng/mL TNF-α, 50 μM CHX, 50 μM CHX/20 ng/mL TNF-α and 50 μM CHX/100 ng/mL TNF-α. (**B**) Cell viability in the treatment groups is expressed as a percentage relative to the untreated control. **, $p < 0.01$, ***, $p < 0.001$.

5.1.5 Morphological changes of HepG2 cells following TNF-α/CHX co-treatment

To assess morphological alterations in HepG2 cells treated with 100 ng/mL TNF-α and/or 50 μM CHX across different time points, cells were examined under a light microscope at 10x magnification (**Figure 5.4**). At 1 hour, HepG2 cells treated with 100 ng/mL TNF-α, 50 μM CHX, or their combination showed no discernible morphological changes compared with the untreated control culture. Similarly, at 3 hours, cells treated with TNF-α or CHX alone exhibited a morphology comparable with that of the control, whereas the TNF-α/CHX co-treatment culture showed slight alterations in cellular appearance, including minor cell rounding and early signs of detachment, indicating the initiation of stress responses. Significant morphological alterations were observed in the co-treated cells at 6 and 18 hours. These cells exhibited definitive apoptotic characteristics, including shrinkage, cytoplasmic condensation, detachment from the substrate, and cellular fragmentation into apoptotic bodies. These changes were not evident in the untreated or single-treatment culture, thereby suggesting a potent cooperative effect of TNF-α and CHX in inducing cell death. The progressive increase in apoptotic features over time in the co-treated culture indicated that TNF-α/CHX co-treatment elicits a more potent apoptotic response than either agent alone. Collectively, the morphological observations suggest that TNF-α/CHX co-treatment induced time-dependent HepG2 cell death. The phenotypic data were consistent with the reduction in cell viability observed in the previous sections.

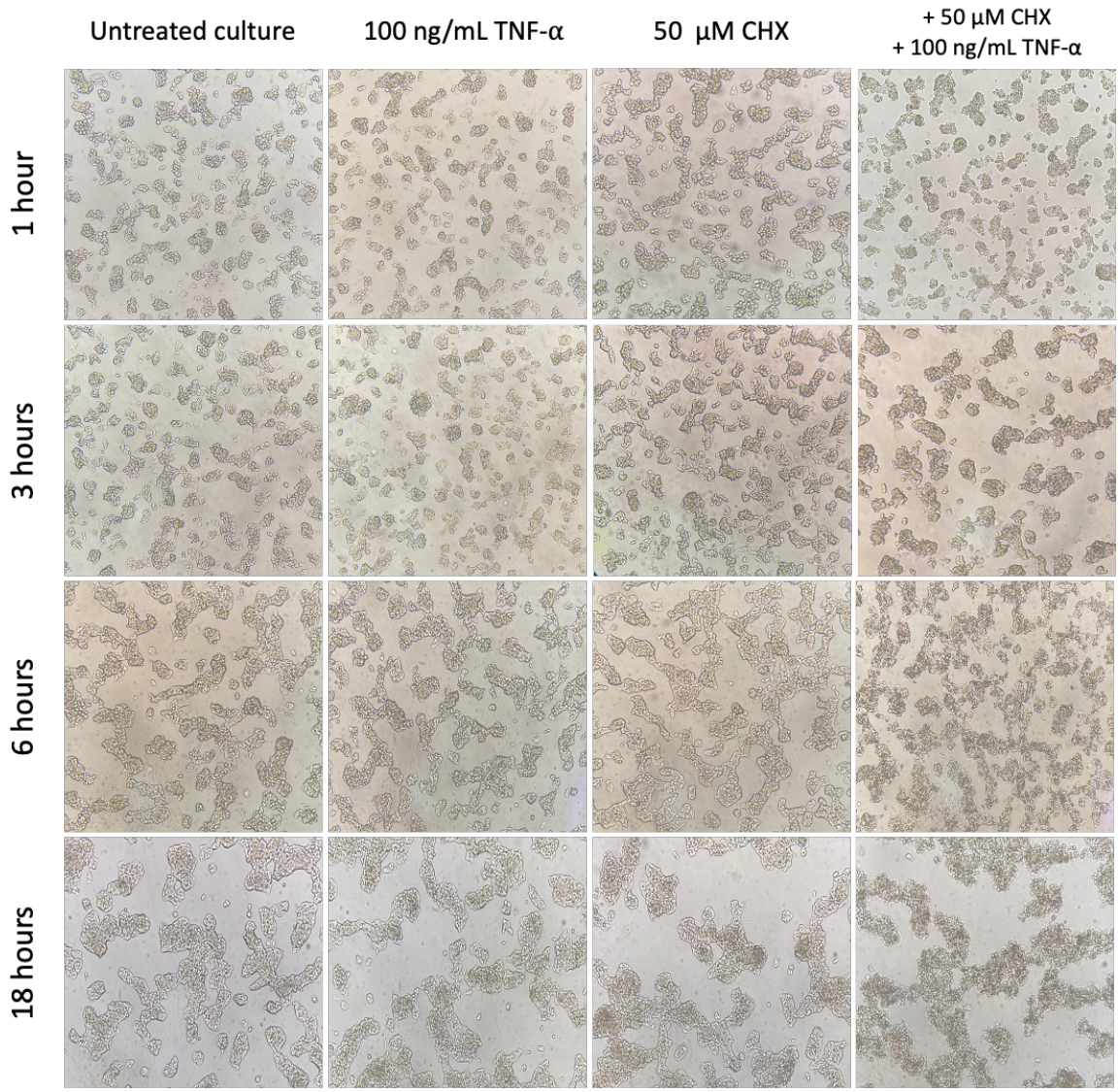

Figure 5.4 Morphological alterations of HepG2 cells under light microscopy at 10X magnification, following the exposure to 100 ng/mL TNF-α, 50 µM CHX, or their combination for 1, 3, 6 and 18 hours compared with the untreated control culture.

5.1.6 Effect of TNF-α alone and CHX/TNF-α co-treatment on HepG2 cell proliferation

To evaluate the proliferative ability of the CHX/TNF-α treated cells, HepG2 cells were either left untreated or treated with 20 or 100 ng/mL TNF-α, 50 μM CHX, or a co-treatment of 20 ng/mL TNF-α with 50 μM CHX for 24 hours (passage 0). **Figure 5.5A** shows viable cell numbers, assessed by trypan blue exclusion assay, in the untreated and treated HepG2 cell cultures across three consecutive subpassages. While cell populations in the untreated controls and cultures treated with TNF-α at 20 and 100 ng/mL steadily increased over three passages, the cultures co-treated with 50 μM CHX- and CHX/TNF-α remained relatively static, showing negligible growth. As shown in **Figure 5.5B**, neither 20 nor 100 ng/mL TNF-α had a significant effect on cell viability compared with the untreated controls throughout the three consecutive passages. In contrast, compared with untreated controls, exposure to 50 μM CHX significantly reduced cell counts during passages 2 and 3 (all $p < 0.05$), whereas the CHX/TNF-α co-treatment significantly reduced viable cell numbers across all three passages ($p < 0.05$ for passage 1 and 3; $p < 0.01$ for passage 2). The data indicated that TNF-α alone did not inhibit cell proliferation, whereas CHX or the co-treatment effectively did. Consequently, these findings suggest the potent capability of the CHX/TNF-α combination to restrict HepG2 cell population expansion.

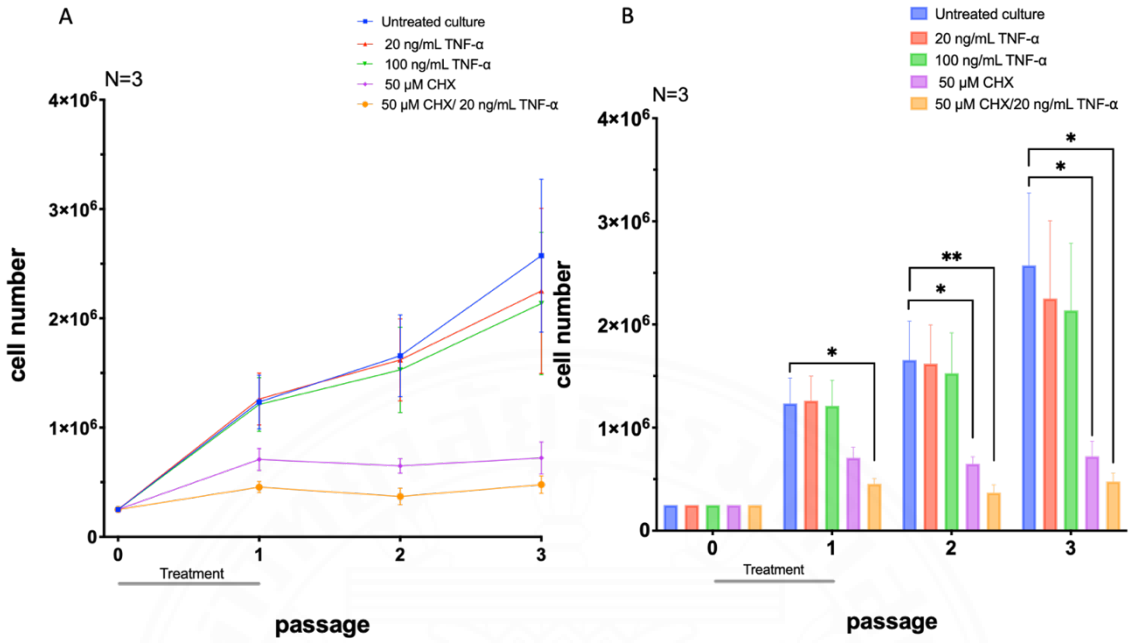

Figure 5.5 Effect of CHX/TNF-α treatment on the proliferative capacity of HepG2 cells, as assessed by a growth arrest assay. (**A**) and (**B**) The cell numbers for HepG2 cells treated with 20 or 100 ng/mL TNF-α, 50 μM CHX, and the co-treatment of 20 ng/mL TNF-α with 50 μM CHX were compared with the untreated culture across three consecutive passages, 1, 2, and 3. *, $p < 0.05$ and **, $p < 0.01$.

5.2 Effect of TNF-α alone and CHX/TNF-α co-treatment on the cell cycle of HepG2 cells

Characterization of CHX/TNF-α treated HepG2 cells was performed by cell-cycle analysis using DNA staining and flow cytometry. Cells were either left untreated or treated with 50 μM CHX, 100 ng/mL TNF-α or a combination of 50 μM CHX and 20 or 100 ng/mL TNF-α, for 24 hours. **Figure 5.6A-F** demonstrated that, compared with untreated culture, treatment with 100 ng/mL TNF-α alone did not alter cell numbers in each phase of the cell cycle. In contrast, compared with the untreated culture, treatment with 50 μM CHX showed a significantly higher percentage of cells in the S-phase (61.3%). Similar portions were observed in the co-treatment combining 50 μM CHX with 20 ng/mL TNF-α (59.7%) or with 100 ng/mL TNF-α (61.3%) ($p < 0.0001$) (**Figure 5.6F**). The data indicate that S-phase arrest in HepG2 cells was induced by either treating with CHX alone or with the CHX/TNF-α co-treatment, suggesting that the effect is driven solely by CHX rather than TNF-α.

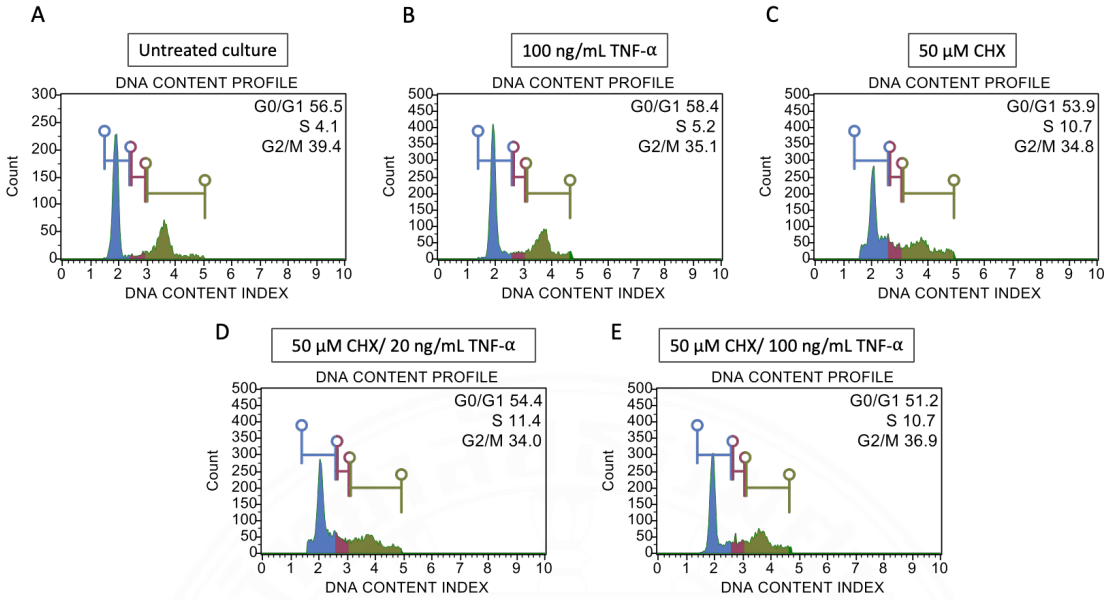
A
Untreated culture
DNA CONTENT PROFILE
G0/G1 56.5
S 4.1
G2/M 39.4
Count
DNA CONTENT INDEX
B
100 ng/mL TNF-α
DNA CONTENT PROFILE
G0/G1 58.4
S 5.2
G2/M 35.1
Count
DNA CONTENT INDEX
C
50 µM CHX
DNA CONTENT PROFILE
G0/G1 53.9
S 10.7
G2/M 34.8
Count
DNA CONTENT INDEX
D
50 µM CHX/ 20 ng/mL TNF-α
DNA CONTENT PROFILE
G0/G1 54.4
S 11.4
G2/M 34.0
Count
DNA CONTENT INDEX
E
50 µM CHX/ 100 ng/mL TNF-α
DNA CONTENT PROFILE
G0/G1 51.2
S 10.7
G2/M 36.9
Count
DNA CONTENT INDEX

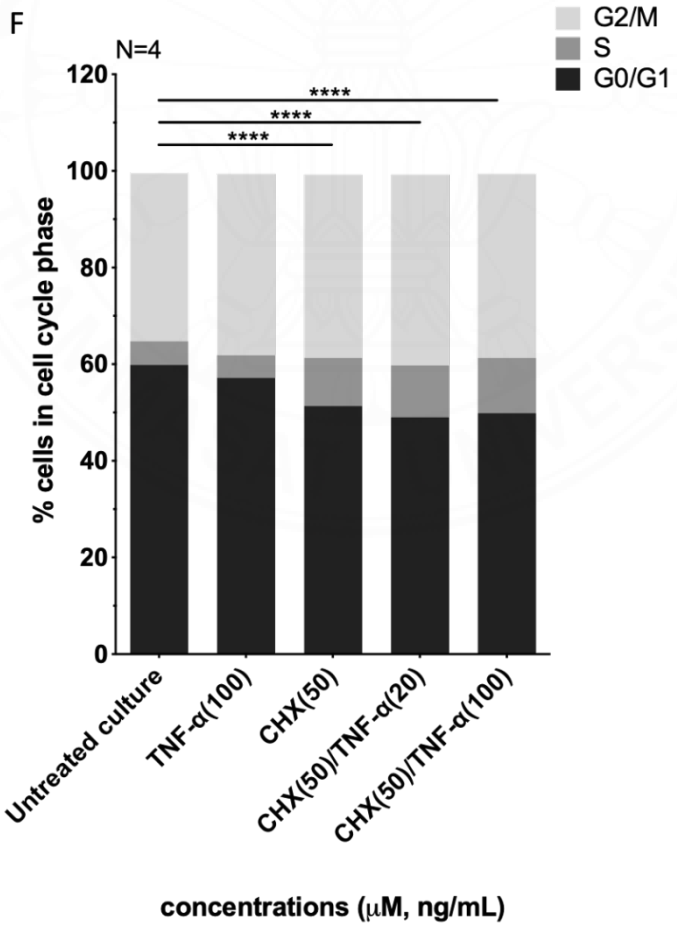
F
N=4
G2/M
S
G0/G1
****
****
****
% cells in cell cycle phase
Untreated culture
TNF-α(100)
CHX(50)
CHX(50)/TNF-α(20)
CHX(50)/TNF-α(100)
concentrations (µM, ng/mL)

Figure 5.6 Effect of CHX/TNF-α treatment on the cell cycle of HepG2 cells. Flow cytometric analysis demonstrates the distribution of cell numbers in each phase of the cell cycle in the untreated culture (**A**), and cultures with 100 ng/mL TNF-α (**B**), 50 μM CHX (**C**), and a combination of 50 μM CHX and 20 ng/mL (**D**) or 100 ng/mL TNF-α (**E**) at 24 hours. The percentages of cells distributed in each phase of the cell cycle in treatment and control cultures are also shown (**F**). ****, $p < 0.0001$

5.3 Effect of TNF-α alone and CHX/TNF-α co-treatment on apoptosis of HepG2 cells

Apoptotic cell death in the CHX/TNF-α-treated HepG2 cells was characterized by Annexin V-apoptosis assay. Cells were either left untreated or treated with 50 μM CHX, 100 ng/mL TNF-α, or a combination of 50 μM CHX and 20 or 100 ng/mL TNF-α for 24 hours. **Figure 5.7** showed that, compared with the control culture, cultures treated with TNF-α at the concentration of 100 ng/mL did not significantly present apoptotic cells. In contrast, treatment of the cells with 50 μM CHX resulted in a significantly higher percentage of apoptotic cells, by 9.2% ($p < 0.01$). Interestingly, the cultures co-treated with 50 μM CHX and 20 or 100 ng/mL TNF-α showed significantly higher percentages, up to 64.5% and 75.8 %, respectively ($p < 0.0001$) (**Figure 5.7F**). The results indicate that TNF-α alone did not induce apoptosis in HepG2 cells. In contrast, treatment with CHX, and its co-treatment with TNF-α exerted an enhanced apoptotic effect on the cell population.

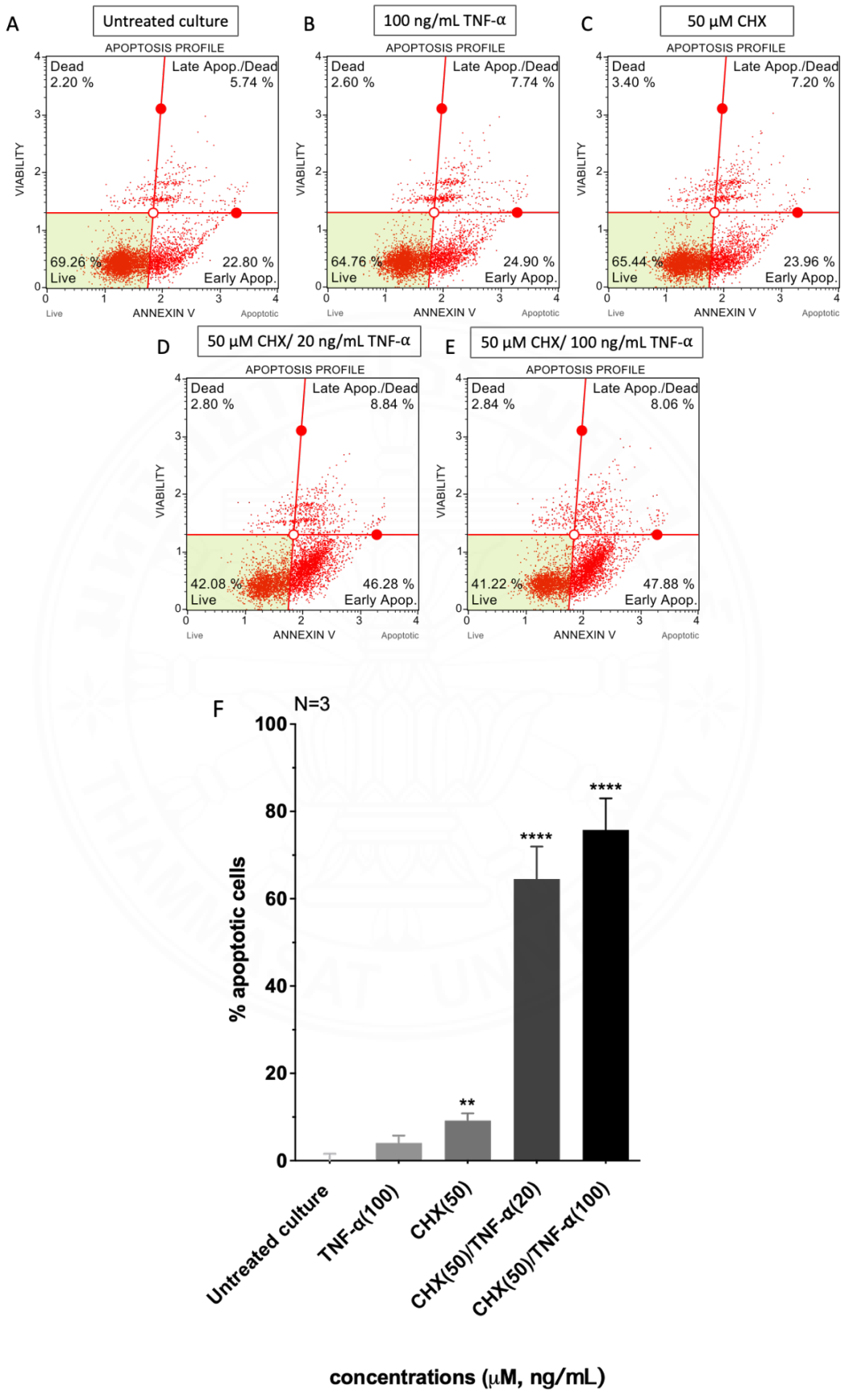
A
Untreated culture
APOPTOSIS PROFILE
Dead
2.20 %
Late Apop./Dead
5.74 %
69.26 %
Live
22.80 %
Early Apop.
VIABILITY
ANNEXIN V
Live
Apoptotic
B
100 ng/mL TNF-α
APOPTOSIS PROFILE
Dead
2.60 %
Late Apop./Dead
7.74 %
64.76 %
Live
24.90 %
Early Apop.
C
50 µM CHX
APOPTOSIS PROFILE
Dead
3.40 %
Late Apop./Dead
7.20 %
65.44 %
Live
23.96 %
Early Apop.
D
50 µM CHX/ 20 ng/mL TNF-α
APOPTOSIS PROFILE
Dead
2.80 %
Late Apop./Dead
8.84 %
42.08 %
Live
46.28 %
Early Apop.
E
50 µM CHX/ 100 ng/mL TNF-α
APOPTOSIS PROFILE
Dead
2.84 %
Late Apop./Dead
8.06 %
41.22 %
Live
47.88 %
Early Apop.
F
N=3
% apoptotic cells
**
****
****
Untreated culture
TNF-α(100)
CHX(50)
CHX(50)/TNF-α(20)
CHX(50)/TNF-α(100)
concentrations (µM, ng/mL)

Figure 5.7 Effect of CHX/TNF-α treatment on apoptosis of HepG2 cells determined by annexinV-7AAD staining and flow cytometry at 24 hours. Dot plot diagrams of apoptotic cells in the control culture without CHX/TNF-α treatment (**A**), and cultures with treatment of 100 ng/mL TNF-α (**B**), 50 μM CHX (**C**), and a combination of 50 μM CHX and 20 ng/mL TNF-α (**D**) or 100 ng/mL TNF-α (**E**) are demonstrated. (**F**) The bar graph illustrates the percentage of apoptotic cells in each treatment culture relative to the untreated control. **, $p < 0.01$ and ****, $p < 0.0001$

5.4 Effect of TNF-α alone and CHX/TNF-α co-treatment on the induction of cellular senescence in HepG2 cells

To determine how TNF-α/CHX treatment affects cellular senescence, cells were stained with SA-β-Galactosidase, which marks senescent cells blue, and observed under a microscope. As shown in **Figure 5.8**, exposure to TNF-α alone at concentrations of 20 or 100 ng/mL shows nearly no effect at the first hour of incubation, and no morphological alterations or SA-β-gal activity were observed compared with untreated controls. However, time-dependent progression toward senescence was observed with blue staining appearing at 3 and 6 hours and becoming much more intense by 18 and 24 hours, when most cells stained dark blue. In contrast, treatment with 50 μM CHX alone, and co-treatment with 20 or 100 ng/mL TNF-α revealed a rapid and complex phenotypic shift. At the early stages of exposure, 1, 3 and 6 hours, cells exhibited intense blue staining, indicating early induction of senescence. After 18-24 hours, the cells showed signs of structural distress, inducing cell shrinkage. Notably, the cells displayed apoptotic features, and the SA-β-gal blue staining was entirely absent. These findings indicate that TNF-α alone may induce cellular senescence, while the addition of CHX alters the cell morphology toward apoptosis. The data indicate that HepG2 cells first briefly enter a senescent state in response to the co-treatment, then progress to a time-dependent apoptotic pathway.

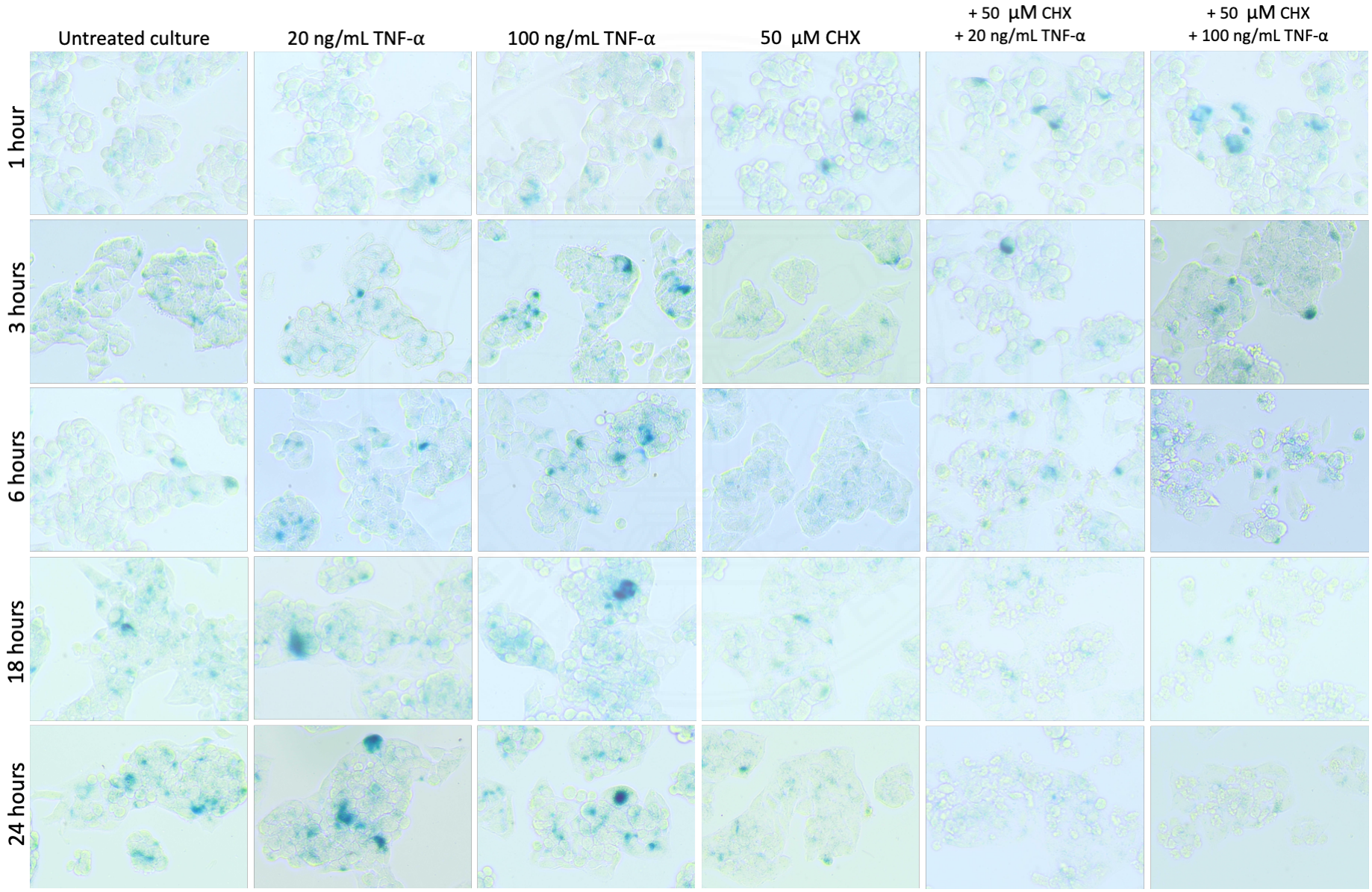
Untreated culture
20 ng/mL TNF-α
100 ng/mL TNF-α
50 µM CHX
+ 50 µM CHX
+ 20 ng/mL TNF-α
+ 50 µM CHX
+ 100 ng/mL TNF-α
1 hour
3 hours
6 hours
18 hours
24 hours

Figure 5.8 The induction of cellular senescence in HepG2 cells following TNF-α/CHX treatments. Cells were left untreated or treated with 20 or 100 ng/mL TNF-α, 50 μM CHX or a combination of 20 or 100 ng/mL TNF-α and 50 μM CHX at 1, 3, 6, 18 and 24 hours. Cellular senescence was evaluated using SA-β-Galactosidase staining and visualized under light microscopy (20X magnification).

5.5 Constitutive expression of tumor necrosis factor receptor 1 in HepG2 cells

To assess the potential for TNF-α-mediated apoptotic signaling in HepG2 cells, the cells were examined for constitutive cell-surface expression of the tumor necrosis factor receptor 1 (TNFR1) under baseline *in vitro* conditions using flow cytometric analysis. The MCF-7 breast cancer cell line, widely recognized for its high endogenous expression of TNFR1, was utilized as a reference control.[98, 99] As shown in **Figure 5.9A** and **B**, compared with isotype control, HepG2 cells expressed TNFR1 at 9.23%, whereas MCF-7 cells exhibited a higher expression level of 26.18%. The results confirmed the presence of TNFR1 on the HepG2 cell surface. Despite the low TNFR1 density in HepG2 cells, the cellular responses to exogenous TNF-α treatment are likely mediated through the TNFR1-dependent pathway

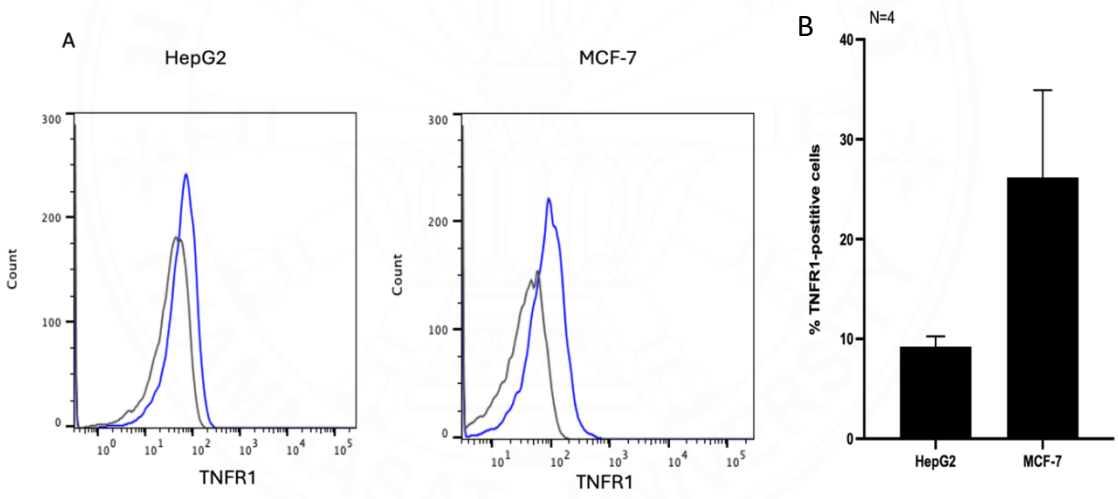

Figure 5.9 Surface expression of TNFR1 on HepG2 and MCF-7 cells. (**A**) Representative flow cytometric histograms showing TNFR1 expression (blue line) versus the isotype control (black line) in HepG2 and MCF-7 cells. (**B**) The bar graph shows the percentage of TNFR1-positive cells, summarized as mean ± SEM from four independent experiments.

5.6 Expression of apoptotic signaling markers in CHX/TNF-α-treated HepG2 cells

To analyze signaling pathways responsible for TNF-α/CHX-mediated HepG2 cell death, expression of key apoptotic markers, caspase-3 and poly (ADP-ribose) polymerase-1 (PARP-1), along with their cleaved isoforms, were examined in HepG2 cells, left untreated or treated with 100 ng/mL TNF-α, 50 μM CHX or their combination at 1, 3, 6, and 18 hours using Western blot analysis (**Figure 5.10**). After 1 hour of culture, their combination did not differ significantly from untreated control cells. Additionally, neither cleaved caspase-3 nor cleaved PARP-1 was detected (**Figure 5.10A** and **B**). However, at 3 hours, cleaved PARP-1 was detected only in the co-treatment cell lysate, although PARP-1 expression remained largely unchanged. Concurrently, procaspase-3 expression was not significantly reduced compared with the untreated control, whereas cleaved caspase-3 was detected in the co-treatment lysate (**Figure 5.10A** and **B**), indicating the induction of apoptotic signaling at this time point. At 6 hours, expression levels of procaspase-3 and PARP-1 were markedly diminished, while their cleaved forms were clearly expressed, consistent with the observations at 3 hours (**Figure 5.10A** and **B**). The results strongly indicated that CHX/TNF-α induced apoptosis in HepG2 cells via the caspase-PARP-1-dependent pathway. Further observation at 18 hours revealed a substantial reduction in PARP-1 alongside the presence of cleaved PARP-1. Notably, procaspase-3 was entirely absent, and no cleaved caspase-3 was detected (**Figure 5.10A** and **B**). The result suggested that procaspase-3 may have been fully degraded, indicating a late phase of cell death. Additionally, it is important to note that, at all-time points, single stimulation by TNF-α or CHX did not cause significant alteration in either the expression levels of procaspase-3 and PARP-1, or the presence of their cleaved forms. This leads to the conclusion that caspase-PARP-dependent apoptosis in HepG2 cells requires the combined effects of TNF-α and CHX rather than individual stimuli. In conclusion, TNF-α/CHX co-treatment induced apoptosis in HepG2 cells through time-dependent activation of caspase-3 and cleavage of PARP-1.

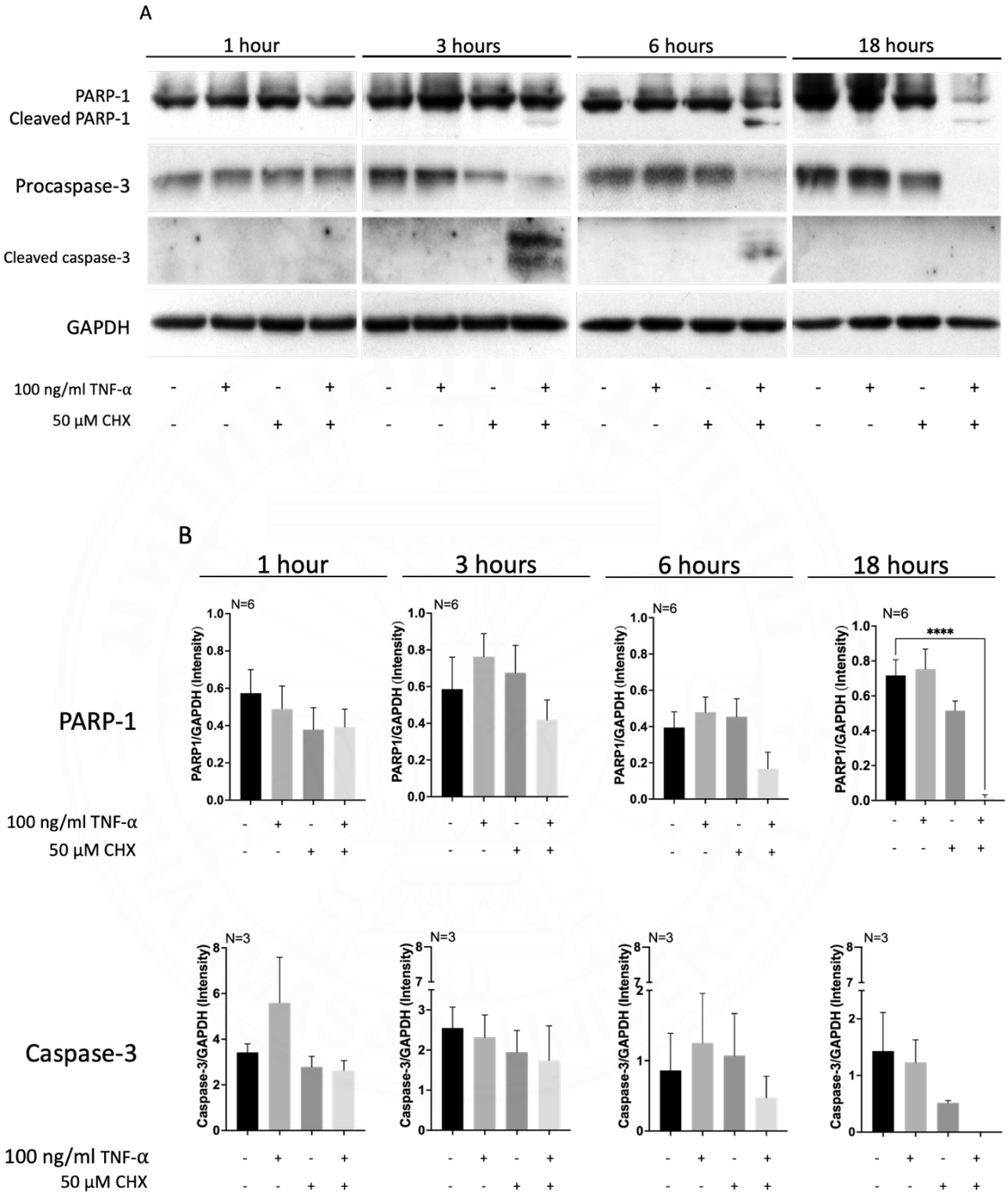

Figure 5.10 Western blot analysis of apoptosis-related markers induced by TNF-α and CHX in HepG2 cells. Cells were exposed to 100 ng/mL TNF-α, 50 μM CHX, or both for various time points. Cell lysates were assayed for total caspase-3, cleaved caspase-3, PARP-1 and cleaved PARP-1, with GAPDH serving as a loading control. (**A**) Representative immunoblots of these markers in 1, 3, 6 and 18 hours, respectively. (**B**) Semi-quantitative analysis of PARP-1 and procaspase-3 expression levels normalized to GAPDH. Data are presented as mean ± SEM from three independent experiments.
****, $p < 0.0001$

5.7 Expression of cell cycle regulatory proteins in CHX/TNF-α-treated HepG2 cells

To elucidate molecular mechanisms underlying S-phase arrest induced by CHX alone or CHX/TNF-α co-treatment, the expression of cell cycle regulatory proteins p21, cyclin A2, and cyclin D1 in HepG2 cells was analyzed by Western blot. Cells were either left untreated or treated with 100 ng/mL TNF-α, 50 μM CHX, or their combination for 1, 3, 6, and 18 hours (**Figure 5.11**). After 1 hour, p21 expression was slightly decreased in both CHX-treated and TNF-α/CHX co-treated cells, compared with untreated controls. Furthermore, exposure to either CHX or the CHX/TNF-α co-treatment for 3, 6, and 18 hours completely abolished p21 expression (**Figure 5.11A** and **B**) ($p < 0.001$, $p < 0.01$ and $p < 0.0001$, respectively, for CHX treatment and the co-treatment). In contrast, treatment with TNF-α alone did not alter p21 expression at all time points, compared with the untreated control, suggesting that the p21 expression was specifically attributable to CHX and its additive effect with TNF-α. Cyclin A2 expression in the treated cells remained unchanged compared with untreated controls, at all time points (**Figure 5.11A** and **B**). When normalized to GAPDH, cyclin A2 expression demonstrated a progressive, time-dependent decrease across all treatments from 1 to 18 hours, with the lowest levels at 18 hours. In contrast, cyclin D1 expression fluctuated over time in response to treatment with TNF-α, CHX, or their combination (**Figure 5.11A** and **B**). After 1 hour of culture, treatment with TNF-α and CHX slightly increased cyclin D1 expression, whereas co-treatment reduced its expression. By 3 hours, cyclin D1 was significantly suppressed in the co-treatment lysate compared with untreated controls. At 6 hours, cyclin D1 levels were equal across all four treatments. At 18 hours, single CHX treatment showed a secondary increase in cyclin D1 expression, while the co-treatment maintained the baseline levels. These results indicated that the dynamic alterations in these cell cycle regulatory proteins, including p21 abolition, downregulation of cyclin A2, and fluctuation of cyclin D1, may drive S-phase arrest and apoptosis caused by treatment with CHX or CHX/TNF-α co-treatment.

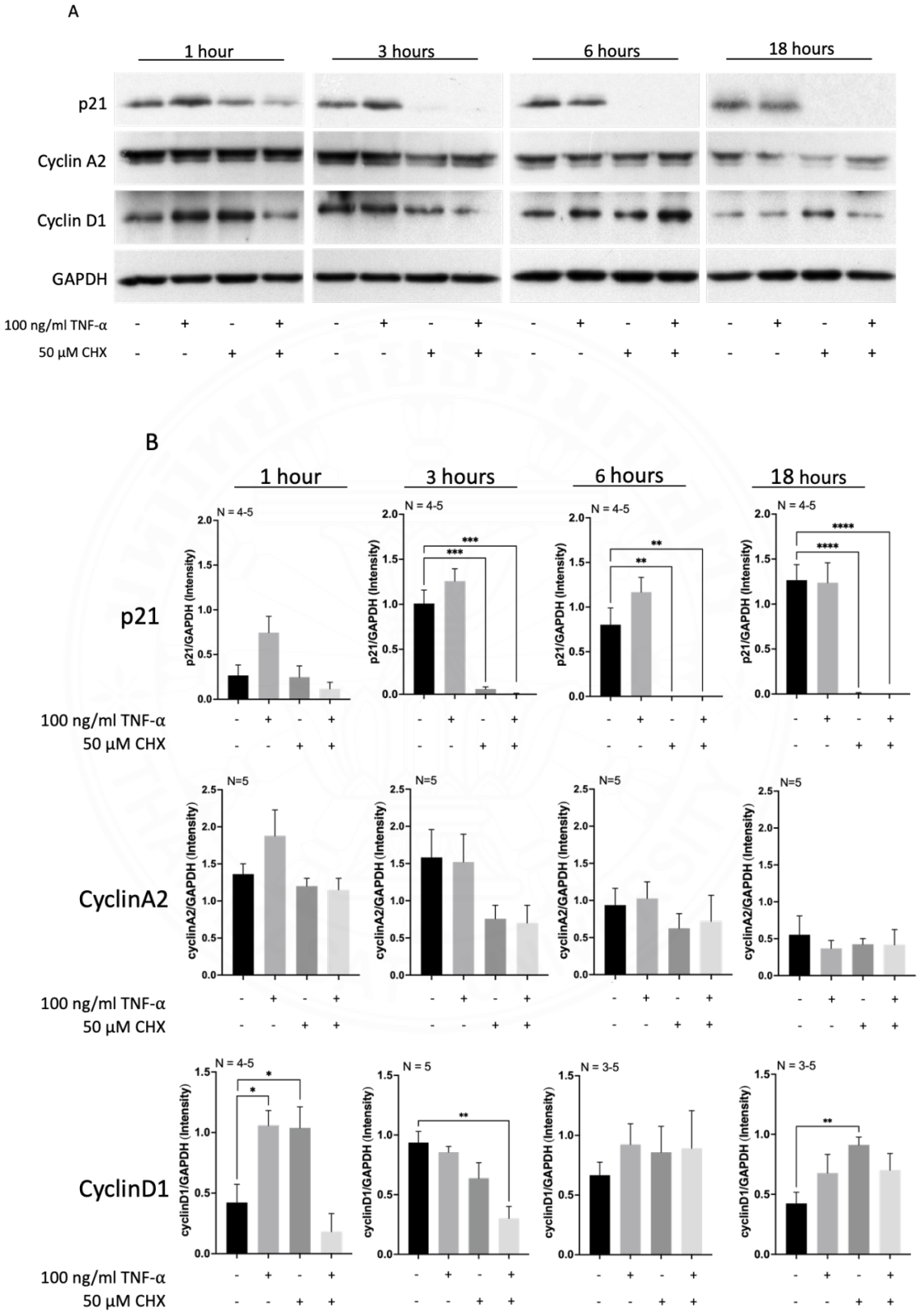
A
1 hour
3 hours
6 hours
18 hours
p21
Cyclin A2
Cyclin D1
GAPDH
100 ng/ml TNF-α
50 μM CHX
B
1 hour
3 hours
6 hours
18 hours
p21
p21/GAPDH (Intensity)
N = 4-5
CyclinA2
cyclinA2/GAPDH (Intensity)
N=5
CyclinD1
cyclinD1/GAPDH (Intensity)
N = 4-5
N = 5
N = 3-5
100 ng/ml TNF-α
50 μM CHX

Figure 5.11 Western blot analysis of cell cycle-related proteins in HepG2 cells following treatments in HepG2 cells. Cells were treated with 100 ng/mL TNF-α, 50 μM CHX, or both for various time points. Cell lysates were assayed for p21, cyclin A2, and cyclin D1, using GAPDH as an internal loading control. (**A**) Representative immunoblots of cell-cycle-associated proteins in 1, 3, 6 and 18 hours, respectively. (**B**) Semi-quantitative analysis of their expression levels normalized to GAPDH. Data are presented as mean ± SEM from three independent experiments. *, $p < 0.05$, **, $p < 0.01$ and ***, $p < 0.001$ ****, $p < 0.0001$

5.8 Proteomic profiling associated with CHX/TNF-α-mediated HepG2 cell death

Since the CHX/TNF-α co-treatment induced S-phase cell-cycle arrest and apoptotic cell death in HepG2 cells, proteomic analysis was performed to identify the molecular pathways associated with these cellular activities. Cell lysates from cultures left untreated or treated with 100 ng/mL TNF-α, 50 μM CHX, or their combination for 1, 3, 18, and 24 hours were subjected to LC-MS/MS analysis. The MS/MS data of 19,482 proteins documented in the database were examined. Proteins were sorted by intensity across various conditions (UT, TNF-α, CHX, and TNF-α/CHX) and time points (1, 3, 18, and 24 hours), yielding 19,351 proteins for further analysis using MetaboAnalyst 6.0. Statistical assessment using ANOVA identified 335 proteins with significant alterations (**Figure 5.12A**). Concurrently, PLS-DA facilitated the differentiation of protein expression patterns across treatments and temporal stages, with VIP score estimates ranging from 1.5-5 from component 1, indicating 2,596 candidate proteins (**Figure 5.12B**). Additionally, SAM analysis identified 24 proteins that were significantly regulated (**Figure 5.12C**). The integration of these findings through a Venn diagram identified 6 proteins that overlapped across all three analytical approaches (**Figure 5.12D**), thereby representing candidates for subsequent investigation. Six key proteins showing differential expression, namely oligodendrocyte lineage transcription factor 2 (OLIG2, Q13516), transmembrane protein ZNF593OS (A0A0U1RRA0, ZNF593OS), zinc finger protein 557 (Q8N988, ZNF557), haloacid dehalogenase-like hydrolase domain-containing 5 (Q9BXW7, CECR5), otoconin 90 (Q02509, OC90), and adenine phosphoribosyltransferase (P07741, APRT), were chosen for subsequent study, as summarized in **Table 5.1**.

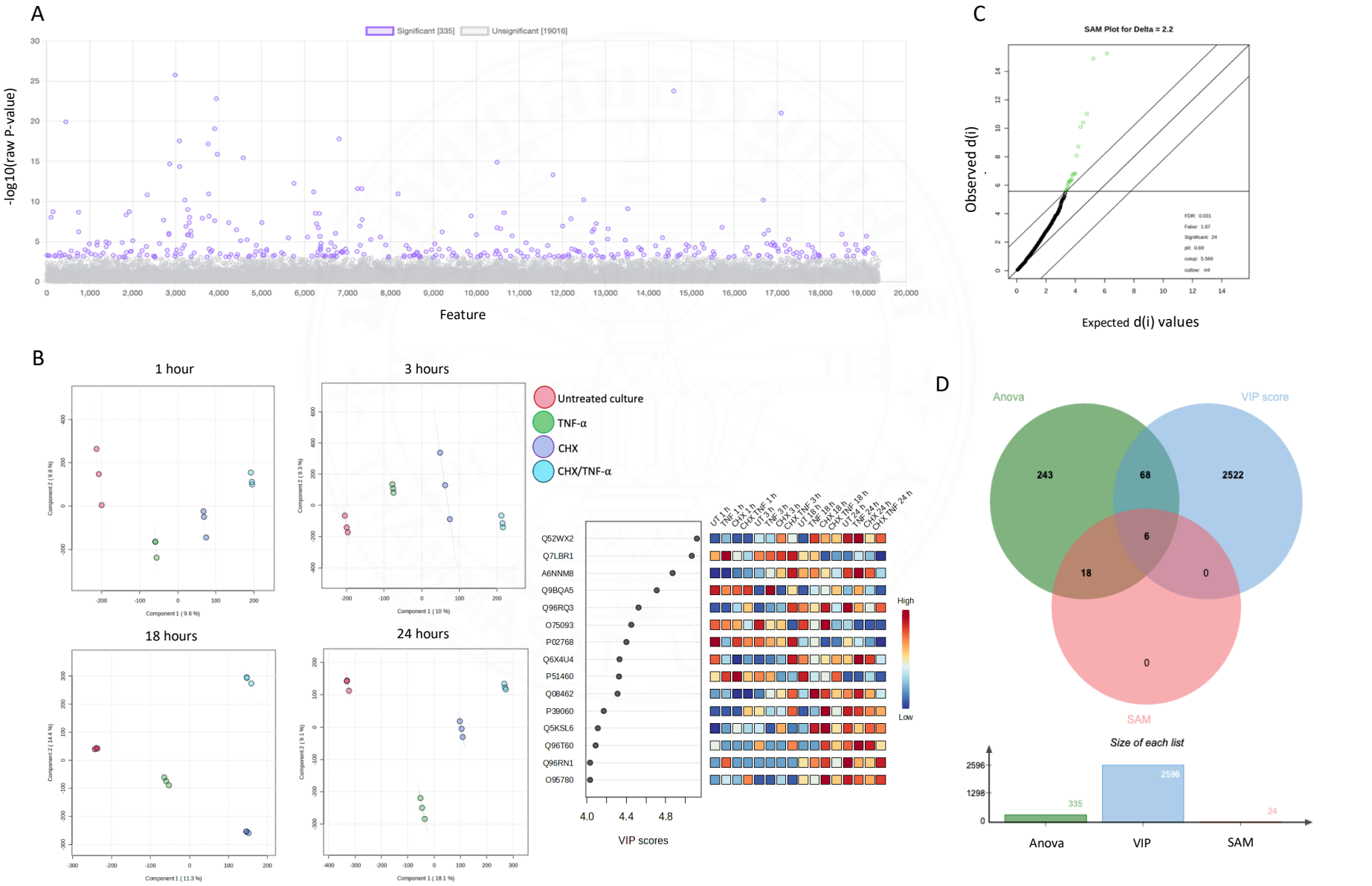

Figure 5.12 Bioinformatic analysis of the HepG2 cell proteome following treatment with CHX and/or TNF-α. Proteins from the cultures left untreated or treated with CHX and/or TNF-α at various time points were identified by LC-MS/MS. (**A**) ANOVA identified 335 significant proteins, based on a *p*-value and FDR < 0.05. (**B**) PLS-DA of protein abundance to distinguish between groups at 1, 3, 18 and 24 hours, and VIP score plot indicating fifteen key proteins that differentiate groups within the PLS-DA model. (**C**) SAM identified 24 differentially expressed proteins, and (**D**) A Venn diagram illustrating the overlap of significant proteins identified across the three statistical methods.

Table 5.1 Lists of six proteins identified through bioinformatic analysis of HepG2 cells following TNF-α/CHX treatment across time points

No.	Accession no.	Peptide sequences	Protein name	False discovery rate (FDR)	p-value
1.	Q13516	EVMPYAHGPSVRK; KLSKIATLLLAR; NYILMLTNSLEEMK; QMTEPELQQLR	Oligodendrocyte transcription factor 2 (Oligo2) (Class B basic helix-loop-helix protein 1) (bHLHb1) (Class E basic helix-loop-helix protein 19) (bHLHe19) (Protein kinase C-binding protein 2) (Protein kinase C-binding protein RACK17)	2.6748E-9	2.488E-12
2.	A0A0U1RRA0	AEPRSLLAGVVATVLAVLGLGGSCYAVWK; MVGQRRVPR;RLTPGYFR	Putative transmembrane protein ZNF593OS (ZNF593 opposite strand protein)	1.1995E-6	1.7977E-9

(Continued over page)

Table 5.1 Lists of six proteins identified through bioinformatic analysis of HepG2 cells following TNF-α/CHX treatment across time points (Cont.)

No.	Accession no.	Peptide sequences	Protein name	False discovery rate (FDR)	p-value
3.	Q8N988	DVMLENCRNLASLGNQVDKPR; EFRTQSIFTRHK; GLTPKLHVFR; GLTPKLHVFRK; HMRTHTGK;IHNGEKPYECNDCGK; MAAVVLPPTAASQR; MAAVVLPPTAASQREGHTEGGELVNELLK; NLASLGNQVDKPR;RRSNLTQHIR; RSNLTQHIR;SFNVLSSVKK;SSLTRHR;SSLTRHRK; SYECSDCGK;VFSTKSSLTR	Zinc finger protein 557	6.8334E-6	1.4125E-8
4.	Q9BXW7	LFSEYHEKR;LKTTPLPR;MAFPLLDMVDLERR; NVVTVDELR;NVVTVDELRMAFPLLDMVDLER; QAERRGWAAPIR;TTPLPRNDFPR; VIPAALK;VIPAALKAFRR; YEGLMGKPSILTYQYAEDLIRR	Haloacid dehalogenase-like hydrolase domain-containing 5 (Cat eye syndrome critical region protein 5)	6.0271E-5	1.6196E-7

(Continued over page)

Table 5.1 Lists of six proteins identified through bioinformatic analysis of HepG2 cells following TNF-α/CHX treatment across time points (Cont.)

No.	Accession no.	Peptide sequences	Protein name	False discovery rate (FDR)	p-value
5.	Q02509	AAIECLAR;ATSPPGSAEIVATR; CPEEFESYGCYCGQEGR; EDLTTLLPR;FEMEGLPVDESDSCCFQHR; FEMEGLPVDESDSCCFQHRR; KIICESKDNCEHLLCTCDK; LSTEVNCVSKK;SLGPLGIGPLHGR	Otoconin-90 (Oc90) (Phospholipase A2 homolog)	2.7115E-4	9.1078E-7
6.	P07741	ADSELQLVEQR;DISPVLKDPASFR; GREKLAPVPFFSLLQYE; IDYIAGLDSR; IRSFPDFPTPGVVFR; LAPVPFFSLLQYE;SFPDFPTPGVVFR	Adenine phosphoribosyltransferase (APRT) (EC 2.4.2.7)	3.7154E-4	1.3501E-6

TNF-α, tumor necrosis factor alpha; CHX, cycloheximide

Six proteins, along with their log_2 intensities, were visualized in a heatmap to show their expression patterns across various treatment conditions and time points. Overall, a heatmap analysis indicated that most proteins were differentially expressed in different conditions and time points. Particularly after 3, 18 and 24 hours, ZNF593OS, ZNF557, CECR5, OC90 and APRT were upregulated in different treatments compared with the expression at 1 hour of culture. Notably, OLIC2, which is highly expressed only in untreated cells at 1 hour of culture, was downregulated at all tested time points. The expression also appeared in TNF-α-treated cells at 3 hours and was downregulated later at 18 and 24 hours. CECR5, which was absent in all treatments at 1 hour, was upregulated in untreated controls and in cultures treated with TNF-α and CHX at 24 hours and 18 hours, respectively, but was absent in the co-treated cells at all tested times. APRT was upregulated at 3 hours of exposure to TNF-α/CHX co-treatment and declined later at 18 and 24 hours, whereas in the untreated control and in cells treated with TNF-α and CHX, it was upregulated later at 18 and 24 hours. The analysis demonstrates the dynamic of protein expression that may be involved in the regulatory effects of CHX/TNF-α on HepG2 cells, potentially leading to S-phase arrest and apoptosis.

To further examine the potential interactions of the six candidate proteins with the TNF-α signaling pathways and the chemical inducer CHX, all six identified proteins were analyzed using STITCH Version 5.0 (**Figure 5.13B**). The input dataset included the six proteins of interest OLIG2, ZNF593OS, ZNF557, CECR5, OC90, and APRT, along with TNF-α and CHX. The interaction network revealed that, ZNF557 and OC90 were not associated with either TNF-α or CHX in the predicted protein-chemical interaction network, whereas the transmembrane protein ZNF593OS was not included in the model, possibly due to the lack of these proteins in STITCH 5.0 database. However, three candidate proteins interacted with the CHX/TNF-α networks, including CECR5, APRT, and OLIG2. Collectively, the protein-protein interaction network suggests that TNF-α and CHX may exert their regulatory effects selectively on these candidate proteins, thereby contributing to intracellular pathways to S-phase arrest and apoptosis in HepG2 cells.

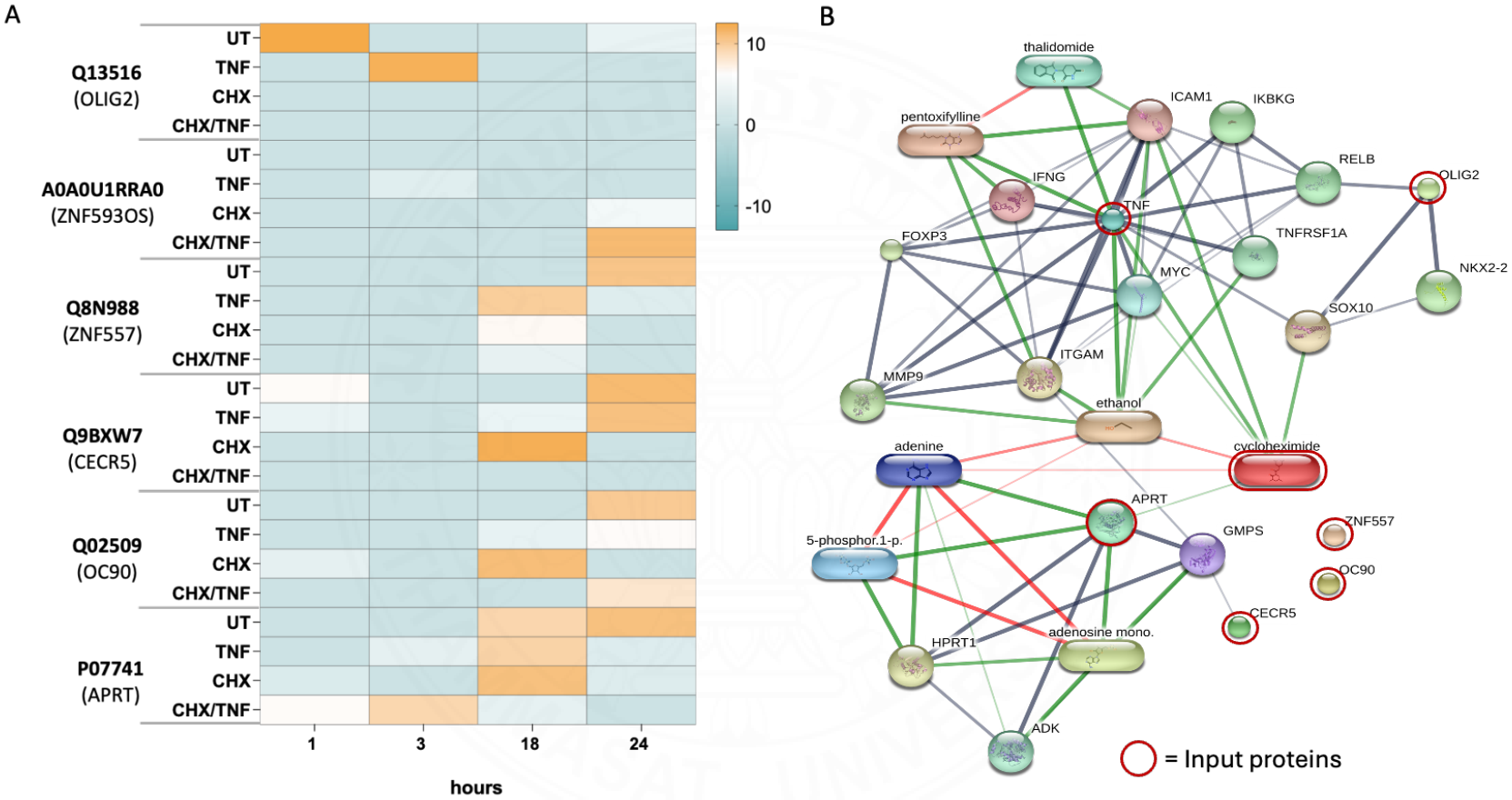
A
Q13516
(OLIG2)
A0A0U1RRA0
(ZNF593OS)
Q8N988
(ZNF557)
Q9BXW7
(CECR5)
Q02509
(OC90)
P07741
(APRT)
UT
TNF
CHX
CHX/TNF
10
0
-10
1
3
18
24
hours
B
thalidomide
pentoxifylline
ICAM1
IKBKG
RELB
OLIG2
IFNG
TNF
FOXP3
TNFRSF1A
MYC
NKX2-2
SOX10
ITGAM
MMP9
ethanol
adenine
cycloheximide
APRT
GMPS
5-phosphor.1-p.
ZNF557
OC90
CECR5
HPRT1
adenosine mono.
ADK
= Input proteins

Figure 5.13 Expression of six candidate proteins and their protein-protein interaction network with the TNF-α-mediated signaling pathways. (**A**) Heatmap analysis shows distinct expression levels of six proteins under different conditions and time points. (**B**) A network of protein-protein interactions generated by STITCH 5.0. A protein-chemical interaction network for these six proteins (Q13516, A0A0U1RRA0, Q8N988, Q9BXW7, Q02509, and P07741) with CHX/TNF-α was demonstrated. Nodes represent proteins or chemicals, and edges indicate data support relationships based on text mining, experimental confidence, database, co-expression, neighborhood, gene fusion, co-occurrence and prediction. Input protein and chemical: APRT, Adenine phosphoribosyltransferase; OLIG2, Oligodendrocyte transcription factor 2; CECR5, Haloacid dehalogenase-like hydrolase domain-containing 5; ZNF593OS, Haloacid dehalogenase-like hydrolase domain-containing 5; ZNF557, Zinc finger protein; OC90, Otoconin-90; TNF, tumor necrosis factor; Cycloheximide. Predicted functional partners: 5-phosphor.1-p, 5-Phosphoribosyl-1-pyrophosphate; Adenine; GMPS, Guanine monphosphate synthetase; IFNG, Interferon gamma; ICAM1, Intercellular adhesion molecule 1; Pentoxifylline; Ethanol; SOX10, Transcription factor SOX-10; ITGAM, Integrin alpha M; HPRT1, Hypoxanthine phosphoribosyltransferase 1; Adenosine mono, Adenosine monophosphate; FOXP3, MMP9, Matrix metallopeptidase 9; NKX2-2, NK2 homeobox 2; IKBKG, NF-kappa-B essential modulator; RELB, Transcription factor RelB; TNFRSF1A, Tumor necrosis factor receptor superfamily member 1A; ADK, Adenosine kinase; Thalidomide and MYC, Myc proto-oncogene protein.

CHAPTER 6
DISCUSSION

Progression toward liver inflammation and fibrosis is a key stage of CLD, caused by different etiologies, including HBV and HCV infections, alcohol-associated liver disease (ALD) and more recently emphasized metabolic dysfunction-associated steatotic liver disease (MASLD/NAFL), eventually leading to HCC.[15, 100-104] Regardless of the underlying etiology, chronic liver inflammation is typically initiated by persistent hepatocyte injury, making this process a key diagnostic and therapeutic target.[105, 106] While numerous studies have indicated the important roles of inflammatory cytokine TNF-α in hepatocyte damage and death,[67, 105, 107] its precise molecular mechanisms are not fully understood.[108] The present study provides a comprehensive characterization of hepatocyte damage and death in the hepatoma HepG2 cell line induced by a combination of TNF-α and translational arrest inducer CHX. This *in vitro* hepatocyte model has been assessed for the capability of cell viability, cell growth and proliferation, cell cycle, cell death and senescence. The key signaling pathways and proteomic profiles associated with TNF-α/CHX-mediated hepatocyte injury and death have also been elucidated, providing a comprehensive explanation of the underlying mechanisms. The findings generated in this study and their significance are detailed in this section.

The primary aim of this study was to establish an *in vitro* TNF-α-medicated hepatic injury and death. HepG2 cells were induced with TNF-α alone, CHX alone or in combination with TNF-α and CHX at various concentrations and times using MTT assay, and it was found that TNF-α and its combination with CHX significantly decrease HepG2 cell viability. TNF-α alone (20 and 100 ng/mL) exhibited a modest but significant effect (5.8% for both concentrations), and co-treatment of 100 ng/mL TNF-α with 50 μM CHX showed an additive effect on HepG2 cell viability (38.4% reduction of cell viability) at 24 hours of exposure. Morphological changes under a microscope and proliferative ability, assessed by a trypan blue exclusion assay, in cultures treated with TNF-α and co-treated with CHX were consistent with the percent reduction of cell viability. This experimental design enabled a comprehensive comparison of how individual and combination conditions influence hepatocyte fate. Consistent with

several previous studies, initial optimization of TNF-α/CHX treatment demonstrated a strictly dose- and time-dependent cellular response.[5, 6]

Further examination was conducted to characterize TNF-α/CHX-treated cells. The data indicated that TNF-α alone decreased cell viability without growth arrest, cell cycle arrest and apoptosis. Normally, TNF-α can bind to TNFR1 and activate two competing downstream pathways, depending on the cellular context and conditions under which TNF-α is encountered.[5] It can engage NF-κB signaling, which promotes the expression of pro-survival and anti-apoptotic genes.[109-111] On the other hand, it can initiate a death-inducing signaling complex that activates caspases and drives apoptosis.[112] Therefore, TNF-α may exert some cytotoxic pressure on HepG2 hepatoma cells and pro-apoptotic signaling is effectively counteracted by active survival mechanisms, most likely NF-κB-driven transcription of short-lived anti-apoptotic proteins.[109, 111] Additionally, HepG2 cells, which are derived from a hepatocellular carcinoma, exhibit constitutively heightened pro-survival signaling, which may explain their inherent resistance to TNF-α alone.[87] In response to a translational inhibitor CHX, HepG2 cells exhibited distinct cellular responses: decreased cell viability, cell growth and S-phase cell cycle arrest, and modest but significant apoptosis. The ability of CHX to induce cell growth and S-phase arrest indicates that translational inhibition alone is sufficient to restrict hepatocyte proliferation, possibly by depleting short-lived proteins required for cell cycle progression.[113-115] However, the limited degree of apoptosis observed in CHX-treated cells aligns with the previous report that CHX protects against serum withdrawal-mediated apoptosis.[113] In this study, the most revealing cellular response observed in HepG2 cells co-treated with TNF-α and CHX was an additive effect on cell viability and cell growth. Moreover, cell cycle arrest was observed specifically at the S-phase together with a robust induction of apoptosis in the co-treatment condition. These results strongly suggest that CHX sensitizes hepatoma cells to TNF-α-mediated apoptosis possibly by depleting the short-lived pro-survival proteins that ordinarily suppress TNFR1-mediated death signaling.[116, 117] Once this protective barrier is removed, TNF-α can fully engage pro-apoptotic pathways, driving cells toward apoptosis in a manner that neither agent could achieve independently.[112] Notably, the S-phase-specific arrest observed under either single CHX treatment or TNF-α/CHX co-treatment further suggests that CHX causes cells to pause replication

before ultimately committing to apoptosis, a possibility that warrants further mechanistic investigation.[118] From a broader biological perspective, these findings are highly relevant to understanding liver pathology. In inflammatory liver diseases such as viral hepatitis, alcoholic liver disease, and drug-induced liver injury, hepatocytes are frequently exposed to elevated TNF-α levels alongside various forms of cellular stress that may compromise protein synthesis.[119-121] The results of this study suggest that under these conditions, hepatocytes that lose their ability to maintain pro-survival protein levels become significantly more vulnerable to TNF-α-driven apoptosis.[122, 123] This has potential implications for understanding the progression of acute liver injury and explaining how specific cellular stress conditions significantly exacerbate TNF-α-associated liver damage.[121] Collectively, the characterization of TNF-α/CHX treatment HepG2 model has provided an understanding of how hepatocyte death is regulated in the context of inflammatory signaling. A distinct cellular outcome for each treatment highlights the critical role of the pro-survival protein synthesis machinery in determining whether TNF-α drives hepatocytes toward survival or apoptosis.[5, 30, 87]

In this study, a TNF-α/CHX-treated model was also preliminarily evaluated for cellular senescence. The data suggested that treatment with TNF-α alone likely induced cellular senescence in a time-dependent manner; however, the growth and cell-cycle arrest, typical characteristics of senescence, were not observed.[124] This TNF-α-induced outcome warrants further clarification. Furthermore, the addition of CHX, either as a single treatment or in combination with TNF-α, likely induced a rapid and complex phenotypic shift toward apoptosis during the early stages of exposure. Ultimately, these data indicate that, at indicated concentrations and times, this TNF-α/CHX-treated HepG2 model represents a progressive cellular response toward S-phase cell-cycle arrest and apoptotic cell death, rather than senescence.

The molecular pathways underlying TNF-α/CHX-mediated cell-cycle arrest and apoptosis in HepG2 cells were further characterized. In this study, HepG2 cells were shown to constitutively express TNFR1 at relatively low levels, measured by immunostaining and flow cytometry, suggesting that TNF-α-mediated responses in this cellular model are likely driven by the TNFR1 signaling pathway.[98, 99] Western blot analysis of p21, Cyclin A2, Cyclin D1, cleaved PARP-1 and cleaved caspase-3 in this TNF-α/CHX model supports the findings at the cellular levels. During apoptotic

induction in the CHX/TNF-α co-treatment condition, decreased pro-caspase and PARP-1 levels alongside the detection of cleaved caspase-3 and cleaved PARP-1 were observed. Caspase-3 is the well-established executioner caspase whose activation marks an irreversible step in both intrinsic and extrinsic apoptotic pathways, and its downstream cleavage of PARP-1 further validates this response.[125, 126] Also, the absence of these cleaved marker forms in the single treatments supports the concept that CHX sensitizes HepG2 cells to TNF-α-induced apoptosis by depleting short-lived pro-survival proteins that ordinarily suppress TNFR1-mediated death signaling.[127, 128] Regarding the expression of the cyclin-dependent kinase inhibitor p21,[46] it progressively decreased under both CHX alone and TNF-α/CHX treatment. This supports the notion that p21 is a short-lived protein required to maintain cell division, and CHX disrupts protein synthesis, including p21, in HepG2 cells.[129] The p21 decline under co-treatment conditions may also reflect a shift from growth arrest to apoptotic commitment, consistent with caspase activation observed in the same condition. Also, TNF-α alone did not alter p21 expression, further confirming its limited molecular impact as a single agent in this model. Cyclin A2 is essential for both S-phase progression and G2/M transition.[107, 130] However, neither CHX nor TNF-α treatments, alone or in combination, affected cyclin A2 expression, even though cyclin A2 levels appeared to decrease over time both in untreated and treated conditions. Thus, cyclin A2 expression in this model does not account for the S-phase arrest observed with CHX treatment alone or TNF-α/CHX co-treatments. Cyclin D1 is known to play important roles in G1-to-S phase transition.[131] In this model, cyclin D1 expression exhibited a more complex and condition-specific pattern. In single treatment, cyclin D1 initially increased, then decreased, possibly reflecting an early compensatory proliferative signal followed by stress-induced suppression. However, under co-treatment, the opposite pattern was observed, with an initial decrease followed by a later rise, suggesting that combined TNF-α and CHX stress engages distinct regulatory mechanisms governing cyclin D1 expression. This divergent behavior suggests that cyclin D1 dynamics may reflect condition-specific signaling rather than a general proliferative response.[132-134] Together, these molecular findings clarify how TNF-α and CHX, alone and in combination, regulate cell cycle and apoptotic pathways. Most

importantly, they highlight that translation inhibition is critical for unlocking TNF-α-induced apoptosis in HepG2 cells.

To explore the proteomic profiles associated with TNF-α-mediated cell death in HepG2 cells. Proteomic analysis identified six proteins with differential expression across multiple conditions, namely CECR5 (HDHD5), ZNF593OS, OC90, APRT, OLIC2, and ZNF557. The mixed pattern of upregulation and downregulation observed among these proteins reflects the complex molecular dynamics of TNF-α/CHX-mediated hepatocyte stress, suggesting the involvement of potentially novel players in cell-cycle arrest and apoptosis. CECR5 or HDHD5, also known as haloacid dehalogenase-like hydrolase domain-containing protein 5, is involved in nucleotide metabolism and has been linked to mitochondrial function.[135] The differential expression observed in this study may link to the well-established role of mitochondrial integrity in regulating the intrinsic apoptotic pathway in hepatocytes.[135, 136] Disruption of mitochondrial homeostasis is a recognized early event in TNF-α-mediated liver cell death, and alterations in HDHD5 may reflect underlying metabolic stress responses triggered by the treatment conditions used in this study.[137, 138] ZNF593OS is a long non-coding RNA overlapping the ZNF593 gene locus. While their precise functions remain poorly characterized, emerging evidence suggests that non-coding RNAs in the ZNF family play regulatory roles in transcriptional stress responses and cell survival.[139, 140] The identification in this proteomic study may suggest an unrecognized regulatory role in TNF-α-mediated signaling in hepatocytes. Further functional studies would be needed to establish the precise role in this context. OC90 is a protein primarily known for its structural role in the extracellular matrix of the inner ear; however, detection in HepG2 cells under treatment conditions suggests a possible stress-related expression pattern.[141, 142] The multiple treatment conditions in this study may reflect broader extracellular matrix remodeling or stress-induced changes in protein expression that accompany hepatocyte apoptosis, though the specific functions in liver cells require further investigation.[143, 144] Adenine phosphoribosyltransferase (APRT) is an enzyme involved in the purine salvage pathway, playing a critical role in maintaining intracellular nucleotide pools.[145] The expression in this study is biologically plausible, as purine metabolism is closely linked to DNA damage responses and cell survival signaling. Disruption of nucleotide homeostasis has been shown to contribute to

replication stress and cell cycle arrest, both of which were observed in the cellular findings of this study.[146-148] The altered expression of APRT may therefore reflect an adaptive metabolic response to the combined stress of translational inhibition and TNF-α signaling. OLIC2 is a relatively uncharacterized protein, and there is currently limited information regarding its function in hepatocytes or apoptotic signaling.[149] Significant differential expression across multiple treatment conditions in this study makes a potentially interesting target for future functional characterization. Given the context of TNF-α-mediated apoptotic cell death, OLIC2 may represent a novel molecular marker or regulator in hepatocyte stress responses that has not yet been fully explored in the study. ZNF557 belongs to the zinc finger protein family, a large group of transcription factors involved in regulating gene expression across diverse biological processes, including stress response, cell cycle and apoptosis.[150, 151] ZNF557 has previously been implicated in modulating NF-κB activity and p53-dependent apoptotic pathways in liver cells.[108, 152, 153] The differential expression of ZNF557 observed in this study may therefore reflect transcriptional reprogramming occurring in HepG2 cells in response to TNF-α and CHX treatment, potentially influencing the balance between pro-survival and pro-apoptotic gene expression. Accordingly, the identification of these six proteins across multiple treatment conditions and time points adds a valuable proteomic dimension to this cellular model. Additionally, the protein-protein interaction network of these six proteins, with the TNF-α signaling and the translational inhibitor CHX, was generated using the STITCH 5.0 database. Three proteins, including CECR5, APRT, and OLIG2, interacted within the network, strengthening their involvement of the three proteins in TNF-α/CHX-mediated HepG2 cell cycle arrest and apoptosis. Future functional studies targeting these proteins individually would help clarify their precise contributions to TNF-α-mediated hepatocyte fate and may reveal new therapeutic targets relevant to inflammatory liver disease.

In conclusion, this study provides insight into TNF-α-mediated cell-cycle arrest and apoptosis in HepG2 cells; however, certain limitations should be considered when interpreting the findings. First, all experiments were conducted exclusively using the HepG2 cell line, which may not fully reflect the biology of normal primary human hepatocytes. Although HepG2 cells retain wild-type p53 function, the findings may still not be directly translatable to normal hepatocyte biology or the complex *in vivo* liver

environment. Second, this study was entirely *in vitro*, which limits the ability to account for multicellular and systemic interactions involving Kupffer cells, hepatic stellate cells, and immune mediators that occur during liver inflammation *in vivo*. Third, the functional roles of the six proteins identified through proteomic analysis remain to be experimentally validated. Future studies should consider validating these findings in primary human hepatocytes and relevant *in vivo* models. Functional characterization of the identified proteins, particularly APRT, OLIG2 and CECR5, would further clarify their roles in TNF-α-mediated hepatocyte apoptosis and senescence.

CHAPTER 7
CONCLUSION

This thesis aimed to characterize *in vitro* TNF-α-mediated hepatocyte death using the human hepatoma cell line HepG2. Through systematic treatment with TNF-α, CHX, and their combination, this study has provided important insights into the cellular and molecular mechanisms governing hepatocyte fate in the context of inflammatory signaling. First, HepG2 cells were treated with TNF-α alone, and a decrease in cell viability was observed, initially suggesting a cytotoxic effect. However, further analysis revealed neither cell cycle arrest nor apoptosis, with the absence of apoptotic markers (cleaved caspase and cleaved PARP-1) and expected cell cycle regulatory shifts (p21, cyclin A2 and cyclin D1). TNF-α is widely regarded as a pro-inflammatory cytokine capable of inducing cell death. The results suggest that cells may possess active survival mechanisms that protect them from TNF-α-mediated killing when TNF-α acts alone. This is consistent with pro-survival pathways, such as NF-κB signaling. Notably, TNF-α-treated cells exhibit SA-β-gal activity, a hallmark of cellular senescence, without cell cycle or growth arrest. The evidence requires more clarification. Second, treatment with CHX alone elicited a distinct response. HepG2 cells exhibited decreased viability, growth and S-phase cell cycle arrest, and a limited degree of apoptosis. Consistently, molecular analysis revealed no detectable apoptotic markers (cleaved caspase and cleaved PARP-1) and downregulated p21 expression. This suggests that CHX can inhibit translation to restrict cell cycle and cell growth without efficiently committing cells to apoptosis. Third, the main finding of this study was obtained from co-treating cells with CHX and TNF-α. The combination produced an additive reduction in cell viability and growth and S-phase arrest, but notably enhanced induction of apoptosis. This study indicates that TNF-α alone is not sufficient to induce apoptosis in hepatoma cells, but when combined with CHX, it becomes a potent driver of cell death. This highlights how context-dependent TNF-α signaling and the balance between survival and death in hepatocytes can shift dramatically in response to changes in the cellular environment. It is worth acknowledging that this study was conducted using a hepatoma cell line, and the results may not fully reflect the behavior of normal primary hepatocytes.

Future work using primary human hepatocytes or relevant *in vivo* models would help determine whether these findings translate to more physiologically relevant settings, particularly in the context of liver diseases such as viral hepatitis or drug-induced liver injury. Additionally, exploring the specific roles of the identified proteins, HDHD5 or CECR5, ZNF593OS, OC90, APRT, OLIC2, and ZNF557, in hepatocyte biology would be a logical and valuable next step based on this work. Ultimately, the characterization of this TNF-α/CHX model provides a valuable framework for understanding immune evasion and stress responses, possibly in CLD and HCC. It not only serves as a reliable *in vitro* tool for modeling inflammatory hepatocyte stress but also offers a critical platform for identifying novel therapeutic targets for hepatocyte apoptosis in liver disease.

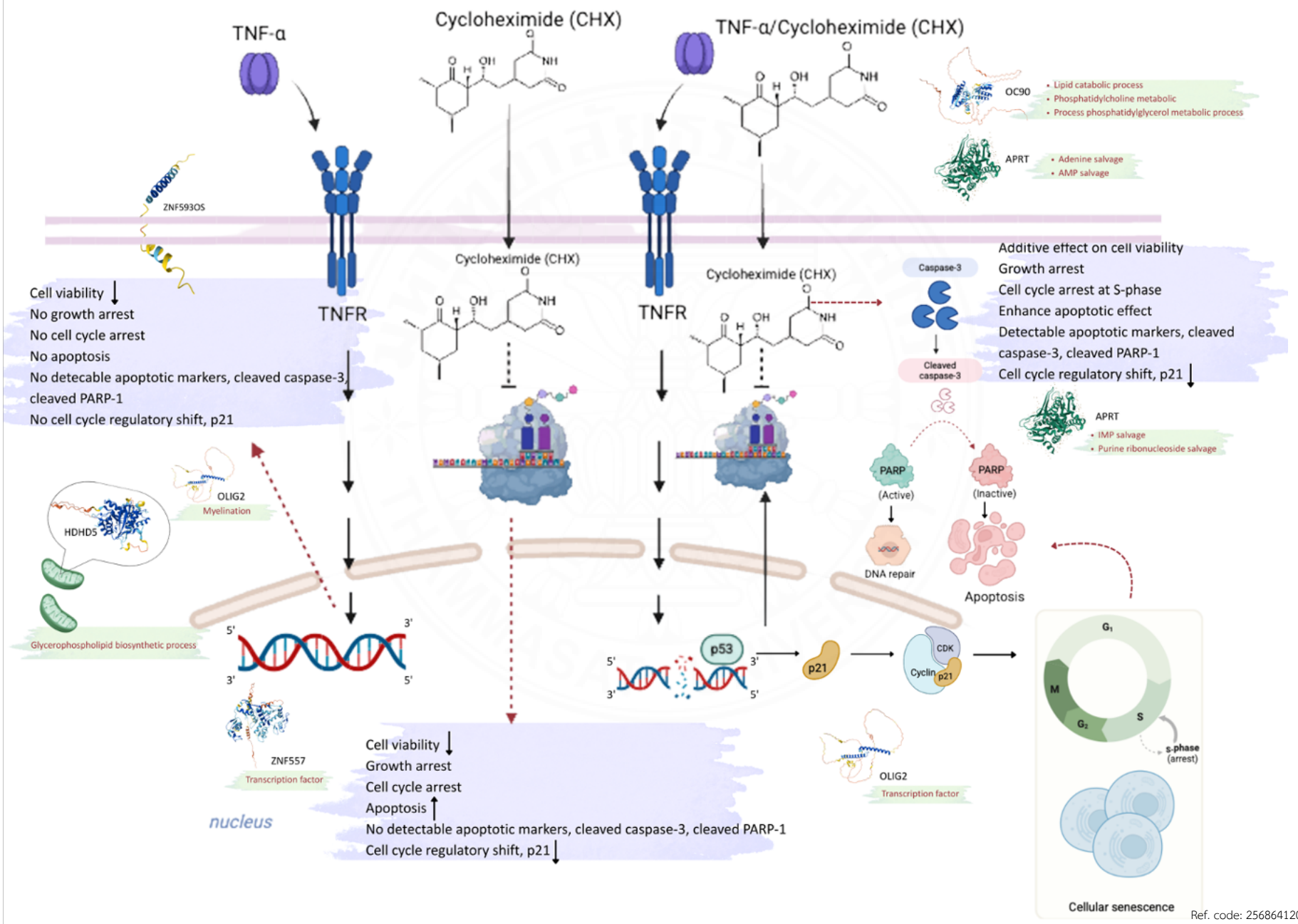

Figure 7.1 Schematic representation of the TNF-α/CHX-mediated hepatocyte death model in a human hepatoma HepG2 cell line. Cellular and molecular responses of HepG2 cells to TNF-α alone, CHX alone and their combination are depicted. Tumor necrosis factor-α (TNF-α), cycloheximide (CHX), Poly [ADP-ribose] polymerase 1 (PARP-1) APRT, Adenine phosphoribosyltransferase; OLIG2, Oligodendrocyte transcription factor 2; CECR5 or HDHD5, Haloacid dehalogenase-like hydrolase domain-containing 5; ZNF593OS, Haloacid dehalogenase-like hydrolase domain-containing 5; ZNF557, Zinc finger protein; OC90, Otoconin-90. Created with BioRender.com.

REFERENCES

1. Roehlen N, Crouchet E, Baumert TF. Liver Fibrosis: Mechanistic Concepts and Therapeutic Perspectives. Cells. 2020;9(4):875.

2. Berumen J, Baglieri J, Kisseleva T, Mekeel K. Liver fibrosis: Pathophysiology and clinical implications. WIREs Mech Dis. 2021;13(1):e1499.

3. Liu P, Tang Q, Chen M, Chen W, Lu Y, Liu Z, et al. Hepatocellular Senescence: Immunosurveillance and Future Senescence-Induced Therapy in Hepatocellular Carcinoma. Front Oncol. 2020;10:589908.

4. Cai X, Guillot A, Liu H. Cellular Senescence in Hepatocellular Carcinoma: The Passenger or the Driver? Cells. 2022;12(1):132.

5. Zhao S, Jiang J, Jing Y, Liu W, Yang X, Hou X, et al. The concentration of tumor necrosis factor-alpha determines its protective or damaging effect on liver injury by regulating Yap activity. Cell Death Dis. 2020;11(1):70.

6. Tiegs G, Horst AK. TNF in the liver: targeting a central player in inflammation. Semin Immunopathol. 2022;44(4):445-59.

7. Leist M, Gantner F, Bohlinger I, Germann PG, Tiegs G, Wendel A. Murine hepatocyte apoptosis induced in vitro and in vivo by TNF-alpha requires transcriptional arrest. J Immunol. 1994;153(4):1778-88.

8. Ni HM, McGill MR, Chao X, Woolbright BL, Jaeschke H, Ding WX. Caspase Inhibition Prevents Tumor Necrosis Factor-alpha-Induced Apoptosis and Promotes Necrotic Cell Death in Mouse Hepatocytes in Vivo and in Vitro. Am J Pathol. 2016;186(10):2623-36.

9. Hu Y, Zhang H, Xie N, Liu D, Jiang Y, Liu Z, et al. Bcl-3 promotes TNF-induced hepatocyte apoptosis by regulating the deubiquitination of RIP1. Cell Death Differ. 2022;29(6):1176-86.

10. Vadrot N, Ghanem S, Braut F, Gavrilescu L, Pilard N, Mansouri A, et al. Mitochondrial DNA maintenance is regulated in human hepatoma cells by glycogen synthase kinase 3beta and p53 in response to tumor necrosis factor alpha. PLoS One. 2012;7(7):e40879.

11. Kandhaya-Pillai R, Miro-Mur F, Alijotas-Reig J, Tchkonia T, Kirkland JL, Schwartz S. TNFalpha-senescence initiates a STAT-dependent positive feedback loop, leading to a sustained interferon signature, DNA damage, and cytokine secretion. Aging (Albany NY). 2017;9(11):2411-35.

12. Li P, Gan Y, Xu Y, Song L, Wang L, Ouyang B, et al. The inflammatory cytokine TNF-alpha promotes the premature senescence of rat nucleus pulposus cells via the PI3K/Akt signaling pathway. Sci Rep. 2017;7:42938.

13. Tatiparthy M, Kammala AK, Urrabaz-Garza R, Thomas TJ, Paul S, Choudhury J, et al. The Impacts of TNF-alpha-Induced Inflammation on Amnion Epithelial Cells: Exploring Stem Cell Gene Expression, Senescence, Inflammatory Responses, and Cellular Transition. Am J Reprod Immunol. 2025;93(6):e70106.

14. Gonzalez-Gualda E, Baker AG, Fruk L, Munoz-Espin D. A guide to assessing cellular senescence in vitro and in vivo. FEBS J. 2021;288(1):56-80.

15. Devarbhavi H, Asrani SK, Arab JP, Nartey YA, Pose E, Kamath PS. Global burden of liver disease: 2023 update. J Hepatol. 2023;79(2):516-37.

16. Rattanamongkolgul S, Wongjitrat C, Puapankitcharoen P. Prevalence of cirrhosis registered in Nakhon Nayok, Thailand. J Med Assoc Thai. 2010;93 Suppl 2:S87-91.

17. Mihm S. Danger-Associated Molecular Patterns (DAMPs): Molecular Triggers for Sterile Inflammation in the Liver. Int J Mol Sci. 2018;19(10):3104.

18. Scaffidi P, Misteli T, Bianchi ME. Release of chromatin protein HMGB1 by necrotic cells triggers inflammation. Nature. 2002;418(6894):191-5.

19. Gardella S, Andrei C, Ferrera D, Lotti LV, Torrisi MR, Bianchi ME, et al. The nuclear protein HMGB1 is secreted by monocytes via a non-classical, vesicle-mediated secretory pathway. EMBO Rep. 2002;3(10):995-1001.

20. Tian J, Avalos AM, Mao SY, Chen B, Senthil K, Wu H, et al. Toll-like receptor 9-dependent activation by DNA-containing immune complexes is mediated by HMGB1 and RAGE. Nat Immunol. 2007;8(5):487-96.

21. Huebener P, Pradere JP, Hernandez C, Gwak GY, Caviglia JM, Mu X, et al. The HMGB1/RAGE axis triggers neutrophil-mediated injury amplification following necrosis. J Clin Invest. 2015;125(2):539-50.

22. Zhan SS, Jiang JX, Wu J, Halsted C, Friedman SL, Zern MA, et al. Phagocytosis of apoptotic bodies by hepatic stellate cells induces NADPH oxidase and is associated with liver fibrosis in vivo. Hepatology. 2006;43(3):435-43.

23. Canbay A, Feldstein AE, Higuchi H, Werneburg N, Grambihler A, Bronk SF, et al. Kupffer cell engulfment of apoptotic bodies stimulates death ligand and cytokine expression. Hepatology. 2003;38(5):1188-98.

24. Canbay A, Higuchi H, Bronk SF, Taniai M, Sebo TJ, Gores GJ. Fas enhances fibrogenesis in the bile duct ligated mouse: a link between apoptosis and fibrosis. Gastroenterology. 2002;123(4):1323-30.

25. Feldstein AE, Canbay A, Angulo P, Taniai M, Burgart LJ, Lindor KD, et al. Hepatocyte apoptosis and fas expression are prominent features of human nonalcoholic steatohepatitis. Gastroenterology. 2003;125(2):437-43.

26. Schafer MJ, White TA, Iijima K, Haak AJ, Ligresti G, Atkinson EJ, et al. Cellular senescence mediates fibrotic pulmonary disease. Nat Commun. 2017;8:14532.

27. Munoz-Espin D, Rovira M, Galiana I, Gimenez C, Lozano-Torres B, Paez-Ribes M, et al. A versatile drug delivery system targeting senescent cells. EMBO Mol Med. 2018;10(9):e9355.

28. van Deursen JM. The role of senescent cells in ageing. Nature. 2014;509(7501):439-46.

29. Childs BG, Durik M, Baker DJ, van Deursen JM. Cellular senescence in aging and age-related disease: from mechanisms to therapy. Nat Med. 2015;21(12):1424-35.

30. Fizikova A, Prokhorova A, Churikova D, Konstantinov Z, Ivanov R, Karabelsky A, et al. Hepatocytes as Model for Investigating Natural Senotherapeutic Compounds and Their Effects on Cell Cycle Dynamics and Genome Stability. Int J Mol Sci. 2025;26(14):6794.

31. Campisi J. Aging, cellular senescence, and cancer. Annu Rev Physiol. 2013;75:685-705.

32. Stojanovic B, Jovanovic I, Dimitrijevic Stojanovic M, Stojanovic BS, Kovacevic V, Radosavljevic I, et al. Oxidative Stress-Driven Cellular Senescence: Mechanistic Crosstalk and Therapeutic Horizons. Antioxidants (Basel). 2025;14(8):987.

33. Kumari R, Jat P. Mechanisms of Cellular Senescence: Cell Cycle Arrest and Senescence Associated Secretory Phenotype. Front Cell Dev Biol. 2021;9:645593.

34. Hernandez Borrero LJ, El-Deiry WS. Tumor suppressor p53: Biology, signaling pathways, and therapeutic targeting. Biochim Biophys Acta Rev Cancer. 2021;1876(1):188556.

35. Xu B, Maimaitijiang A, Nuerbiyamu D, Su Z, Li W. The Multifaceted Role of p53 in Cancer Molecular Biology: Insights for Precision Diagnosis and Therapeutic Breakthroughs. Biomolecules. 2025;15(8):1088.

36. Kuilman T, Michaloglou C, Mooi WJ, Peeper DS. The essence of senescence. Genes Dev. 2010;24(22):2463-79.

37. Manohar S, Estrada ME, Uliana F, Vuina K, Alvarez PM, de Bruin RAM, et al. Genome homeostasis defects drive enlarged cells into senescence. Mol Cell. 2023;83(22):4032-46 e6.

38. Blagosklonny MV. Cell cycle arrest is not senescence. Aging (Albany NY). 2011;3(2):94-101.

39. Liao Z, Yeo HL, Wong SW, Zhao Y. Cellular Senescence: Mechanisms and Therapeutic Potential. Biomedicines. 2021;9(12):1769.

40. Blagosklonny MV. Geroconversion: irreversible step to cellular senescence. Cell Cycle. 2014;13(23):3628-35.

41. Aird KM, Zhang R. Detection of senescence-associated heterochromatin foci (SAHF). Methods Mol Biol. 2013;965:185-96.

42. Alam MT, Mansoor MAM, Ashiqueali SA, Golusinski P, Golusinska-Kardach E, Strzelczyk JK, et al. The Impact of Senescence-Associated Secretory Phenotype (SASP) on Head and Neck Cancers: From Biology to Therapy. Cancers (Basel). 2025;17(24):4024.

43. Dong Z, Luo Y, Yuan Z, Tian Y, Jin T, Xu F. Cellular senescence and SASP in tumor progression and therapeutic opportunities. Mol Cancer. 2024;23(1):181.

44. Thangavelu L, Altamimi ASA, Ghaboura N, Babu MA, Roopashree R, Sharma P, et al. Targeting the p53-p21 axis in liver cancer: Linking cellular senescence to tumor suppression and progression. Pathol Res Pract. 2024;263:155652.

45. Engeland K. Cell cycle regulation: p53-p21-RB signaling. Cell Death Differ. 2022;29(5):946-60.

46. Yan J, Chen S, Yi Z, Zhao R, Zhu J, Ding S, et al. The role of p21 in cellular senescence and aging-related diseases. Mol Cells. 2024;47(11):100113.

47. Chen J. The Cell-Cycle Arrest and Apoptotic Functions of p53 in Tumor Initiation and Progression. Cold Spring Harb Perspect Med. 2016;6(3):a026104.

48. Senturk E, Manfredi JJ. p53 and cell cycle effects after DNA damage. Methods Mol Biol. 2013;962:49-61.

49. Kari S, Subramanian K, Altomonte IA, Murugesan A, Yli-Harja O, Kandhavelu M. Programmed cell death detection methods: a systematic review and a categorical comparison. Apoptosis. 2022;27(7-8):482-508.

50. Zhang Y, Fujita N, Tsuruo T. Caspase-mediated cleavage of p21Waf1/Cip1 converts cancer cells from growth arrest to undergoing apoptosis. Oncogene. 1999;18(5):1131-8.

51. Abbas T, Dutta A. p21 in cancer: intricate networks and multiple activities. Nat Rev Cancer. 2009;9(6):400-14.

52. Yadav M, Kandhari K, Mathan SV, Ali M, Singh RP. Fisetin induces G2/M phase arrest and caspase-mediated cleavage of p21(Cip1) and p27(Kip1) leading to apoptosis and tumor growth inhibition in HNSCC. Mol Carcinog. 2024;63(9):1697-711.

53. Nishitsuji H, Funami K, Shimizu Y, Ujino S, Sugiyama K, Seya T, et al. Hepatitis C virus infection induces inflammatory cytokines and chemokines mediated by the cross talk between hepatocytes and stellate cells. J Virol. 2013;87(14):8169-78.

54. Luedde T, Kaplowitz N, Schwabe RF. Cell death and cell death responses in liver disease: mechanisms and clinical relevance. Gastroenterology. 2014;147(4):765-83 e4.

55. Leroux A, Ferrere G, Godie V, Cailleux F, Renoud ML, Gaudin F, et al. Toxic lipids stored by Kupffer cells correlates with their pro-inflammatory phenotype at an early stage of steatohepatitis. J Hepatol. 2012;57(1):141-9.

56. Bieghs V, Hendrikx T, van Gorp PJ, Verheyen F, Guichot YD, Walenbergh SM, et al. The cholesterol derivative 27-hydroxycholesterol reduces steatohepatitis in mice. Gastroenterology. 2013;144(1):167-78.

57. Pellicoro A, Ramachandran P, Iredale JP, Fallowfield JA. Liver fibrosis and repair: immune regulation of wound healing in a solid organ. Nat Rev Immunol. 2014;14(3):181-94.

58. Tacke F, Zimmermann HW. Macrophage heterogeneity in liver injury and fibrosis. J Hepatol. 2014;60(5):1090-6.

59. Nishikawa K, Osawa Y, Kimura K. Wnt/beta-Catenin Signaling as a Potential Target for the Treatment of Liver Cirrhosis Using Antifibrotic Drugs. Int J Mol Sci. 2018;19(10):3103.

60. Cai X, Li Z, Zhang Q, Qu Y, Xu M, Wan X, et al. CXCL6-EGFR-induced Kupffer cells secrete TGF-beta1 promoting hepatic stellate cell activation via the SMAD2/BRD4/C-MYC/EZH2 pathway in liver fibrosis. J Cell Mol Med. 2018;22(10):5050-61.

61. Liu RM, Desai LP. Reciprocal regulation of TGF-beta and reactive oxygen species: A perverse cycle for fibrosis. Redox Biol. 2015;6:565-77.

62. Reth M. Hydrogen peroxide as second messenger in lymphocyte activation. Nat Immunol. 2002;3(12):1129-34.

63. Zhang Q, Raoof M, Chen Y, Sumi Y, Sursal T, Junger W, et al. Circulating mitochondrial DAMPs cause inflammatory responses to injury. Nature. 2010;464(7285):104-7.

64. Luangmonkong T, Suriguga S, Mutsaers HAM, Groothuis GMM, Olinga P, Boersema M. Targeting Oxidative Stress for the Treatment of Liver Fibrosis. Rev Physiol Biochem Pharmacol. 2018;175:71-102.

65. van Loo G, Bertrand MJM. Death by TNF: a road to inflammation. Nat Rev Immunol. 2023;23(5):289-303.

66. Osawa Y, Kojika E, Hayashi Y, Kimura M, Nishikawa K, Yoshio S, et al. Tumor necrosis factor-alpha-mediated hepatocyte apoptosis stimulates fibrosis in the steatotic liver in mice. Hepatol Commun. 2018;2(4):407-20.

67. Yang YM, Seki E. TNFalpha in liver fibrosis. Curr Pathobiol Rep. 2015;3(4):253-61.

68. Tarrats N, Moles A, Morales A, Garcia-Ruiz C, Fernandez-Checa JC, Mari M. Critical role of tumor necrosis factor receptor 1, but not 2, in hepatic stellate cell

proliferation, extracellular matrix remodeling, and liver fibrogenesis. Hepatology. 2011;54(1):319-27.

69. Simeonova PP, Gallucci RM, Hulderman T, Wilson R, Kommineni C, Rao M, et al. The role of tumor necrosis factor-alpha in liver toxicity, inflammation, and fibrosis induced by carbon tetrachloride. Toxicol Appl Pharmacol. 2001;177(2):112-20.

70. Kitamura K, Nakamoto Y, Akiyama M, Fujii C, Kondo T, Kobayashi K, et al. Pathogenic roles of tumor necrosis factor receptor p55-mediated signals in dimethylnitrosamine-induced murine liver fibrosis. Lab Invest. 2002;82(5):571-83.

71. Wandrer F, Liebig S, Marhenke S, Vogel A, John K, Manns MP, et al. TNF-Receptor-1 inhibition reduces liver steatosis, hepatocellular injury and fibrosis in NAFLD mice. Cell Death Dis. 2020;11(3):212.

72. Brenner D, Blaser H, Mak TW. Regulation of tumour necrosis factor signalling: live or let die. Nat Rev Immunol. 2015;15(6):362-74.

73. Yamada Y, Kirillova I, Peschon JJ, Fausto N. Initiation of liver growth by tumor necrosis factor: deficient liver regeneration in mice lacking type I tumor necrosis factor receptor. Proc Natl Acad Sci U S A. 1997;94(4):1441-6.

74. Yamada Y, Webber EM, Kirillova I, Peschon JJ, Fausto N. Analysis of liver regeneration in mice lacking type 1 or type 2 tumor necrosis factor receptor: requirement for type 1 but not type 2 receptor. Hepatology. 1998;28(4):959-70.

75. Aggarwal BB. Signalling pathways of the TNF superfamily: a double-edged sword. Nat Rev Immunol. 2003;3(9):745-56.

76. Canbay A, Friedman S, Gores GJ. Apoptosis: the nexus of liver injury and fibrosis. Hepatology. 2004;39(2):273-8.

77. Hernandez-Munoz I, de la Torre P, Sanchez-Alcazar JA, Garcia I, Santiago E, Munoz-Yague MT, et al. Tumor necrosis factor alpha inhibits collagen alpha 1(I) gene expression in rat hepatic stellate cells through a G protein. Gastroenterology. 1997;113(2):625-40.

78. Saile B, Matthes N, Knittel T, Ramadori G. Transforming growth factor beta and tumor necrosis factor alpha inhibit both apoptosis and proliferation of activated rat hepatic stellate cells. Hepatology. 1999;30(1):196-202.

79. Knittel T, Mehde M, Kobold D, Saile B, Dinter C, Ramadori G. Expression patterns of matrix metalloproteinases and their inhibitors in parenchymal and non-

parenchymal cells of rat liver: regulation by TNF-alpha and TGF-beta1. J Hepatol. 1999;30(1):48-60.

80. Pradere JP, Kluwe J, De Minicis S, Jiao JJ, Gwak GY, Dapito DH, et al. Hepatic macrophages but not dendritic cells contribute to liver fibrosis by promoting the survival of activated hepatic stellate cells in mice. Hepatology. 2013;58(4):1461-73.

81. Rivera CA, Bradford BU, Hunt KJ, Adachi Y, Schrum LW, Koop DR, et al. Attenuation of CCl(4)-induced hepatic fibrosis by GdCl(3) treatment or dietary glycine. Am J Physiol Gastrointest Liver Physiol. 2001;281(1):G200-7.

82. Amara S, Lopez K, Banan B, Brown SK, Whalen M, Myles E, et al. Synergistic effect of pro-inflammatory TNFalpha and IL-17 in periostin mediated collagen deposition: potential role in liver fibrosis. Mol Immunol. 2015;64(1):26-35.

83. Kumar P, Smith T, Raeman R, Chopyk DM, Brink H, Liu Y, et al. Periostin promotes liver fibrogenesis by activating lysyl oxidase in hepatic stellate cells. J Biol Chem. 2018;293(33):12781-92.

84. Lu TF, Yang TH, Zhong CP, Shen C, Lin WW, Gu GX, et al. Dual Effect of Hepatic Macrophages on Liver Ischemia and Reperfusion Injury during Liver Transplantation. Immune Netw. 2018;18(3):e24.

85. Choi HJ, Kim NE, Kim BM, Seo M, Heo JH. TNF-alpha-Induced YAP/TAZ Activity Mediates Leukocyte-Endothelial Adhesion by Regulating VCAM1 Expression in Endothelial Cells. Int J Mol Sci. 2018;19(11):3428.

86. Chaisson ML, Brooling JT, Ladiges W, Tsai S, Fausto N. Hepatocyte-specific inhibition of NF-kappaB leads to apoptosis after TNF treatment, but not after partial hepatectomy. J Clin Invest. 2002;110(2):193-202.

87. Faletti L, Peintner L, Neumann S, Sandler S, Grabinger T, Mac Nelly S, et al. TNFalpha sensitizes hepatocytes to FasL-induced apoptosis by NFkappaB-mediated Fas upregulation. Cell Death Dis. 2018;9(9):909.

88. Luedde T, Assmus U, Wustefeld T, Meyer zu Vilsendorf A, Roskams T, Schmidt-Supprian M, et al. Deletion of IKK2 in hepatocytes does not sensitize these cells to TNF-induced apoptosis but protects from ischemia/reperfusion injury. J Clin Invest. 2005;115(4):849-59.

89. Park J, Kang W, Ryu SW, Kim WI, Chang DY, Lee DH, et al. Hepatitis C virus infection enhances TNFalpha-induced cell death via suppression of NF-kappaB. Hepatology. 2012;56(3):831-40.

90. Leist M, Gantner F, Jilg S, Wendel A. Activation of the 55 kDa TNF receptor is necessary and sufficient for TNF-induced liver failure, hepatocyte apoptosis, and nitrite release. J Immunol. 1995;154(3):1307-16.

91. Eggert T, Wolter K, Ji J, Ma C, Yevsa T, Klotz S, et al. Distinct Functions of Senescence-Associated Immune Responses in Liver Tumor Surveillance and Tumor Progression. Cancer Cell. 2016;30(4):533-47.

92. Guo F, Wu R, Xu J. Salicin prevents TNF-alpha-induced cellular senescence in human umbilical vein endothelial cells (HUVECs). Artif Cells Nanomed Biotechnol. 2019;47(1):2618-23.

93. Tyciakova S, Valova V, Svitkova B, Matuskova M. Overexpression of TNFalpha induces senescence, autophagy and mitochondrial dysfunctions in melanoma cells. BMC Cancer. 2021;21(1):507.

94. Lowry OH, Rosebrough NJ, Farr AL, Randall RJ. Protein measurement with the Folin phenol reagent. J Biol Chem. 1951;193(1):265-75.

95. Tyanova S, Temu T, Cox J. The MaxQuant computational platform for mass spectrometry-based shotgun proteomics. Nat Protoc. 2016;11(12):2301-19.

96. Pang Z, Lu Y, Zhou G, Hui F, Xu L, Viau C, et al. MetaboAnalyst 6.0: towards a unified platform for metabolomics data processing, analysis and interpretation. Nucleic Acids Res. 2024;52(W1):W398-W406.

97. Lee SY, Teng Y, Son M, Ku B, Moon HS, Tergaonkar V, et al. High-dose drug heat map analysis for drug safety and efficacy in multi-spheroid brain normal cells and GBM patient-derived cells. PLoS One. 2021;16(12):e0251998.

98. Zhao Y, Yang F, Li W, Xu C, Li L, Chen L, et al. miR-29a suppresses MCF-7 cell growth by downregulating tumor necrosis factor receptor 1. Tumour Biol. 2017;39(2):1010428317692264.

99. Martinez-Reza I, Diaz L, Garcia-Becerra R. Preclinical and clinical aspects of TNF-alpha and its receptors TNFR1 and TNFR2 in breast cancer. J Biomed Sci. 2017;24(1):90.

100. Butt MA, Aby ES, Debes JD. The global epidemiology of hepatocellular carcinoma. Hepatol Commun. 2026;10(5):102446.

101. Sung H, Ferlay J, Siegel RL, Laversanne M, Soerjomataram I, Jemal A, et al. Global Cancer Statistics 2020: GLOBOCAN Estimates of Incidence and Mortality Worldwide for 36 Cancers in 185 Countries. CA Cancer J Clin. 2021;71(3):209-49.

102. Ringelhan M, Pfister D, O'Connor T, Pikarsky E, Heikenwalder M. The immunology of hepatocellular carcinoma. Nat Immunol. 2018;19(3):222-32.

103. Roerecke M, Vafaei A, Hasan OSM, Chrystoja BR, Cruz M, Lee R, et al. Alcohol Consumption and Risk of Liver Cirrhosis: A Systematic Review and Meta-Analysis. Am J Gastroenterol. 2019;114(10):1574-86.

104. Younossi ZM, Kalligeros M, Henry L. Epidemiology of metabolic dysfunction-associated steatotic liver disease. Clin Mol Hepatol. 2025;31(Suppl):S32-S50.

105. Schwabe RF, Luedde T. Apoptosis and necroptosis in the liver: a matter of life and death. Nat Rev Gastroenterol Hepatol. 2018;15(12):738-52.

106. Malhi H, Gores GJ. Cellular and molecular mechanisms of liver injury. Gastroenterology. 2008;134(6):1641-54.

107. Liu X, Yang JM, Zhang SS, Liu XY, Liu DX. Induction of cell cycle arrest at G1 and S phases and cAMP-dependent differentiation in C6 glioma by low concentration of cycloheximide. BMC Cancer. 2010;10:684.

108. Luedde T, Schwabe RF. NF-kappaB in the liver--linking injury, fibrosis and hepatocellular carcinoma. Nat Rev Gastroenterol Hepatol. 2011;8(2):108-18.

109. Czauderna C, Castven D, Mahn FL, Marquardt JU. Context-Dependent Role of NF-kappaB Signaling in Primary Liver Cancer-from Tumor Development to Therapeutic Implications. Cancers (Basel). 2019;11(8):1053.

110. Sadati S, Khalaji A, Bonyad A, Khoshdooz S, Hosseini Kolbadi KS, Bahrami A, et al. NF-kappaB and apoptosis: colorectal cancer progression and novel strategies for treatment. Eur J Med Res. 2025;30(1):616.

111. Schoemaker MH, Ros JE, Homan M, Trautwein C, Liston P, Poelstra K, et al. Cytokine regulation of pro- and anti-apoptotic genes in rat hepatocytes: NF-kappaB-regulated inhibitor of apoptosis protein 2 (cIAP2) prevents apoptosis. J Hepatol. 2002;36(6):742-50.

112. Guerrache A, Micheau O. TNF-Related Apoptosis-Inducing Ligand: Non-Apoptotic Signalling. Cells. 2024;13(6):521.

113. Bai J, Cederbaum AI. Cycloheximide protects HepG2 cells from serum withdrawal-induced apoptosis by decreasing p53 and phosphorylated p53 levels. J Pharmacol Exp Ther. 2006;319(3):1435-43.

114. Goodall KJ, Finch-Edmondson ML, van Vuuren J, Yeoh GC, Gentle IE, Vince JE, et al. Cycloheximide Can Induce Bax/Bak Dependent Myeloid Cell Death Independently of Multiple BH3-Only Proteins. PLoS One. 2016;11(11):e0164003.

115. Miao Y, Du Q, Zhang HG, Yuan Y, Zuo Y, Zheng H. Cycloheximide (CHX) Chase Assay to Examine Protein Half-life. Bio Protoc. 2023;13(11):e4690.

116. Pajak B, Gajkowska B, Orzechowski A. Cycloheximide-mediated sensitization to TNF-alpha-induced apoptosis in human colorectal cancer cell line COLO 205; role of FLIP and metabolic inhibitors. J Physiol Pharmacol. 2005;56 Suppl 3:101-18.

117. Zou X, Zhang D, Song Y, Liu S, Long Q, Yao L, et al. HRG switches TNFR1-mediated cell survival to apoptosis in Hepatocellular Carcinoma. Theranostics. 2020;10(23):10434-47.

118. Luschen S, Ussat S, Scherer G, Kabelitz D, Adam-Klages S. Sensitization to death receptor cytotoxicity by inhibition of fas-associated death domain protein (FADD)/caspase signaling. Requirement of cell cycle progression. J Biol Chem. 2000;275(32):24670-8.

119. Mahdavi Sharif P, Jabbari P, Razi S, Keshavarz-Fathi M, Rezaei N. Importance of TNF-alpha and its alterations in the development of cancers. Cytokine. 2020;130:155066.

120. Hora S, Wuestefeld T. Liver Injury and Regeneration: Current Understanding, New Approaches, and Future Perspectives. Cells. 2023;12(17):2129.

121. Shen H, Liangpunsakul S, Iwakiri Y, Szabo G, Wang H. Immunological mechanisms and emerging therapeutic targets in alcohol-associated liver disease. Cell Mol Immunol. 2025;22(10):1190-204.

122. Liu W, Lin YT, Han DG, Shi AC, Liu Q, Jing ZT. Enhancement of Tumor Necrosis Factor-alpha-Mediated Hepatic Apoptosis and Liver Injury by Hepatitis B Virus Surface Antigen. Am J Pathol. 2025;195(10):1854-68.

123. New-Aaron M, Adepoju LA, Pathania AS, Kharbanda KK, Osna NA. Hepatocyte-Derived Apoptotic Bodies as Pathological Intercellular Messengers in the Liver. Biomolecules. 2026;16(2):198.

124. Ajoolabady A, Pratico D, Bahijri S, Eldakhakhny B, Tuomilehto J, Wu F, et al. Hallmarks and mechanisms of cellular senescence in aging and disease. Cell Death Discov. 2025;11(1):364.

125. Los M, Mozoluk M, Ferrari D, Stepczynska A, Stroh C, Renz A, et al. Activation and caspase-mediated inhibition of PARP: a molecular switch between fibroblast necrosis and apoptosis in death receptor signaling. Mol Biol Cell. 2002;13(3):978-88.

126. Wen X, Lin ZQ, Liu B, Wei YQ. Caspase-mediated programmed cell death pathways as potential therapeutic targets in cancer. Cell Prolif. 2012;45(3):217-24.

127. Santiago-Lomeli M, Gomez-Quiroz LE, Ortiz-Ortega VM, Kershenobich D, Gutierrez-Ruiz MC. Differential effect of interleukin-10 on hepatocyte apoptosis. Life Sci. 2005;76(22):2569-79.

128. Ogura K, Terasaki Y, Miyoshi-Akiyama T, Terasaki M, Moss J, Noda M, et al. Vibrio cholerae Cholix Toxin-Induced HepG2 Cell Death is Enhanced by Tumor Necrosis Factor-Alpha Through ROS and Intracellular Signal-Regulated Kinases. Toxicol Sci. 2017;156(2):455-68.

129. Lee MS, Seo J, Choi DY, Lee EW, Ko A, Ha NC, et al. Stabilization of p21 (Cip1/WAF1) following Tip60-dependent acetylation is required for p21-mediated DNA damage response. Cell Death Differ. 2013;20(4):620-9.

130. Kim HM, Kang MK, Seong SY, Jo JH, Kim MJ, Shin EK, et al. Meiotic Cell Cycle Progression in Mouse Oocytes: Role of Cyclins. Int J Mol Sci. 2023;24(17):13659

131. Tchakarska G, Sola B. The double dealing of cyclin D1. Cell Cycle. 2020;19(2):163-78.

132. Moneo V, del Valle Guijarro M, Link W, Carnero A. Overexpression of cyclin D1 inhibits TNF-induced growth arrest. J Cell Biochem. 2003;89(3):484-99.

133. Montalto FI, De Amicis F. Cyclin D1 in Cancer: A Molecular Connection for Cell Cycle Control, Adhesion and Invasion in Tumor and Stroma. Cells. 2020;9(12):2648.

134. Chen S, Li L. Degradation strategy of cyclin D1 in cancer cells and the potential clinical application. Front Oncol. 2022;12:949688.

135. Qi Y, Guo S, Cai X, Liu C, Dong Y, Chen X, et al. HADHA in Cardiovascular Disease: From Mitochondrial Dysfunction to Therapeutic Targets. Ageing Res Rev. 2026:103106.

136. Zhang S, Rao S, Yang M, Ma C, Hong F, Yang S. Role of Mitochondrial Pathways in Cell Apoptosis during He-Patic Ischemia/Reperfusion Injury. Int J Mol Sci. 2022;23(4):2357.

137. Pierce RH, Campbell JS, Stephenson AB, Franklin CC, Chaisson M, Poot M, et al. Disruption of redox homeostasis in tumor necrosis factor-induced apoptosis in a murine hepatocyte cell line. Am J Pathol. 2000;157(1):221-36.

138. Arumugam MK, Gopal T, Kalari Kandy RR, Boopathy LK, Perumal SK, Ganesan M, et al. Mitochondrial Dysfunction-Associated Mechanisms in the Development of Chronic Liver Diseases. Biology (Basel). 2023;12(10):1311

139. Cassandri M, Smirnov A, Novelli F, Pitolli C, Agostini M, Malewicz M, et al. Zinc-finger proteins in health and disease. Cell Death Discov. 2017;3:17071.

140. Zhang Y, Tang X, Wang C, Wang M, Li M, Li X, et al. Zinc finger protein 593 promotes breast cancer development by ensuring DNA damage repair and cell-cycle progression. iScience. 2024;27(12):111513.

141. Hartman BH, Durruthy-Durruthy R, Laske RD, Losorelli S, Heller S. Identification and characterization of mouse otic sensory lineage genes. Front Cell Neurosci. 2015;9:79.

142. Xu Y, Yang L, Zhao X, Zhang Y, Jones TA, Jones SM, et al. Functional cooperation between two otoconial proteins Oc90 and Nox3. J Vestib Res. 2021;31(6):441-9.

143. Mlynarska E, Kowalik A, Krajewska A, Krupinska N, Marcinkowska W, Motor J, et al. Inflammaging and Senescence-Driven Extracellular Matrix Remodeling in Age-Associated Cardiovascular Disease. Biomolecules. 2025;15(10):1452.

144. Rizzo MG, Fazio E, De Pasquale C, Sciuto EL, Cannata G, Multisanti CR, et al. Physiopathological Features in a Three-Dimensional In Vitro Model of Hepatocellular Carcinoma: Hypoxia-Driven Oxidative Stress and ECM Remodeling. Cancers (Basel). 2025;17(18):3082.

145. Glockzin K, Meek TD, Katzfuss A. Characterization of adenine phosphoribosyltransferase (APRT) activity in Trypanosoma brucei brucei: Only one of the two isoforms is kinetically active. PLoS Negl Trop Dis. 2022;16(2):e0009926.

146. Diehl FF, Miettinen TP, Elbashir R, Nabel CS, Darnell AM, Do BT, et al. Nucleotide imbalance decouples cell growth from cell proliferation. Nat Cell Biol. 2022;24(8):1252-64.

147. Chen S, Zhang S, Wang Z, Li J, Yuan Y, Li T, et al. Purine metabolism-related gene expression signature predicts survival outcome and indicates immune microenvironment profile of gliomas. Front Pharmacol. 2022;13:1038272.

148. Qi S, Fu J, Li Y, Fei C, Zhang J, Sui L, et al. Electrochemical response mechanism of DNA damaged cells: DNA damage repair and purine metabolism activation. Bioelectrochemistry. 2025;161:108832.

149. Lee JE, Ahn S, Jeong H, An S, Myung CH, Lee JA, et al. Olig2 regulates p53-mediated apoptosis, migration and invasion of melanoma cells. Sci Rep. 2021;11(1):7778.

150. Rakhra G, Rakhra G. Zinc finger proteins: insights into the transcriptional and post transcriptional regulation of immune response. Mol Biol Rep. 2021;48(7):5735-43.

151. Liu S, Sima X, Liu X, Chen H. Zinc Finger Proteins: Functions and Mechanisms in Colon Cancer. Cancers (Basel). 2022;14(21):5242.

152. Schnabl B, Czech B, Valletta D, Weiss TS, Kirovski G, Hellerbrand C. Increased expression of zinc finger protein 267 in non-alcoholic fatty liver disease. Int J Clin Exp Pathol. 2011;4(7):661-6.

153. Zhang X, Zheng Q, Yue X, Yuan Z, Ling J, Yuan Y, et al. ZNF498 promotes hepatocellular carcinogenesis by suppressing p53-mediated apoptosis and ferroptosis via the attenuation of p53 Ser46 phosphorylation. J Exp Clin Cancer Res. 2022;41(1):79.

BIOGRAPHY

Name	Thanawan Soimanee
Educational Attainment	2013: B.S. (Veterinary Technology) Faculty of Veterinary Technology, Kasetsart University, Thailand. 2021: M.Sc. student Graduate Program in Biomedical Sciences, Faculty of Allied Health Science, Thammasat University, Thailand.

Publication

1. Chareeporn Akekawatchai*, Chada Phuegsilp, Khaimuk Changsri, Thanawan Soimanee, Warisara Sretapunya. Distribution of +874T/A IFN-γ and -509C/T TGF-β1 Single Nucleotide Polymorphisms in Human Immunodeficiency Virus-infected Thais. Journal of Medical virology 94(3), 2022. doi.org/10.1002/jmv.27567
2. Chareeporn Akekawatchai*, Khaimuk Changsri, Apikhun Tunkor, Chada Phuegsilp, Thanawan Soimanee, Madtika Fungkrajai, Thitiilat Chiraunyanann, Warisara Sretapunya. Lack of Association between IFN-γ, CXCL10 and TGF-β1 Gene Polymorphisms and Liver Complication in HIV-infected Thais. Asian Pac J Cancer Prev, 23 (4), 1279-1284. DOI:10.31557/APJCP.2022.23.4.1279
3. Khaimuk Changsri*, Thitimonrat Duangchanda*, Thanawan Soimanee, Waraporn Fuckpo, Duangnate Pipatsatitpong, Chareeporn Akekawatchai. Distribution and Clinical Significance of Hepatitis B virus A1762T/G1764A Double Mutation in Chronic Hepatitis B Patients: A Cross-Sectional Study. Asian Pac J Cancer Prev, 25 (2), 371-377.DOI:10.31557/APJCP.2024.25.2.371.

4. Chewaporn Tarnathummanan, Thanawan Soimanee, Janya Khattiya, Warisara Sretapunya, Narumon Phaonakrop, Sittiruk Roytrakul and Chareeporn Akekawatchai. Biomedical report 21: 155, 2024. DOI: 10.3892/br.2024.1843.

Presentation in scientific meetings

Thanawan Soimanee and Chareeporn Akekawatchai

IN VITRO model for hepatocyte death and inflammation. The 30th FAOBMB & 8th BMB Conference, Bangkok, Nov 22-25, 2023. (Poster presentation)

Thanawan Soimanee, Sittiruk Roytrakul and Chareeporn Akekawatch

Characterization of *IN VITRO* hepatocyte death by proteomic analysis. The 12th Joint Symposium Tentative Theme: "Harmonizing Healthcare: Bridging interprofessional Collaboration", University of Santo Tomas, Manila, Philippines, Mar 17-18, 2026. (Poster presentation)